INFORMATION TO USERS

This manuscript has been reproduced from the microfilm master. UMI films the text directly from the original or copy submitted. Thus, some thesis and dissertation copies are in typewriter face, while others may be from any type of computer printer.

The quality of this reproduction is dependent upon the quality of the copy submitted. Broken or indistinct print, colored or poor quality illustrations and photographs, print bleedthrough, substandard margins, and improper alignment can adversely affect reproduction.

In the unlikely event that the author did not send UMI a complete manuscript and there are missing pages, these will be noted. Also, if unauthorized copyright material had to be removed, a note will indicate the deletion.

Oversize materials (e.g., maps, drawings, charts) are reproduced by sectioning the original, beginning at the upper left-hand corner and continuing from left to right in equal sections with small overlaps.

ProQuest Information and Learning
300 North Zeeb Road, Ann Arbor, MI 48106-1346 USA
800-521-0600

Complexation of Probe Molecules to the Different Binding Sites of Bile Salt Aggregates

by

Olga Rinco
B.Sc., McMaster University, 1997

A Dissertation Submitted in Partial Fulfillment of the
Requirements for the Degree of

DOCTOR OF PHILOSOPHY

in the Department of Chemistry

We accept this dissertation as conforming
to the required standard

Dr. Cornelia Bohne, Supervisor (Department of Chemistry)

Dr. Thomas M. Fyles, Departmental Member (Department of Chemistry)

Dr. David A. Harrington, Departmental Member (Department of Chemistry)

Dr. Barbara J. Hawkins, Outside Member (Department of Biology)

Dr. Mónica Barra, External Examiner (Department of Chemistry, University of Waterloo)

© Olga Rinco, 2002
University of Victoria

All right reserved. This thesis may not be reproduced in whole or in part, by photocopy or other means, without the permission of the author.

Ethylnaphthalene, 2-ethylnaphthalene, 1-acetonaphthone, 2-acetonaphthone, 1-naphthyl-1-ethanol and 2-naphthyl-1-ethanol were studied. 1-Ethylnaphthalene and 2-ethylnaphthalene were contained within the primary binding site, while 1-naphthyl-1-ethanol, 2-naphthyl-1-ethanol, 1-acetonaphthone and 2-acetonaphthone were contained within the secondary binding site. The effect of the position of the substituent was only noticed when the probe molecules formed weak interactions with the outside of the primary aggregate, and not when the probe was complexed to one of the binding sites present in the NaCh system.

The naphthalene probe molecules were also used to study the effect of ionic strength on NaCh aggregate formation. It was found that primary aggregation occurred at lower NaCh concentration as the ionic strength was increased. No effect of ionic strength was observed on the formation of secondary aggregates.

All the findings in this study are consistent with an aggregation model in which two distinct binding sites are present. The shape of the probe as well as its hydrophobicity are critical to its interaction with the NaCh aggregates. From these dynamic studies it was found that only a small number of NaCh monomers (6-13) are needed to define both the primary and secondary binding sites.

Examiners:

Dr. Cornelia Bohne, Supervisor (Department of Chemistry)

Dr. Thomas M. Fyles, Departmental Member (Department of Chemistry)

Dr. David A. Harrington, Departmental Member (Department of Chemistry)

Dr. Barbara J. Hawkins, Outside Member (Department of Biology)

Dr.Mónica Barra, External Examiner (Department of Chemistry, University of Waterloo)

TABLE OF CONTENTS

PRELIMINARY PAGES

Abstract....ii
Table of Contents....iv
List of Tables....ix
List of Figures....xii
List of Schemes....xvi
Acknowledgements....xvii
Dedication....xviii
List of Abbreviations....xix

1 INTRODUCTION....1

1.1 Photophysics[1-3]....1
1.1.1 Photophysical processes....1
1.1.2 Photophysics involving unimolecular processes....3
1.1.2.1 Non-radiative Processes....5
1.1.2.2 Radiative Processes....6
1.1.2.2.1 Absorption of light....6
1.1.2.2.2 Fluorescence emission....8
1.1.2.2.3 Phosphorescence emission....8
1.1.2.3 Kinetic measurements of lifetimes....9
1.1.2.4 Quantum yields....10
1.1.3 Bimolecular photophysical processes....11
1.1.3.1 Excited state quenching....11
1.1.3.1.1 Quenching within supramolecular systems....14

1.2 Fast kinetic techniques....18
1.2.1 Laser flash photolysis....18

1.2.2 Fluorescence spectroscopy 20
1.2.3 Time-resolved fluorescence emission measurements: single photon counting 22

1.3 Bile salts 25
1.3.1 Biological significance of bile acids 25
1.3.2 Structure of bile salts 26
1.3.2.1 Primary/secondary aggregate model for bile salts in solutions 29
1.3.2.2 Helical model 37
1.3.2.3 Effect of ionic strength on the aggregation pattern of bile salts 40

1.4 Probe molecules for the studies within NaCh aggregates 42
1.4.1 Benzophenone and 4,4'-dimethylbenzophenone 43
1.4.2 Naphthalene and derivatives 46

1.5 Project Proposal 48

2 EXPERIMENTAL 50

2.1 Materials 50

2.2 General sample preparation 50
2.2.1 Sodium cholate solutions 51
2.2.2 Benzophenone and 4,4'-dimethylbenzophenone solutions 52
2.2.3 Solutions for naphthalene derivatives 53
2.2.3.1 Probe and NaCh solutions 53
2.2.3.2 Quencher solutions 53

2.3 Sample preparation for experiments conducted at constant ionic strength 54
2.3.1 Preparation of NaCh/NaCl solutions for quenching experiments 55
2.3.2 Sample preparation for fluorescence quenching experiments 55
2.3.3 Sample preparation for laser flash photolysis quenching experiments 56

2.4 Instrumentation 57

2.4.1 UV-Vis absorption spectroscopy 57
2.4.2 Fluorescence spectroscopy 58
2.4.2.1 Steady-state experiments 58
2.4.2.2 Time-resolved experiments 59
2.4.3 Laser flash photolysis 60

2.5 Procedures 66
2.5.1 Determination of molar absorptivities for Bp and DMBp 66
2.5.2 Detection of solvated electrons 67

3 PHOTOCHEMISTRY OF BENZOPHENONE AND 4,4'-DIMETHYLBENZOPHENONE IN SODIUM CHOLATE 68

3.1 Results 68
3.1.1 Molar absorptivities of Bp and DMBp in water and sodium cholate aggregates 68
3.1.2 Photochemistry of Bp and DMBp in water 70
3.1.2.1 Transient absorption spectra 70
3.1.2.2 Transient kinetics of Bp and DMBp in water 72
3.1.2.3 Quenching studies 73
3.1.2.3.1 Nitrite as a triplet excited state quencher 73
3.1.2.3.2 Oxygen as a triplet excited state quencher 74
3.1.2.3.3 2-propanol as a triplet excited state quencher 74
3.1.3 Photochemistry of Bp and DMBp when complexed to NaCh aggregates 75
3.1.3.1 Transient absorption spectra of Bp and DMBp in presence of NaCh aggregates 75
3.1.3.2 Kinetic processes for Bp and DMBp in NaCh aggregates monitored in the 600 nm region 77
3.1.3.2.1 Effect of Bp or DMBp concentration on the kinetic processes at 600 nm 80
3.1.3.3 Kinetic processes for Bp and DMBp in NaCh aggregates in the 540 nm region 83

4.2.1.1 Emission spectra 151
4.2.1.2 Singlet excited state quenching of naphthalene probes by sodium iodide..... 151
4.2.2 Laser flash photolysis: investigation of the effect of ionic strength on the complexation dynamics of the triplet excited states of the Np probes with NaCh aggregates 156
4.2.2.1 Transient spectra and kinetic decays 156
4.2.2.2 Quenching studies of the excited triplet states of Np with nitrite..... 156
4.3 Discussion on the dynamics of probe binding to bile salt aggregates at varying ionic strength..... 162
4.3.1 Mechanism of quenching for singlet excited state Np probe molecules. 166
4.3.2 Effect of the probe hydrophobicity on guest binding with NaCh aggregates..... 166
4.3.2.1 1-Ethylnaphthalene and 2-ethylnaphthalene as probe molecules in NaCh aggregates..... 167
4.3.2.2 1-Naphthyl-1-ethanol and 2-naphthyl-1-ethanol as probe molecules in NaCh aggregates..... 174
4.3.2.3 1-Acetonaphthone and 2-acetonaphthone as probe molecules in NaCh aggregates..... 177
4.3.2.4 Summary of the findings for Np probe complexation in experiments carried out with varying ionic strength 179
4.4 Discussion on the dynamics of probe binding to bile salt aggregates at constant ionic strength..... 183
4.4.1 Effect of ionic strength on primary aggregate formation 184
4.4.2 Effect of ionic strength on secondary aggregate formation 187
5 CONCLUSIONS..... 189
5.1 Benzophenone complexation 189
5.2 Naphthalene complexation..... 191
6 REFERENCES..... 193

LIST OF TABLES

Table 2.1 Sample preparation for fluorescence quenching experiments performed at a constant ionic strength (μ). (a) μ = 0.03 M (top), (b) μ = 0.2 M (middle) and (c) μ = 0.4 M (bottom) (blank refers to solutions with no probe added that were used for baseline readings) 56

Table 3.1 Dependence of the relative triplet concentration, measured in terms of the absorbance at 600 nm, and the relative contribution of the initial fast decay (A_1 / A_t) on the NaCh and Bp concentrations. Errors are average deviations of two independent experiments. 79

Table 3.2 Dependence of the relative triplet concentration, measured in terms of the absorbance at 600 nm, and the relative contribution of the initial fast decay (A_1 / A_t) on the NaCh and DMBp concentrations. Errors are average deviations of two independent experiments. 80

Table 3.3 Dependence of the relative ratios of ketyl absorption to the total absorption and the 2k/εl values on varying concentrations of NaCh and Bp at 540 nm. Errors are average deviations of two independent experiments. 87

Table 3.4 Dependence of the relative ratios of ketyl absorption to the total absorption and the 2k/εl values on varying concentrations of NaCh and DMBp at 540 nm. Errors are average deviations of two independent experiments. 88

Table 4.1 Stern-Volmer constants obtained from steady-state fluorescence quenching of the Np probes in the presence of varying concentrations of NaCh. The numbers in parentheses indicate the number of independent experiments performed to arrive at the average value. 122

Table 4.2 Single photon counting results: values for τ_0 (or $<\tau_0>$), K_{sv} values and k_q (or $<k_q>$) values for the hydroxy and alkyl substituted Np derivatives in the presence of 0 mM, 10 mM, 20 mM and 40 mM of NaCh. Errors were recovered from data analysis as each experiment was performed once. 131

Table 4.3 Lifetimes in the absence of quencher, average pre-exponential factors (A), and quenching rate constants for the species with different lifetimes for 1-EtNp and 2-EtNp in the presence of various concentrations of NaCh. Data for both alkane

substituted probes in the absence of NaCh gave rise to monoexponential decays; therefore, only one lifetime and one value of k_q were reported. 134

Table 4.4 Lifetimes in the absence of quencher, average pre-exponential factors (A), and quenching rate constants for the species with different lifetimes for 1-NpOH and 2-NpOH in the presence of various concentrations of NaCh. Data for both alcohol substituted probes in the absence of NaCh gave rise to monoexponential decays; therefore, only one lifetime and one value of k_q were reported. 135

Table 4.5 Triplet quenching rate constants for the linear quenching plots of the naphthalene derivatives in the absence of NaCh and 1-NpOH in the presence of 10 mM of NaCh. The number in parentheses represents the number of independent experiments performed. 142

Table 4.6 Quenching rate constants (or ranges) ($k_q(H)$) for the triplet excited states of 1-EtNp, 2-EtNp, 1-NpOH, 2-NpOH, 1-NpO, and 2-NpO in the bile salt aggregates quenched by nitrite for experiments that led to curved quenching plots. The number in parentheses represents the number of independent experiments performed. 144

Table 4.7 Dissociation rate constants for the triplet naphthalene derivatives in the presence of 10 mM, 20 mM, and 40 mM of NaCh. The number in parentheses represents the number of independent experiments performed. 146

Table 4.8 Values for the association rate constants divided by the aggregation number for the naphthalene series of probes, in the presence of 10 mM, 20 mM, and 40 mM of NaCh. The number in parentheses represents the number of independent experiments performed. 150

Table 4.9 Effect of ionic strength on the Stern-Volmer constants for 1-EtNp in the presence and absence of NaCh. The number in parentheses indicates the number of independent experiments performed. 153

Table 4.10 Effect of ionic strength on the Stern-Volmer constants for 1-NpOH in the presence and absence of NaCh. The number in parentheses indicates the number of independent experiments performed. 154

Table 4.11 Quenching rate constants for 1-EtNp in the absence of NaCh, and 1-NpOH in the absence of NaCh and in the presence of 10 of mM of NaCh, at constant ionic

strength. Two independent experiments were performed for each probe at each bile salt and NaCl concentration. 157

Table 4.12 Quenching rate constants (or ranges) for 1-EtNp in the presence of 10 mM, and 40 mM of NaCh and 1-NpOH in the presence of 40 mM of NaCh at constant ionic strengths. Two independent experiments were performed for each probe at each bile salt and NaCl concentration. 158

Table 4.13 Dissociation rate constants for 1-EtNp in the presence of 10 mM, and 40 mM of NaCh and 1-NpOH in the presence of 40 mM of NaCh at constant ionic strengths. Two independent experiments were performed for each probe at each bile salt and NaCl concentration. 159

Table 4.14 Values for the association rate constants divided by the aggregation number for 1-EtNp in the presence of 10 mM, and 40 mM of NaCh and 1-NpOH in the presence of 40 mM of NaCh at constant ionic strengths. Two independent experiments were performed for each probe at each bile salt and NaCl concentration. 160

Table 4.15 Comparison of the triplet excited state quenching rate constants between the varying ionic strength experiments and the constant ionic strength experiments at μ = 0.2 M 161

Table 4.16 Comparison of the dissociation rate constants for the triplet excited states between the varying ionic strength experiments and the constant ionic strength experiments at μ = 0.2 M. 161

Table 4.17 Association rate constants for the triplet excited state of the probe molecules located within the primary aggregate of NaCh calculated based on an aggregation number of 4. 182

Table 4.18 Association rate constants for the triplet excited state of the probe molecules located within the secondary aggregate of NaCh calculated, based on an aggregation number of 10. 182

LIST OF FIGURES

Figure 1.1 The electromagnetic spectrum (adapted from ref. 1). 3

Figure 1.2 Jablonski energy level diagram: Solid arrows represent radiative processes (absorption (Abs), fluorescence (F), phosphorescence (P), and triplet-triplet absorption ($T\text{-}T_{Abs}$)), while zigzagged arrows represent non-radiative process (internal conversion (IC), intersystem crossing (ISC), and vibrational relaxation (VR)). 5

Figure 1.3 Mechanisms for dynamic and static quenching 12

Figure 1.4 Simplified diagram of a fluorescence spectrometer 21

Figure 1.5 A schematic representation of a single photon counter. Light source (1), "start" photomultiplier detector (2), excitation monochromator (3), sample (4), detection monochromator (5), "stop" photomultiplier detector (6), time-amplitude converter (7) and multichannel analyzer (8).[13] 23

Figure 1.6 Structure of the most common bile salt monomer: NaCh. The structure on the right emphasizes the planar polarity of the NaCh molecule. 27

Figure 1.7 Structures of other commonly studied bile salts. 28

Figure 1.8 Primary and secondary aggregate interactions of NaCh. Each cluster represents a primary aggregate, while the grouping of two or more of the primary aggregates forms a secondary aggregate. The black portion of the aggregates are the hydrocarbons within the NaCh, while the gray circles represent the position of the hydrophilic alcohol and carboxy groups. 30

Figure 1.9 Disk-like model of primary aggregation (left). Incorporation of a spin probe (right) into a primary "disk-like" aggregate.[50] (Kawamura et al., Spin-Label Studies of Bile Salt Micelles, © ACS 1989/ CANCOPY.) 32

Figure 1.10 Early schematic representation of pyrene incorporated within a NaTC primary aggregate.[54] (Thomas et al., Kinetic Studies in Bile Acid Micelles, ©ACS 1975/ CANCOPY.) 33

Figure 1.11 Probe molecules: Pyrene (left), anthracene (center) and naphthalene (Np) (right). 35

Figure 1.12 Probe molecule: xanthone. 36

Figure 1.13 Crystal structure of RbTC which supports the helical model for bile salt aggregation.[58] (Conte et al., Nuclear Magnetic Resonance and X-ray studies on Micellar Aggregates of Sodium Deoxycholate, © ACS 1984/ CANCOPY.) 38

Figure 1.14 Probe molecules: benzophenone (Bp, left) and 4,4'-dimethylbenzophenone (DMBp, right).....44

Figure 1.15 Probe molecules: 1-ethylnaphthalene (1-EtNp), 2-ethylnaphthalene (2-EtNp), 1-acetonaphthone (1-NpO), 2-acetonaphthone (2-NpO), 1-naphthyl-1-ethanol (1-NpOH) and 2-naphthyl-1-ethanol (2-NpOH).....47

Figure 3.1 Ground state absorption spectra of Bp in the absence of NaCh and in the presence of 40 mM of NaCh, to show the difference in the absorption of Bp ([Bp] = 0.6 mM) due to the presence of NaCh, at the excitation wavelength, 308 nm.....69

Figure 3.2 Transient absorption spectra for Bp in water (0.2 M NaCl), in the absence (0, delay = 9.9 μs) and in the presence (▲, delay = 12 μs) of 0.62 M of 2-propanol. The two spectra were normalized at the peak maximum in order to emphasize the shift in the spectrum upon the formation of ketyl radicals. The third spectrum (∇, delay = 30 μs) is the signal for Bp in water observed for a long delay after the laser pulse. The solid lines were included to guide the eye.....71

Figure 3.3 Self-quenching plot for the triplet excited state of Bp in water, with a self-quenching rate constant of 1.2×10^8 $M^{-1}s^{-1}$.....73

Figure 3.4 Quenching plot for the triplet excited state of Bp in water quenched with sodium nitrite. A quenching rate constant of 3.4×10^9 $M^{-1}s^{-1}$ was recovered.....74

Figure 3.5 Transient absorption spectra of Bp in the presence of 40 mM of NaCh at varying time delays after the laser pulse (0.07 μs (∇), 0.3 μs (●), 4.9 μs (O)). The solid lines were included to guide the eye.....76

Figure 3.6 Decay at 600 nm fitted to the sum of two exponentials ($\tau_1 = 0.07$ μs, $\tau_2 = 5.6$ μs) for the transients formed when irradiating Bp in the presence of 40 mM of NaCh. The inset shows the decay on a long time scale in order to determine the values for τ_2 and A_3.....78

Figure 3.7 Dependence with ketone concentration of the observed rate constant for the fast triplet decay at 600 nm, of Bp (A) and DMBp (B) in the presence of NaCh. The open symbols are solutions in the presence of 10 mM of NaCh while closed symbols

are solutions in the presence 40 mM of NaCh. The different symbols correspond to independent experiments. 82

Figure 3.8 Transient kinetics at 540 nm in the presence of 10 mM of NaCh for Bp (●, 1.0 mM) and DMBp (O, 0.44 mM) 83

Figure 3.9 Kinetics at 540 nm in the presence of 40 mM of NaCh. (A) Normalized transient decays for Bp (●, 2.7 mM) and DMBp (O, 2.2 mM) illustrating the growth observed for Bp. (B) Decay of the Bp ketyl radical after the growth shown in A. The solid line represents the fit to a bimolecular decay and the residuals for the fit are shown in the inset. 85

Figure 3.10 nitrite quenching plot, for one of the independent experiments, for the triplet excited state of Bp at 600 nm. Fast (●) and slow (Δ) triplet components in the presence of 10 mM of NaCh. 91

Figure 3.11 Nitrite quenching plot for the fast component of the triplet excited state decay of DMBp in the presence of 10 mM of NaCh(❑) and 40 mM of NaCh (O,●, two independent experiments), and the slow component of the decay in the presence of 40 mM of NaCh(▲). 93

Figure 4.1 Normalized fluorescence emission spectra for the singlet excited states of 2-NpOH (top) and 2-EtNp (bottom) in the absence of NaCh (a) and in the presence of 40 mM of NaCh (b). 118

Figure 4.2 Quenching of the fluorescence emission spectra of 2-EtNp in the presence of 10 mM of NaCh with the following NaI concentrations: a = 0 mM, b = 10 mM, c = 20 mM, d = 30 mM, e = 40 mM and f = 50 mM 120

Figure 4.3 Stern-Volmer plots for the quenching by iodide of the singlet excited state of 2-EtNp in the presence of 0 mM (●), 10 mM (▲) and 40 mM (■) of NaCh. 121

Figure 4.4 Single exponential fluorescence decay for 2-EtNp in water (top). The resicuals for the fit of the experimental data for a single exponential decay (middle). The residuals for the fit of the experimental data to the sum of two exponentials (Equations 2.2) (bottom) 125

Figure 4.5 Fluorescence decay for 1-NpOH in the presence of 10 mM of NaCh, and 30 mM of NaI, fitted to the sum of two exponentials (top). The residuals for the fit of the experimental data for the sum of two exponentials (Equations 2.2) (middle). The

residuals for the fit of the experimental data for a single exponential decay (bottom). 126

Figure 4.6 Stern-Volmer plot for 2-NpOH in the presence of 10 mM (◆), 20 mM (●) and 40 mM (▲) of NaCh, data using average lifetimes obtained from single photon counting experiments..... 128

Figure 4.7 Stern-Volmer plot for the excited state species with two different lifetimes obtained from the SPC experiments; singlet excited state quenching by NaI for 1-EtNp in the presence of 20 mM of NaCh. 133

Figure 4.8 Transient absorption spectra of 2-NpOH in the absence of NaCh (●, delay = 6.5 μs) and in the presence of 40 mM of NaCh (Δ, delay = 12 μs). The spectra have been normalized at the absorption maximum at 420 nm. The solid line represents a smooth curve through the data in the presence of 40 mM of NaCh. Only one curve was shown as both sets of data gave rise to a similar spectrum..... 138

Figure 4.9 Kinetic decay traces of 1-EtNp in the absence of NaCh (A) and in the presence of 40 mM of NaCh (B). All traces were fitted to a monoexponential decay and the residuals for the fit are shown in the insets..... 140

Figure 4.10 Linear quenching plot for triplet 2-EtNp in the absence of NaCh quenched by sodium nitrite..... 141

Figure 4.11 Curved quenching plot for the quenching of triplet 1-EtNp in the presence of 10 mM of NaCh by nitrite..... 143

Figure 4.12 Nitrite quenching plot for 1-NpOH and 2-NpOH in the presence of 10 mM of NaCh to show the difference in curvature based on the position of the substituent on the Np ring structure. 148

Figure 4.13 Comparison of the triplet excited state quenching plots for (A) 1-EtNp and (B) 1-NpOH by nitrite in the presence of 0 mM, 10 mM and 40 mM of NaCh to highlight the presence of two distinct binding sites. 165

Acknowledgements

I wish to express my thanks and sincere appreciation to many people without whom this dissertation would not be possible. Firstly, to my supervisor Dr. Cornelia Bohne for her guidance and assistance throughout my research project. She inspired me to pursue a higher level of education and has been a wonderful role model. Special thanks to Dr. Tom Fyles, who helped overcome some of the final hurdles in order to complete the dissertation.

Special thanks goes out to Marie-Christine Nolet and Robyn Ovans, both of whom worked on the naphthalene project presented within this thesis. Lois Atkinson was kind enough to help with some editing in the latter stages of the writing of this work. Luis Netter's support with technical aspects of the lab as well as in many other ways was sincerely appreciated.

Many colleges over the years have helped me both professionally and personally and for that I thank them. Mark Kleinman, Scott Murphy, Sarah Monahan, Jason Anema, Molina Sheepwash, Andria Dyck, Laurie Amundson, Jessy Oake, Chelsea Carter, Christina de Barros, and Laura Okano, thanks for all your support! Also, thanks to the entire chemistry department, including the secretarial and technical staff for all their support, as well as my fellow graduate students for the friendly and social environment they helped create.

Completing a project such as this also takes support from external friends and family. My thanks go out to my extended "family" of friends here in Victoria especially those of you associated with my theatre and skydiving life. Thank-you for helping balance my life, which allowed me to finish this thesis.

Last, but never least my thanks to my family, especially my mother, without whose support it would have been impossible for me to finish this thesis.

Dedication

***To my mother**: for inspiring my life and always believing in me.*

***In memory of my father**: without his courage and love, I wouldn't be the same.*

List of Abbreviations

2k/εl	apparent first order rate constant
Abs	absorbance
ACS	American Chemical Society
Agg	aggregate
BDE	bond dissociation energy
Bp	benzophenone
c	velocity of light (3×10^8 ms^{-1})
ca	approximately
CD	circular dichroism
DMBp	4,4'-dimethylbenzophenone
E	energy
ESR	electron spin resonance
1-EtNp	1-ethylnaphthalene
2-EtNp	2-ethylnaphthalene
F	fluorescence
GC	gas chromatography
h	hours
h	Plank's constant (6.63×10^{-34} J s)
HOMO	highest occupied molecular orbital
I	intensity of transmitted light
IC	internal conversion
I_o	intensity of incident light
IR	infrared
IRF	instrument response function
ISC	intersystem crossing
k_-	dissociation rate constant
K	equilibrium constant
k_+	association rate constant
k_f	rate constant for fluorescence
k_o	intrinsic decay rate constant

k_{obs}	observed rate constant
k_q	quenching rate constant
k_{sq}	self-quenching rate constant
K_{SV}	Stern-Volmer constant
LFP	laser flash photolysis
τ	lifetime
LUMO	lowest unoccupied molecular orbital
MCA	multichannel analyzer
MeOH	methanol
min	minutes
mJ	millijoules
mL	milliliters
mM	millimolar
Mol	moles
ε	molar absorptivity
ms	milliseconds
N	aggregation number
NaCh	sodium cholate
NaTC	sodium taurocholate
nm	nanometers
NMR	nuclear magnetic resonance
Np	naphthalene
1-NpO	1-acetonaphthone
2-NpO	2-acetonaphthone
1-NpOH	1-naphthyl-1-ethanol
2-NpOH	2-naphthyl-1-ethanol
nr	non-radiative process
ns	nanoseconds
P	phosphorescence
ps	picoseconds
Q	quencher

r	radiative process
%RSD	percent relative standard deviation
s	seconds
SDS	sodium dodecyl sulfate
SPC	single photon counting
$T\text{-}T_{Abs}$	Triplet-triplet absorption
TAC	time-to-amplitude converter
UV	ultraviolet
vis	visible
VR	vibrational relaxation
λ	wavelength
Xan	xanthone
ΔA	change in absorbance
ΔA_{max}	maximum transient absorbance in a LFP kinetic trace
Φ	quantum yield
λ_{ex}	excitation wavelength
μm	micrometers
μs	microseconds
ν	frequency (s^{-1})

1 Introduction

1.1 Photophysics[1-3]

The interaction of light with matter occurs with one of two main outcomes. If the chemical nature of the matter is altered, resulting in the formation of a new chemical species, the study of the interaction is known as photochemistry. If no chemical reaction occurs, but there is a change in the quantum state of the molecule, the study of this interaction is known as photophysics. Understanding the photophysics of molecules helps not only in predicting photochemical mechanisms, but is also of use in understanding the interactions of molecules in complex supramolecular systems.

1.1.1 Photophysical processes

Molecules undergo photophysical changes upon interaction with light of a certain energy. Light in the ultraviolet (UV) and visible (vis) region of the electromagnetic spectrum is most often used to induce electronic transitions within organic molecules. Smaller amounts of energy are typically needed for rotational and vibrational transitions to occur.

The most common pictorial description of light is that of an electromagnetic wave of energy.[3] The light absorbed by a molecule takes the form of a quantized packet of energy known as a photon. The energy of a photon is critical for its interaction with an organic molecule. The energy of a photon is calculated using Equation 1.1,

$E = h\nu$

Equation 1.1

where E is energy (J), *h* is Plank's constant (6.63×10^{-34} J s), ν is the frequency of the light (s^{-1}).

As is clear from Equation 1.1, the energy of the photon increases as the frequency of light is increased. In photophysical studies, the frequency of light is often reported in terms of the wavelength of light (λ) measured in nanometers. Wavelength increases proportionally with a decrease in the energy of the photon, thus re-writing Equation 1.1 leads to Equation 1.2,

$E = hc/\lambda$

Equation 1.2

where c is the speed of light (3.0×10^{8} ms^{-1}). Figure 1.1 shows the span of the electromagnetic spectrum.

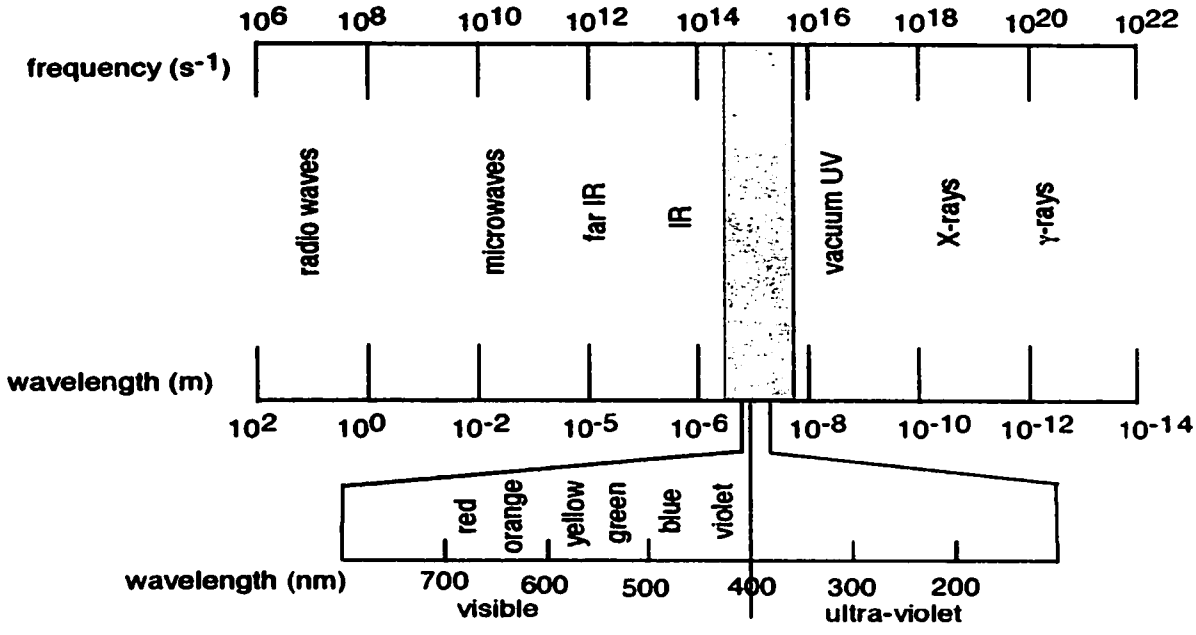

Figure 1.1 The electromagnetic spectrum (adapted from ref. 1).

Upon excitation, a molecule in the electronic ground state is excited to a higher energy state. The transition with the lowest energy occurs from the molecule's highest occupied molecular orbital (HOMO) to the (previously) lowest unoccupied molecular orbital (LUMO). For a closed shell organic molecule, the HOMO is most often a σ or π bonding orbital or a non-bonding orbital (n). The LUMO, on the other hand, is most often a σ^* or π^* anti-bonding orbital. The most common electronic transition for alkenes, alkynes and aromatic molecules to undergo is a π to π^* transition, whereas molecules containing a carbonyl functional group often undergo an n to π^* transition.

1.1.2 Photophysics involving unimolecular processes

Upon the absorption of light, a molecule is excited from its electronic ground state to a higher energy electronic state. There are a number of deactivation pathways that a

molecule can undergo in order to return to the ground state. The pathways are classified in two main categories: if the molecule emits light as it returns to the ground state, the process is classified as a radiative transition; if there is no emission involved in the deactivation of the molecule, the process is classified as a non-radiative transition. The deactivation pathway that occurs depends on numerous factors in regard to each molecule, including the solvent that is used, the electronic state of the molecule and/or the presence of other molecules. Figure 1.2 is a schematic energy level diagram developed by Jablonski that shows the excitation of a molecule and all the possible unimolecular deactivation pathways.[2]

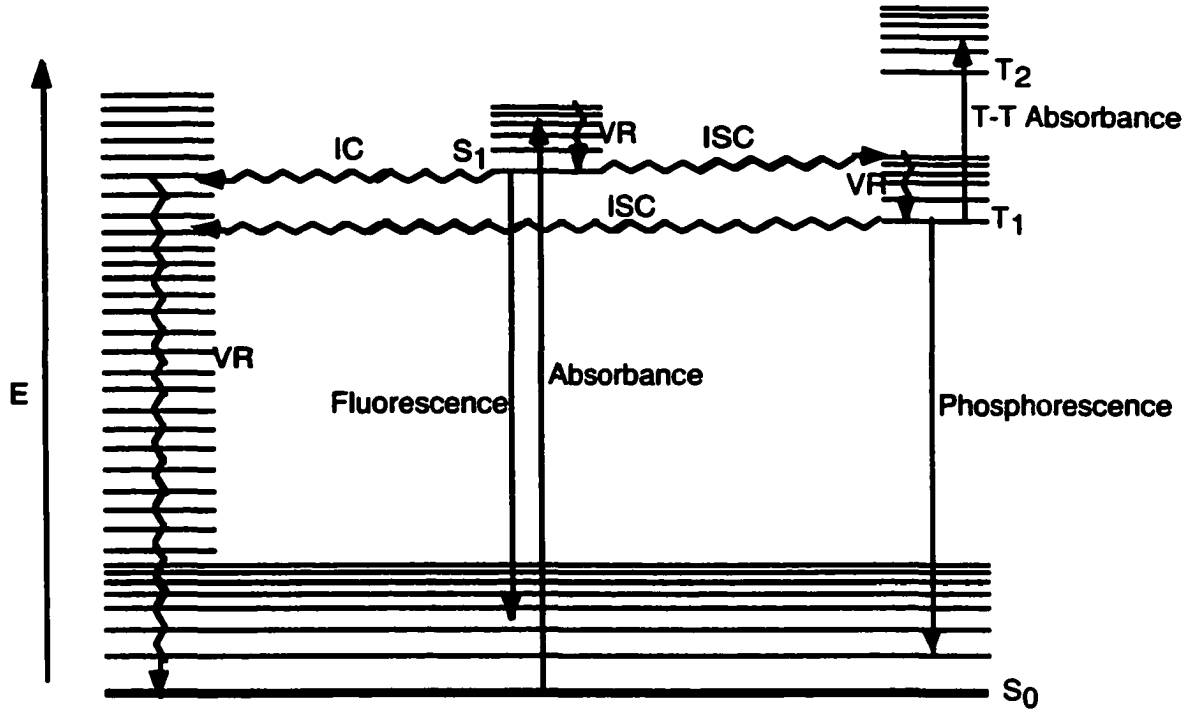

Figure 1.2 Jablonski energy level diagram: Solid arrows represent radiative processes (absorption (Abs), fluorescence (F), phosphorescence (P), and triplet-triplet absorption ($T\text{-}T_{Abs}$)), while zigzagged arrows represent non-radiative process (internal conversion (IC), intersystem crossing (ISC), and vibrational relaxation (VR)).

1.1.2.1 Non-radiative Processes

Closed-shell organic molecules usually exist in singlet ground states, where all electrons are paired. The multiplicity of a molecule is calculated by Equation 1.3, where S is the total electron spin. Thus, a singlet state multiplicity arises when all electrons are paired (total spin (S) = 0).

$$\text{Multiplicity} = 2S + 1$$

Equation 1.3

Vibrational relaxation occurs between vibrational levels of the same electronic state (e.g. between v = 3 and v = 0 of S_0). In solution, due to the interaction with solvent molecules, this process is known to occur very rapidly (10^{-11} s).[3] Internal conversion occurs for a transition between two electronic states that have the same spin multiplicity (e.g. S_1 to S_0). Intersystem crossing occurs for a transition between two electronic states that have different spin multiplicity (e.g. S_1 to T_1) and is known as a forbidden process. Any process involving a spin flip is a forbidden process. The term "forbidden" typically refers to transitions that are not probable but may still occur. Transitions are considered forbidden based upon the symmetry selection rules, which state that if the overlap integral of the wavefunctions is equal to one the transition is allowed; whereas if the integral is equal to zero the transition is forbidden. As singlet-singlet transitions have an overlap integral of one, while singlet-triplet transitions lead to an integral of zero, the former are spin-allowed transitions, while the latter are considered spin-forbidden. However, mixing between the zeroth-order molecular wavefunctions, due to coupling between electronic and nuclear motion, allows some symmetry-forbidden transitions to occur.

1.1.2.2 Radiative Processes

1.1.2.2.1 Absorption of light

Absorption involves the interaction of a photon of light that has the correct energy, with the chromophore (light absorbing portion) of a molecule. The absorbance of a solution is measured by comparing the intensity of the incident light (I_o) to the intensity of transmitted light (I). Alternatively, the absorbance of a sample can be determined if the

concentration of the sample (c), the pathlength the light must travel through the sample (l), and the molar absorptivity coefficient (ε) are known. This relationship is shown in Equation 1.4, and is known as the Beer-Lambert Law,

$$Abs = -\log (I/I_o) = \varepsilon cl$$

Equation 1.4

where Abs is the absorbance, I_o is the intensity of incident light, I is the intensity of transmitted light, c is the concentration of the absorbing species, ε is the molar absorptivity of the absorbing species, and l is the pathlength through which the light must travel.

The probability of light absorption occurring is affected by factors such as the energy of the light, and the likelihood of the transition, which is dependent upon the polarizability of the molecule. The probability of a transition occurring will be higher for an allowed process than for a forbidden one. The polarizability is important, because as light interacts with a molecule it will induce a dipole moment in the molecule's electron cloud, which in turn will allow the promotion of an electron from one type of orbital to another (vide infra). The probability of light absorption occurring is contained within the ε term of the Beer-Lambert law.

The structure of the absorption spectrum relies on the difference in the molecule's ground state and excited state structure, which depends upon the molecule's rigidity. Based on the Frank-Condon principle, the strongest electronic transition occurs between the lowest vibrational level (ν_0) of the electronic ground state (S_0) and the vibrational level (ν_n) of the excited state (S_1) of a molecule, where the largest overlap of vibrational wavefunctions occurs. If there is little change in the nuclear configuration of the two

states, the transition will occur at a lower overall energy. However, if there is a large change in the nuclear configuration the transition will occur at a higher energy. The rigidity of the molecule also helps in understanding the effects of the structure on the absoption spectra. In a rigid molecule, the vibrational levels are further apart, leading to a vibrationally structured absorption spectra; this is not the case for a flexible molecule, as the vibrational levels are closer together.

1.1.2.2.2 Fluorescence emission

Fluorescence is the emission of radiation that takes a molecule from an excited state to a lower energy state with retention of the spin multiplicity. The most common fluorescence emission involves transitions between the S_1 and S_0 electronic states of the molecule. Though this is the only fluorescence emission illustrated in the Jablonski diagram (Fig. 1.2), it should be noted that fluorescence may occur between any two different excited states with the same multiplicity.

1.1.2.2.3 Phosphorescence emission

Phosphorescence is similar to the radiative process of fluorescence, the major difference being that deactivation occurs with a change in the spin multiplicity. The most common phosphorescence emission occurs for molecules decaying from the excited T_1 state to the S_0 ground state. Phosphorescence does not occur readily for most organic molecules as ISC is a more predominant process.

1.1.2.3 Kinetic measurements of lifetimes

With modern day instrumentation it is possible to measure the lifetime for the deactivation process of excited molecules. The lifetime of an excited molecule is measured as the time it takes for the concentration of a species to fall to 1/e of the initial value. The deactivation kinetics for the excited states of most organic molecules occur in the microsecond to nanosecond time domain. The lifetime of the molecule gives important insight into the molecule's reactivity. Scheme 1.1 shows the deactivation of a molecule M* to a lower energy state.

$$M^* \longrightarrow M + h\nu + \Delta E$$

Scheme 1.1

As all radiative (r) and non-radiative (nr) processes occur simultaneously, experimentally it is impossible to measure the rate constant for a radiative process independently. This being the case, intrinsic rate constants are more commonly measured, and the intrinsic rate constant, k_0 (Equation 1.5), takes into account all deactivation pathways possible.

$$k_o = \Sigma k_r + \Sigma k_{nr}$$

Equation 1.5

The rate law for the deactivation of an excited state species is expressed as a sum of all the processes that lead to the deactivation. For example, the rate law for the

deactivation of the singlet excited state would take into account fluorescence, intersystem crossing, and internal conversion (Equation 1.6).

$$-\frac{d}{dt}[M^*] = (k_f + k_{ISC} + k_{IC})[M^*] = k_o[M^*]$$

Equation 1.6

Integrating Equation 1.6 leads to Equation 1.7, where $[M^*]_0$ is the initial concentration of the excited species M*.

$$[M^*] = [M^*]_o e^{-k_o t}$$

Equation 1.7

The lifetime (τ_o) related to the decay of M* in Equation 1.7 is the reciprocal of the sum of the rate constants for all the deactivation pathways possible (Equation 1.8).

$$\tau_o = \frac{1}{(\Sigma k_r + \Sigma k_{nr})} = \frac{1}{k_o}$$

Equation 1.8

1.1.2.4 Quantum yields

The quantum yield of a radiative process is given as the number of photons emitted by that process relative to the total number of photons absorbed. For example, the

fluorescence quantum yield, defined by the rate constants of the various deactivation processes, is given by Equation 1.9.

$$\Phi_f = \frac{k_f}{k_f + k_{ISC} + k_{IC}} = k_f \tau_o$$

Equation 1.9

1.1.3 Bimolecular photophysical processes

1.1.3.1 Excited state quenching

Quenching is a deactivation pathway for excited state molecules which differs from the processes described in Section 1.1.2 above. As quenching introduces a new deactivation pathway, it will affect the lifetime and/or concentration of excited state molecules. Quenching reactions can be studied, as long as a measurable quantity such as excited state lifetime, transient absorbance, or singlet excited state emission intensity is affected by the addition of the quencher. Scheme 1.2 shows the bimolecular reaction of an excited probe molecule (M^*) and a quencher (Q).

$$M^* + Q \longrightarrow M + Q^*$$

Scheme 1.2

The rate for the disappearance of the excited state probe (M^*) in the presence of a quencher is given by Equation 1.10.

$$-\frac{d}{dt}[M^*] = k_o[M^*] + k_q[M^*][Q]$$

Equation 1.10

Quenching studies are normally carried out under pseudo-first order conditions, where one of the reagents is present in excess over the other ([Q]>>[M*]). In the presence of a quencher, the observed rate constant is therefore related to k_o (the intrinsic rate constant or the inverse of the lifetime), k_q (the quenching rate constant), and the concentration of quencher as is shown in Equation 1.11.

$$k_{obs} = k_o + k_q[Q] \quad \text{or} \quad \frac{1}{\tau_{obs}} = \frac{1}{\tau_o} + k_q[Q]$$

Equation 1.11

Quenching reactions occur via numerous mechanisms, including energy transfer, electron transfer, or charge transfer. The nature of these interactions may also vary from collisional in nature (dynamic quenching), to occurring due to the complexation of a ground state molecule with a quencher molecule before excitation (static quenching). Figure 1.3 shows a combination of both the static and dynamic quenching mechanisms.

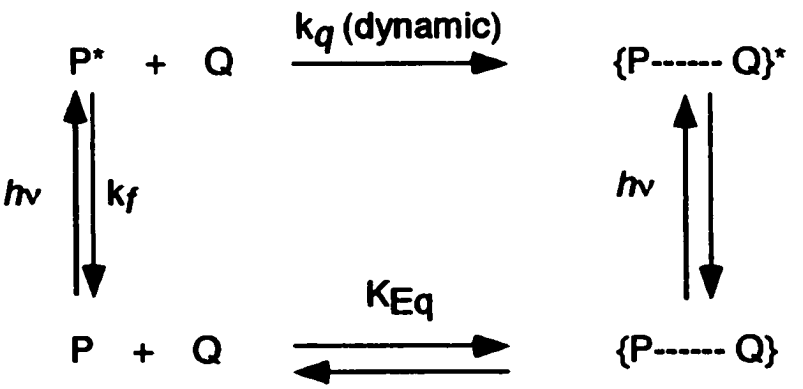

Figure 1.3 Mechanisms for dynamic and static quenching

Equation 1.11 gave the relationships used to determine the quenching rate constants. Multiplying the second of these equations by τ_o leads to Equation 1.12, which is used in time-resolved fluorescence studies. When studying the effect of quenching using lifetime measurements, only the dynamic quenching mechanism is investigated. Thus, Equation 1.12 gives rise to the dynamic quenching rate constant,

$$\frac{\tau_o}{\tau_{obs}} = 1 + \tau_o k_q [Q] = 1 + K_{SV}[Q]$$

Equation 1.12

where K_{sv} is the Stern-Volmer constant.

Steady-state fluorescence quenching gives information on both static and dynamic quenching. This is due to the fact that the area of the emission spectra, or the intensity of emission, is affected by a decrease in the excited state lifetime (dynamic quenching) as well a decrease in the number of fluorophores emitting (static quenching).

An equation (Equation 1.13) can be arrived at for steady-state fluorescence quenching, which is similar to the equation used for time-resolved quenching (Equation 1.12). In this case, both static and dynamic quenching would contribute to the overall value for the apparent Stern-Volmer constant (K_{sv}(app)).

$$\frac{A_o}{A} = \frac{I_o}{I} = 1 + (\tau_o k_q + K_{Eq})[Q] = 1 + K_{SV}(app)[Q]$$

Equation 1.13

where Ao/A and Io/I are the area of emission and intensity ratios, respectively.

The value for K_{SV} can be determined for time-resolved experiments, while the K_{SV}(app) is determined for steady-state experiments. It is of interest to note that in many cases the mechanisms of static and dynamic quenching may be in competition with one another. For static quenching, only the intensity of emission (or area of emission spectra) is affected as there are fewer fluorophores emitting, but the lifetime of the fluorophore would not be altered. By performing lifetime measurements, only the effect of dynamic quenching is measured. By comparing results of lifetime measurements to those done in the steady-state, conclusions can be drawn as to which quenching mechanism is occurring. If the Stern-Volmer constant agrees with the apparent Stern-Volmer constant, only dynamic quenching is occurring. If the two constants disagree then most likely both quenching mechanisms are occurring. If static quenching does compete with dynamic quenching, it would be expected that the plot of τ_o/τ versus quencher concentration would have a lower K_{SV} value than the K_{SV}(app) for a plot of A_o/A versus quencher concentration.

1.1.3.1.1 Quenching within supramolecular systems

Quenching is of special interest when studying the interaction of a probe molecule with a supramolecular system. The probe molecule may be located within various environments due to the presence of the supramolecular system, and quenching studies help identify the location in which the probe resides. In the simplest case, some excited probe molecules may be located within the aqueous phase of a system, while others are located within one supramolecular binding site. If the probe molecule is located within a protected environment (binding site), the access of aqueous quenchers to the probe will

be decreased. Thus, by following the quenching efficiency, the location of the probe can be hypothesized.

When performing time-resolved fluorescence measurements in the presence of a supramolecular system, more than one excited state species may be present. If the probe molecules are located within two separate environments (i.e.: aqueous phase and one binding site), the decay trace obtained will be the sum of the two decaying species. In this situation, it is still necessary to compare steady-state to time-resolved data in order to elucidate the mechanism of quenching for the system. In such situations, an average lifetime has to be established for all the species decaying (Equation 1. 14),[4]

$$<\tau>=\frac{\Sigma a_i \tau_i}{\Sigma a_i}$$

Equation 1.14

where $<\tau>$ is the average lifetime of the species decaying, a_i is the pre-exponential factor associated with the i^{th} term, and τ_i is the lifetime associated with the i^{th} term, Σa_i is equal to one, as the sum of all pre-exponential factors is normalized to one when fitting the lifetime data.

Equation 1.14 represents the methodology of "amplitude average lifetime", which is favored over "intensity average lifetime" (Equation 1.15). The latter of these methodologies is unreliable when there is a possibility of static quenching occurring, as it emphasizes the longer lived component(s).[4,5]

$$<\tau>=\frac{\Sigma a_i \tau_i^2}{\Sigma a_i \tau_i}$$

Equation 1.15

In time-resolved analysis, the static quenching component may be indicated by a fast decay, and not only by the non-radiative process outlined in Figure 1.2. By using Equation 1.15 as the basis for the analysis, the fast component would be underestimated, giving rise to inaccurate data. Whether a fast component is present or not, using the average lifetime equation (Equation 1.14) leads to a reliable comparison of the total integrated area under the decay trace and the area under the steady-state spectrum.[4-6]

Performing quenching studies on a laser flash photolysis system (see below) helps in the understanding of the dynamic interactions of a probe molecule with a supramolecular system. The assignment for the location of the probe molecule within the supramolecular system (arrived at in the fluorescence experiments) can be supported by quenching data for the triplet excited state or transient species. A new kinetic scheme (Scheme 1.3) for the quenching process is necessary in order to take into account all the processes occurring.

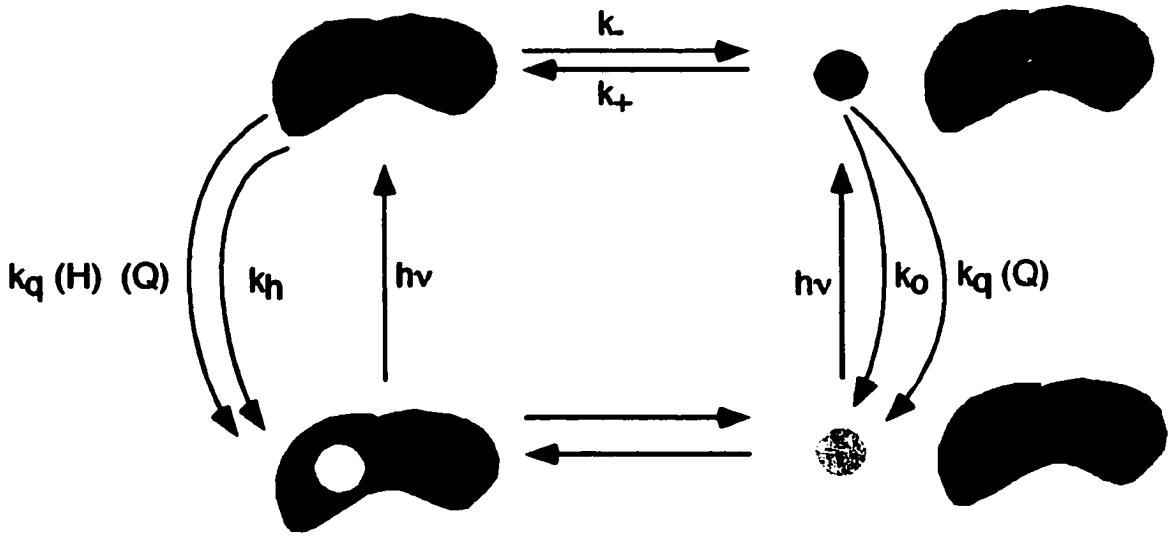

Scheme 1.3 Schematic representation of quenching within a supramolecular system, where circles and shaded areas represent probe molecules and supramolecular systems, respectively,

$$k_{obs} = k_h + k_- + k_q(H)[Q] - \frac{k_- k_+ [H]}{k_+ [H] + k_o + k_q\ [Q]}$$

Equation 1.16[7]

where k_{obs} is the observed first order rate constant, k_h is the decay of the species within the host system, k_- is the dissociation rate constant, $k_q(H)$ is the quenching rate constant of the probe within the host system, [Q] is the concentration of quencher, k_+ is the association rate constant, [H] is the concentration of host, k_o is the intrinsic decay rate constant in water, and k_q is the quenching rate constant in water.

At low quencher concentrations, a quencher that resides mainly in the aqueous phase will interact with the most accessible excited probe molecules, usually those

located within the aqueous phase. At high quencher concentrations, the decay of the probe in aqueous systems becomes very fast and the exit of the probe from the supramolecular system becomes the rate-determining step.[8] Mathematically, it can be seen that at high quencher concentrations, the last term in Equation 1.16 becomes negligible and the function defined by the equation becomes linear.

The methodology for quenching of probes within a supramolecular system (Scheme 1.3 and Equation 1.16) was originally developed for the study of mobility of arenes in micelles.[7] The kinetic treatment takes into account different quenching efficiencies for probes in the homogeneous phase, as opposed to those included within the supramolecular system. The key assumption of this model is that the concentration of free probe (in the homogeneous phase) is small in comparison to the amount of probe complexed.[7-9] If this assumption is valid, and the kinetics of the probe molecule follows a first-order decay, Equation 1.16 may be used.

1.2 Fast kinetic techniques

1.2.1 Laser flash photolysis

The triplet excited state data collected in this study used the technique of laser flash photolysis (LFP). This technique is an expansion of the conventional flash photolysis technique,[10] which won Porter and Norrish the Nobel prize in 1967. The LFP technique makes use of modern day inventions such as gated photomultipliers, multichannel analyzers, and computers. The details of the particular experimental setup used in this study have been described previously,[11] and are highlighted as they apply to this work in chapter two. Lasers are considered a major breakthrough for photochemistry

because they allow processes that take place on extremely fast time scales (ns and ps) to be measured.

LASER stands for light amplification by the stimulated emission of radiation. One requirement for laser action is the existence of a metastable excited state, with a lifetime long enough to participate in stimulated emission.[12] A second critical characteristic for lasers is the existence of a greater population in the metastable state than in the ground state.[12] This population inversion is achieved by different methods, depending upon the type of laser used.

Two different types of lasers were used in this work. The first was an Nd:YAG laser. The active medium for this instrument is neodymium incorporated into an yttrium aluminum garnet (YAG) crystal. The Nd:YAG laser is a four level laser with the main absorptions occurring at 730 and 800 nm. The laser transition is at 1064 nm and for electronic excitations of molecules this frequency is doubled, tripled or quadrupled to give light at wavelengths of 532 nm, 355 nm, or 266 nm, respectively.

The second of the two lasers used was an Excimer laser. This name is actually a misnomer, as the active medium within an excimer laser depends upon the formation of exciplexes and not excimers. This laser is a gas state laser with a gas mixture comprised of Xe, HCl and He (buffer). An electric discharge through the gas mixture produces excited Cl atoms, which then attach to the ground state Xe atoms to form the exciplex XeCl*. This exciplex survives for ca. 10 ns, which is the time needed for a laser action at 308 nm to occur. As soon as the photon is released, the atoms separate.

The importance of the LFP technique is its ability to provide critical spectral and kinetic information on (excited state) transients of all sorts, from excited triplet states to

radical species. This method allows the absorption and kinetics of an excited state and subsequent intermediates to be monitored directly. The basic principle behind the LFP system is the following: the molecular excited states are generated by a short laser pulse (ca. 5 to 10 ns). A monitoring beam of light is passed through the sample before and after excitation and the change in light intensity is related to the change in the absorbance of the excited-state probe molecule. The concentration of the excited species is proportional to the absorption, and as such, the excited species can be followed by kinetic treatments. The LFP technique allows the determination of lifetimes for processes occurring in the time scale range of tens of nanoseconds to hundreds of microseconds. It is important to understand that the absorbances measured using LFP are ΔA values (the change in absorbance) because the absorbance of the transient is measured relative to the absorbance of the chromophore before excitation occurs. A transient spectrum can be obtained by plotting the ΔA values, obtained on the same time scale in the kinetic traces, for various monitoring wavelengths.

1.2.2 Fluorescence spectroscopy

A fluorescence emission spectrum is measured by keeping the wavelength of excitation constant, while varying the monitoring wavelength. As was previously mentioned, the fluorescence emission usually occurs from the first excited singlet state (S_1). Since fluorescence occurs from the lowest possible vibrational level within the S_1 state (VR is fast to arrive at this state), fluorescence emission is a lower energy process than the corresponding absorption. This leads to an emission spectrum at longer wavelengths than is observed for the ground state absorption of the same molecule. As

the radiative decay may occur to various vibrational levels within the S_0 ground state of the molecule, vibrational fine structure in the fluorescence emission spectra is possible.

Fluorescence spectra are measured on a fluorescence spectrophotometer (fluorimeter). The essential components of the system are shown in Figure 1.4. The typical excitation source for the fluorimeter is a Xenon-arc lamp, which provides a continuous source of light at a constant intensity during measurements. In order to minimize the interference from scattered light, the emission is detected at right angles to the incident excitation light within the sample chamber.

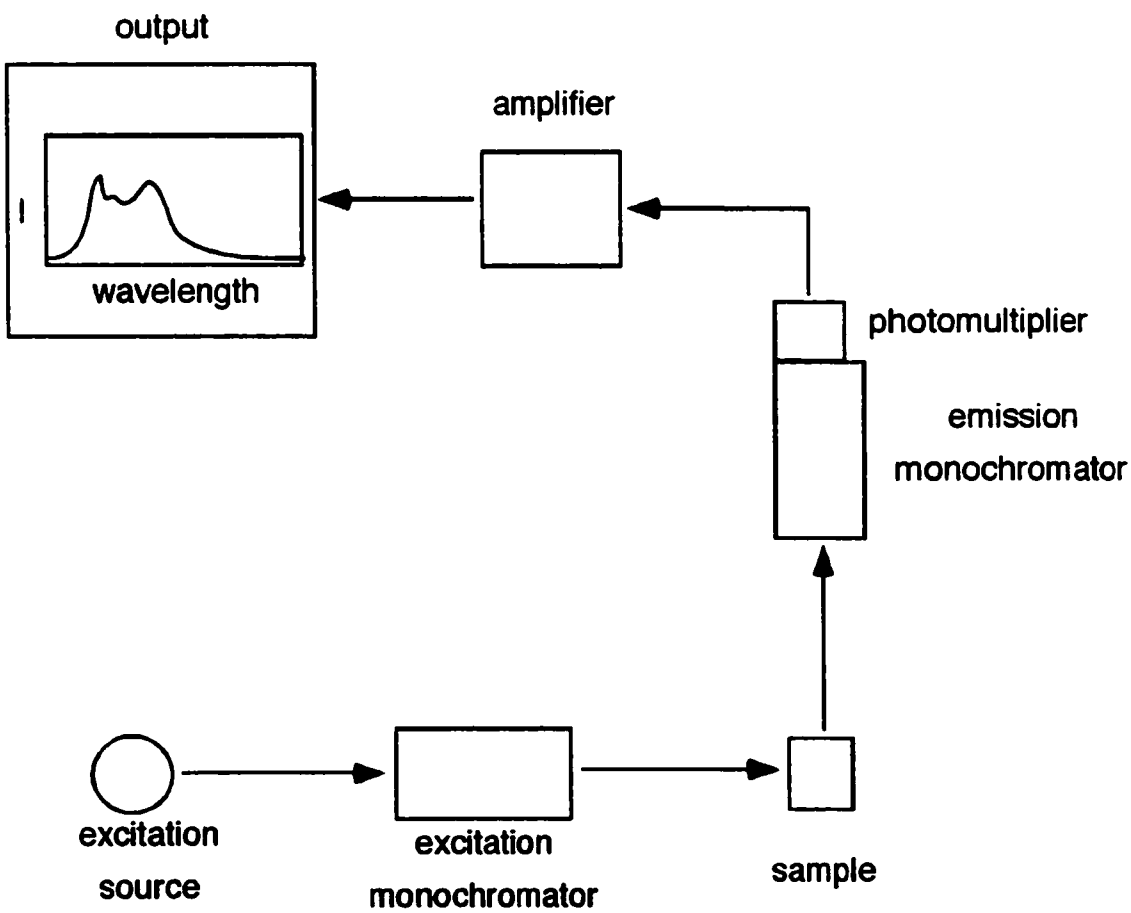

Figure 1.4 Simplified diagram of a fluorescence spectrometer

1.2.3 Time-resolved fluorescence emission measurements: single photon counting

Single photon counting (SPC) is a technique in which fluorescence measurements are made as a function of time, as opposed to energy, as is the case in steady-state fluorimetery. This technique is extremely important as it allows the differentiation between species with different lifetimes. The key components of the SPC system are shown schematically in Figure 1.5.

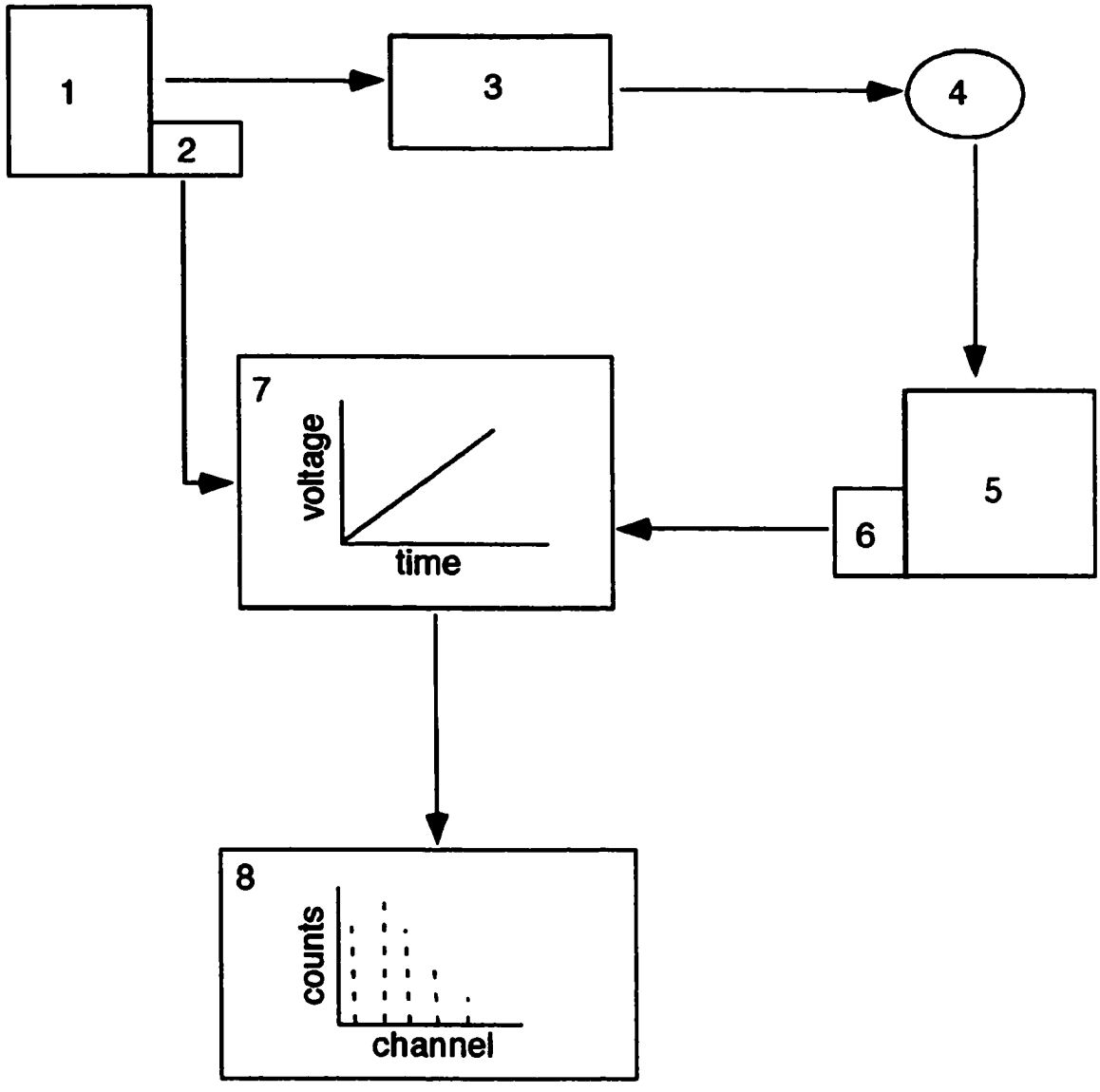

Figure 1.5 A schematic representation of a single photon counter. Light source (1), "start" photomultiplier detector (2), excitation monochromator (3), sample (4), detection monochromator (5), "stop" photomultiplier detector (6), time-amplitude converter (7) and multichannel analyzer (8).[13]

The light source (1) is a hydrogen flash lamp, which has a pulse duration of approximately 2 ns. The duration of the pulse limits the capability of this technique to

measure only lifetimes of excited singlet states that are greater than 2 ns. The light passes through an excitation monochromator (3) that selects the wavelength at which to excite the sample. A second monochromator located by the sample chamber selects the emission wavelength of interest for both the sample and the scatterer (5). Upon excitation of the sample, the photomultiplier detector attached to the excitation source is triggered, which results in an electronic signal (the "start" pulse) (2). This signal is sent to the time-to-amplitude converter (TAC) (7). Once the "start" pulse has been detected at the TAC, a voltage ramp that is linear with time is initiated. When the first photon reaches the photomultiplier detector (6) attached to the detection monochromator, a "stop" pulse is recorded and the voltage ramp at the TAC is stopped. The difference in voltage between the start and the stop trigger is related to a time delay for the emitting species. The multichannel analyzer (MCA) (8) is pre-calibrated before each experiment, and is capable of sorting data in 512 separate channels. The channels represent the various time delays, between the start and the stop pulse, recorded for the photons. Each start/stop event leads to a count that is then stored in the appropriate channel on the MCA. The time dependence of the fluorescence emission is obtained by retrieving the data for all the channels in the MCA; this gives rise to the decay for the species being detected. This process relies on the fact that the experiment follows a statistical Poisson distribution. As such, it is critical that for each run of an experiment only a single photon is being detected. This is achieved by assuring that the rate at which photons are counted is kept below 2 % of the rate at which the excitation pulse of the system is generated.[13] To achieve the best results, 10 000 counts are collected for the channel of maximum intensity.

When fitting the exponential decay, the shape of the lamp pulse must be taken into account as it is not finite. While some molecules have already decayed, the end of the excitation pulse will still excite other ground state molecules. Thus, to measure the effect of the lamp pulse, the instrument response function (IRF) of the SPC is collected using a scattering sample at the same excitation wavelength as the sample being monitored. The lamp profile is then convoluted with simulated data based on the model expected for the data obtained. This convoluted profile is compared to the experimental profile and if the two match, the model is considered acceptable. The statistical conditions under which the fits were considered acceptable are outlined in chapter two.

1.3 Bile salts

Bile salts are considered by many to be the most important biological detergent-like molecules discovered to date.[14-17] Bile salts (or bile acids) play a role in the physiology of humans as well as many other living creatures.[15,18] Chemists' interest in these structures arose in the middle of last century.[19] The following sections give the background necessary in order to understand bile salt aggregates as they were employed in this study.

1.3.1 Biological significance of bile acids

The main biological function of bile salt aggregates within the human organism is to solubilize dietary lipids and aid in accelerating their absorption.[15] In order to perform this function efficiently, there are many organs involved within the human body.[15] The primary bile acids (such as sodium cholate (NaCh)) are synthesized from cholesterol in

the liver, and are then secreted. The bile acids are concentrated in the gallbladder.[15] The gallbladder is also responsible for the storage of excess bile acids. In the small intestine, bile salts form mixed aggregates with lecithin and cholesterol and these mixed aggregates are capable of solubilizing fatty acids and monoglycerides.[14] The mixed aggregates also solubilize dietary lipids within the small intestine and aid with phospholipid transformations.[15]

After ingestion of a meal, the bile acids stored in the gallbladder are expelled to facilitate absorption of dietary lipids. The bile acids are subsequently resorbed and returned to the liver. The bile (in form of mixed aggregates) within our bodies circulates between six and ten times a day, and contains 3 to 5 g of bile and 0.25 g of cholesterol.[15] Maintaining a healthy bile system is critical to survival, since an elevated concentration of total cholesterol is a major risk factor in coronary heart disease.[15]

1.3.2 Structure of bile salts

The structure of mixed aggregates of bile salts is not yet understood.[20-25] In fact, despite many efforts to elucidate the structure of simple bile salt aggregates in aqueous solutions, a debate continues to grow in the literature (see below).[19,26-60] The focus of this study was the interaction of probe molecules with simple NaCh aggregates, and as such information is only presented on simple bile salt aggregates (in the absence of lipids, cholesterol, etc.) in aqueous solutions.

Bile salts are bi-polar molecules, due to the fact that all the hydrophilic groups are found on one side of the molecule, leaving a hydrophobic backbone on the opposite side. Figure 1.6 shows a monomer of sodium cholate (NaCh) the bile salt of interest for this

study, while Figure 1.7 shows some of the other bile salts commonly studied in the works that debate the structure of bile salts cited above. The major changes from the cholesterol parent molecule are: saturation of the double bond, epimerization of the hydroxyl group at the C_3 carbon, addition of the hydroxy groups at the C_7 and C_{12} carbons, and oxidative cleavage at C_{24} to form the carboxylic acid group.[14] The NaCh molecule is about 20 Å long and the cross section of the molecule is not flat, and has been shown to be nearly circular with a diameter of ca. 7 Å.[14]

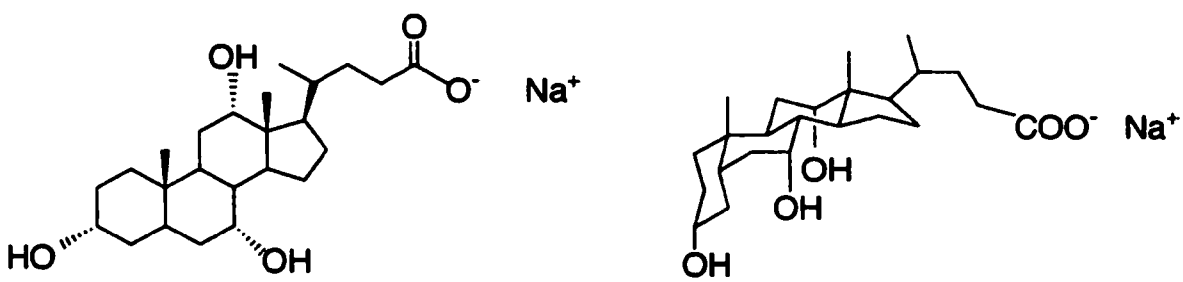

Figure 1.6 Structure of the most common bile salt monomer: NaCh. The structure on the right emphasizes the planar polarity of the NaCh molecule.

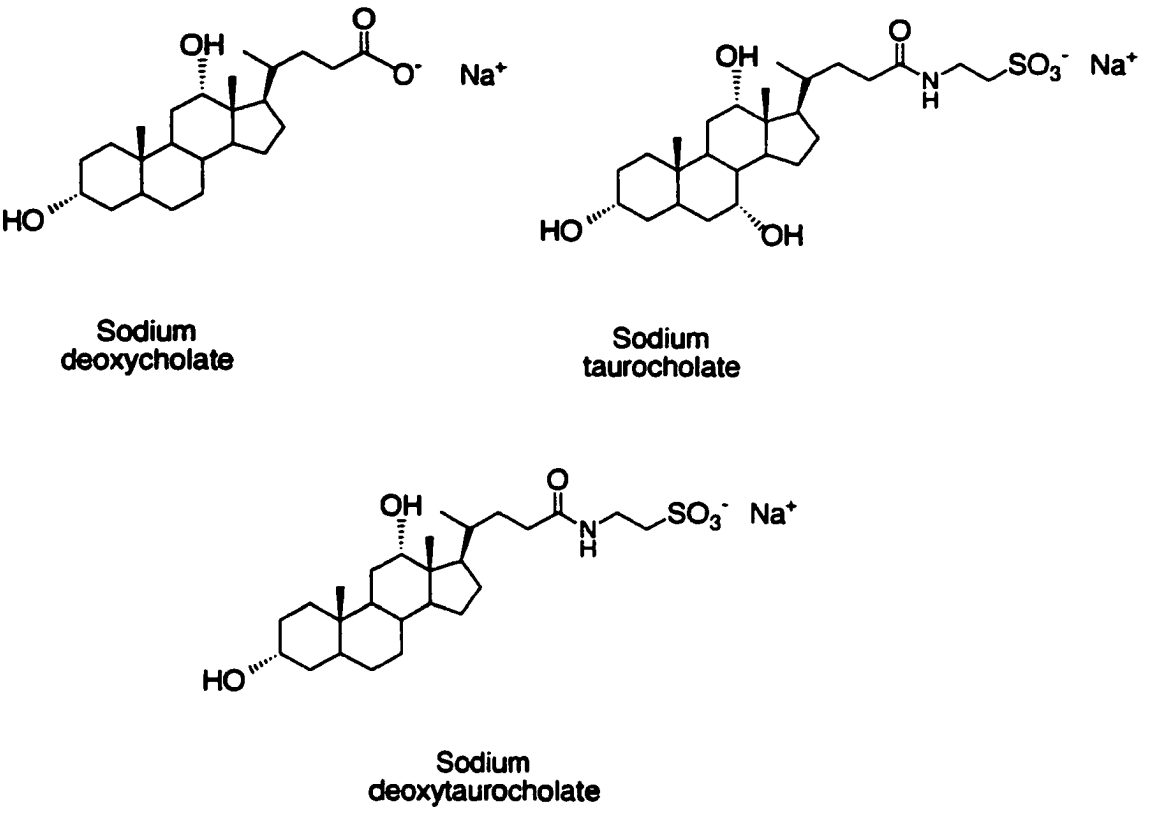

Figure 1.7 Structures of other commonly studied bile salts.

The first model for the aggregation of bile salts in aqueous medium compared the aggregation of bile salts to the aggregation of micelles.[19] Micelles are self-assemblies formed from surfactants that contain an alkyl chain and a hydrophilic head group. In solution, these structures have been classified as forming pseudo-phases from the bulk solvent. The dynamics of micelles are such that the monomers exchange on a microsecond time scale.[61] It is believed that bile salt aggregates are not pseudo phases and that, in fact, the binding sites in bile salts can be more restrictive than those found within the aggregates of micelles.

1.3.2.1 Primary/secondary aggregate model for bile salts in solutions

There are two competing models for the aggregation of bile salts in the literature; the first model is one of primary and secondary aggregation,[19,28,29,31-54,62-64] while the second is best described as a helical model.[55-59,65] The primary and secondary aggregation model suggests that aggregation is a balance between hydrophobic interactions or hydrogen bonds, which are attractive in nature, and electrostatic repulsion of the negative head groups. In this model, the planar polarity of the bile salt monomers aids in aggregation of the NaCh monomers at low concentration. At low NaCh concentrations, ca. 10 mM, the clustering of the hydrophobic backbones of the monomers to form primary aggregates introduces a very well protected hydrophobic binding site. Though an aggregation number is not known for bile salts, as it is for micelles, estimates on the number of monomers within a primary site range from four to ten in the case of sodium cholate.[28,48,66,67] The onset of secondary aggregation begins at higher NaCh concentrations (around 15 mM to 25 mM), at room temperature in the presence of counterions.[19,33,34,38,39] Our research group uses 20 mM of NaCh as the concentration at which secondary aggregates are formed, in the presence of 0.2 M NaCl at 20 °C.[52] The formation of secondary aggregates is hypothesized to occur based on the balance of attractive hydrogen bonding and repulsive electrostatic interactions of the primary aggregates (Fig. 1.8).

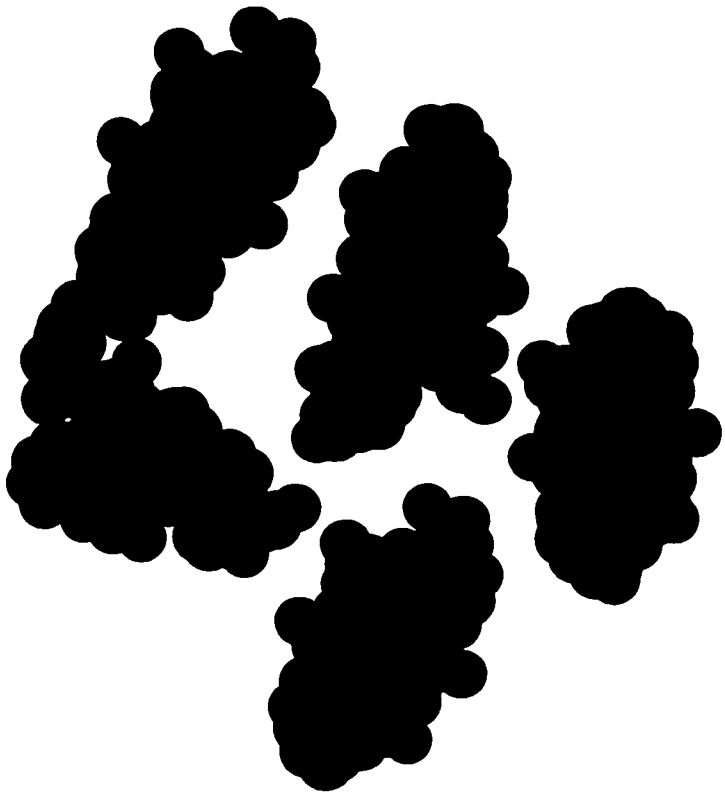

Figure 1.8 Primary and secondary aggregate interactions of NaCh. Each cluster represents a primary aggregate, while the grouping of two or more of the primary aggregates forms a secondary aggregate. The black portion of the aggregates are the hydrocarbons within the NaCh, while the gray circles represent the position of the hydrophilic alcohol and carboxy groups.

The evidence for this first model of aggregation spans research in numerous fields including surface tension,[39] light scattering,[36,41,48] fluorescence,[32,33,38,40,42,44,46,47,52] laser flash photolysis studies,[40,51,54] ESR,[50] pulse radiolysis,[54] and NMR.[19] The majority of the work was carried out in the solution phase, which is of greatest interest to the work described in this thesis. The earliest proposal of this model comes from Small et al., who proposed the model mainly based on NMR results.[19] These researchers studied proton shifts in

NMR spectra as a function of bile salt concentration. Their results showed that at concentrations at which primary aggregates are believed to exist, protons contained along the hydrophobic side of the bile salt molecules gave rise to signal changes in the NMR spectra while protons located on the hydrophilic side of the molecule did not. By observing the line broadening of the NMR spectra with increasing bile salt concentration, the researchers concluded that the hydrophobic sides of the molecules must have been clustering together from the onset of aggregation, thus forming the primary aggregates.

In one study, Kratohvil and co-workers carried out spin-labeling work in hopes of supporting the model proposed by Small.[50] In these experiments, ESR (electron spin resonance) rotational correlation times at different bile salt concentrations were compared. The value for the correlation time is considered to be a measure of the immobilization degree of a probe, and thus offers information on the restraint of the probe in its environment. The findings in this study were consistent with the probe being surrounded by the hydrophobic sides of the bile salt monomers, but the researchers proposed a slight variation to the model. In this case, the researchers propose that the structure of the primary aggregate is really a "disk-like" aggregate in which the probe can slip in and out through an opening near the top or bottom of the aggregate (Fig. 1.9).[50] According to the researchers, an aggregate with the hydrophilic groups oriented toward the interior would not explain the immobilization observed in the study.[50]

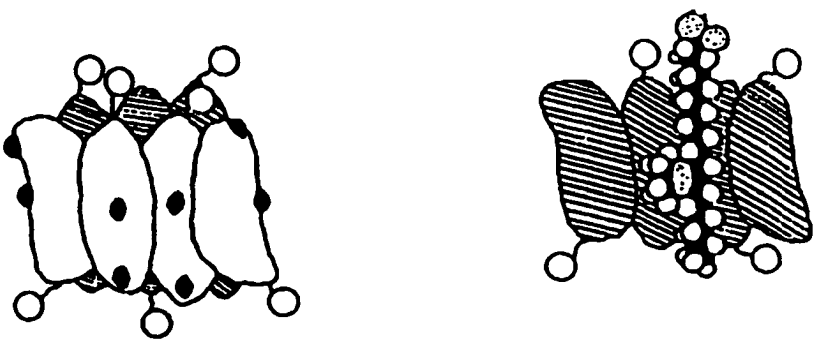

Figure 1.9 Disk-like model of primary aggregation (left). Incorporation of a spin probe (right) into a primary "disk-like" aggregate.[50] (Kawamura et al., Spin-Label Studies of Bile Salt Micelles, © ACS 1989/ CANCOPY.)

In work done by O'Connor and co-workers, the critical concentrations at which a change in the aggregation pattern of the bile salts occurs was investigated.[39] These researchers found that the aggregation pattern of many of the commonly studied bile salts changed as the concentration of bile salt was increased. This study used surface tension measurements to interpret the concentrations at which the aggregation pattern for the bile salts changed drastically, suggesting that at these concentrations the formation of secondary aggregates occurred. Most of the bile salts studied showed changes in the surface tension measurements at bile salt concentrations between 15 mM and 50 mM. For NaCh, the researchers found that secondary aggregates formed at a NaCh concentration between 13 mM and 18 mM.

Light scattering data were key in the initial estimates of the size of primary aggregates. Using the technique of light scattering, Mazer and co-workers[48] also found that the aggregation of bile salts is a step-wise process (primary aggregates form initially, followed by secondary aggregates). Further, calculating the mean radii from the scattered light, the researchers found that at low bile salt concentrations, the aggregation number

for primary aggregates lies between four and ten. These findings were supported by the researchers' theoretical calculations,[48] as well as by their dynamic light scattering results.[41]

Thomas and co-workers were among the first researchers to study the interactions of probe molecules with bile salt aggregates, using the techniques of fluorescence, pulse radiolysis and laser flash photolysis.[54] These researchers found that pyrene (a common photophysical probe, see below) was located in a very protected environment (Fig. 1.10), surrounded by the hydrophobic sides of the bile salt monomers. The result was obtained by using pulse radiolysis of pyrene in the presence of less than 20 mM of sodium taurocholate (NaTC). This finding is consistent with a hydrophobic binding site being present at low bile salt concentrations.

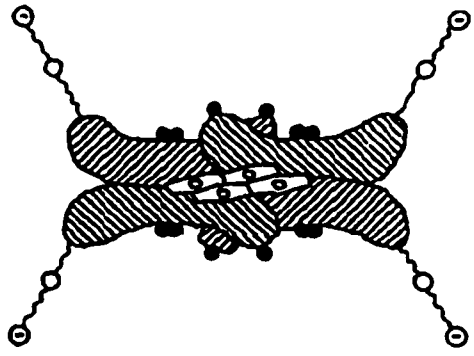

Figure 1.10 Early schematic representation of pyrene incorporated within a NaTC primary aggregate.[54] (Thomas et al., Kinetic Studies in Bile Acid Micelles, ©ACS 1975/ CANCOPY.)

Work done by McGown and co-workers provided further evidence for the primary and secondary aggregation model from fluorescence studies.[42,44,46,47] These

researchers studied the interaction of pyrene with NaTC. Pyrene is a well studied photophysical probe because it is well documented that the fluorescence emission spectra is sensitive to changes in the environmental polarity.[68] The pyrene emission spectrum has five characteristic vibrational peaks. A comparison of the I/III vibrational peak ratio for the probe gives information on the surrounding polarity because the first band is sensitive to the polarity of its environment while the third band is unaffected by changes in polarity.[68] McGown's studies showed that NaTC had a unique binding site for the hydrophobic pyrene that other organized systems, such as sodium dodecyl sulfate (SDS) micelles, did not posses. Using anisotropy, the researchers were able to establish that the mobility of the probe in the presence of NaTC was restricted, compared to the same probe in the presence of SDS micelles. In a second study by the same researchers,[42] the critical concentrations at which the aggregation pattern of bile salts was altered in solution was studied. Using many fluorescent based techniques (spectral intensity, lifetimes and anisotropy), the researchers found that a definite change in protection of fluorescent probes was observed in the presence of 8 mM to 12 mM of NaTC. At this concentration, which falls within the range for primary aggregates, a higher degree of protection was observed for larger hydrophobic probe molecules.

Preliminary research done in our research group provided convincing support for the primary/secondary aggregation model by studying the interaction of probe molecules with bile salt aggregates in solution.[51,52] The first study[52] used the fluorescence quenching methodology and the probes studied were anthracene, pyrene, and naphthalene (Np) (Fig 1.11). This study allowed for a hypothesis of the location of these probe molecules within

the aggregates to be made by studying the accessibility of an aqueous quencher to the probes within the supramolecular framework.[52]

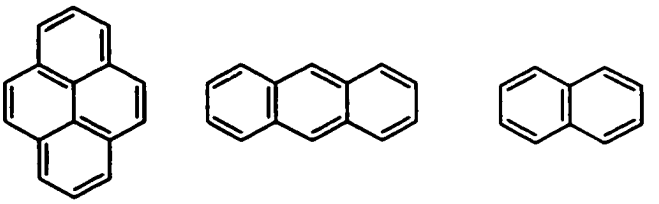

Figure 1.11 Probe molecules: Pyrene (left), anthracene (center) and naphthalene (Np) (right).

The goal for studying this series of probe molecules was to investigate the effect of the shape of the probe on its location within the various binding sites of bile salt aggregates. It was found that all three probes were incorporated within the primary aggregate. Within the study the ratio of quenching rate constants of the probes (by NaI) in the absence and presence of bile salt ($k_q/k_q(H)$) was calculated. The lower the value for k_q, the higher the level of protection for the excited probe molecule in the bile salt aggregates from reaction with the aqueous quencher. Thus, the higher the ratio of k_q^0/k_q the higher the level of protection for the probe in the aggregates. The ratio for Np in the presence of 20 mM of NaCh was 51 ± 1, while the ratio for pyrene was 36 ± 1, at the same NaCh concentration. These initial findings suggest that the size of the probe is a factor in the extent of incorporation within the primary aggregates.

A second preliminary study[51] looked at the effect of the polarity of probe molecules on the complexation dynamics with bile salts by comparing naphthalene to

xanthone (Xan) (Fig. 1.12) as probes bound to bile salt aggregates. In this case, both fluorescence and laser flash photolysis experiments were carried out.

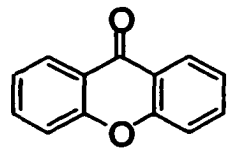

Figure 1.12 Probe molecule: xanthone.

Naphthalene is a small, hydrophobic probe and it was located within the primary aggregate; it was concluded that xanthone, a larger and more hydrophilic molecule, resided in the secondary aggregate.[51] The dynamic data from laser flash photolysis experiments supported this finding. The dissociation rate constant for Np in the presence of 40 mM of NaCh was found to be (1.0 ± 0.4) x 10^6 s^{-1}, while the dissociation rate constant for Xan under the same conditions was found to be (5 ± 4) x 10^6 s^{-1}. This suggested that, within experimental error, no difference was observed for the dissociation rate constants in the presence of NaCh for Np and Xan. A difference in dissociation rate constants was observed when Np and Xan were studied in the presence of 40 mM of NaTC. The dissociation rates for Np and Xan respectively were (2.2 ± 0.5) x 10^6 s^{-1} and (25 ± 8) x 10^6 s^{-1}. These results support the presence of two distinct binding sites, and further suggest that the polarities of the two sites are different.

1.3.2.2 Helical model

This model is in sharp contrast to the primary/secondary aggregation model as it suggests that the primary interaction occurring is the interaction of the monomers to form a very solvated aqueous cavity, as opposed to a hydrophobic binding site. In this model, the interactions, which are critical for the formation of the helical structure are dependant upon intermolecular forces involving the cation from the bile salt. It is proposed that ion-ion and ion-dipole interactions (involving the cation) as well as hydrogen bonding, cause the primary helix to form; the non-polar face of the bile salts are oriented toward the aqueous medium.[59] There is no binding site in the helical model that would account for a greater level of protection from the aqueous bulk for hydrophobic probes than for hydrophilic probes. Researchers proposing the helical model consider it astonishing that the hydrophobic backbones of the molecules are oriented towards the aqueous bulk solvent;[59] however, their crystal structures support these findings (Fig. 1.13). In the case of the helix, the growth of the supramolecular system is postulated to take place either by a stepwise addition of bile salt monomers or by joining numerous smaller helices together to form a larger supramolecular system.

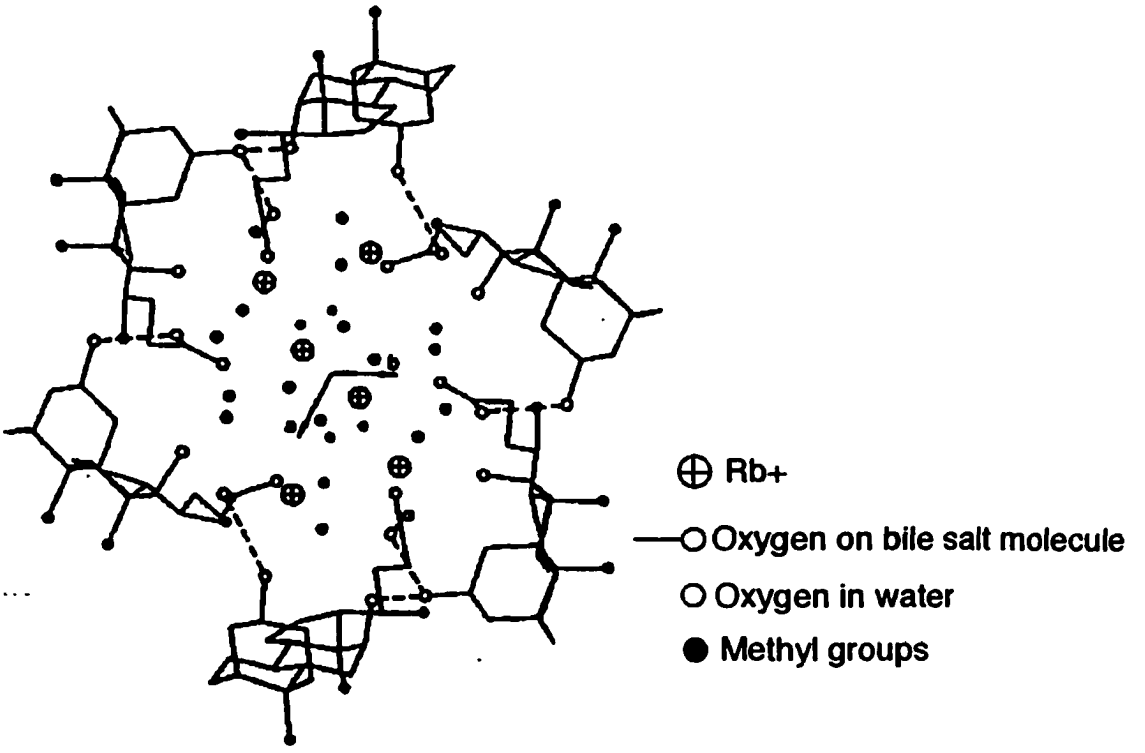

Figure 1.13 Crystal structure of RbTC which supports the helical model for bile salt aggregation.[58] (Conte et al., Nuclear Magnetic Resonance and X-ray studies on Micellar Aggregates of Sodium Deoxycholate, © ACS 1984/ CANCOPY.)

The evidence for the helical model comes from experiments done using circular dichroism (CD),[55-57] nuclear magnetic resonance (NMR),[55,56,58] electron spin resonance (ESR),[60] X-ray light scattering,[57,58,60] and crystallographic studies.[57,58,60] The crystallographic work lends the strongest support to this model; however, it must be pointed out that the data are collected in the solid state.

Giglio and co-workers[58] are the leading group publishing crystal structures in support of the helical model. In one study, to support the crystal structures recovered, these researchers performed NMR measurements, and X-ray diffraction on gel fibers

extracted from the bile salt solutions.[58] In order to obtain the gel fibers from the solutions used for NMR studies, the researchers had to perform the following alterations: the pH and the temperature of the solution were lowered and the ionic strength and pressure on the solution were increased. After making these alterations to the solution, the gel-like fibers were studied. The X-ray diffraction data for the gel phase suggested a helical structure, although "the helix of the crystal is not equal to that of the fiber".[58] Since the transformation of the solution used in NMR to the gel-like state used to isolate fibers, "seems to be continuous",[58] the researchers conclude that the structure isolated by X-ray diffraction and crystallography is the same as the structure present in solution.

The researchers presented NMR data in the solution phase to support their crystal structures. It is important to point out that the researchers work "well above the cmc for NaTC",[58] which leads to NMR solutions in which the concentration of NaTC is greater than 100 mM. Using mainly large aromatic probe molecules, the researchers observed proton shifts in the NMR spectra of certain hydrogens located on the bile salt structure. The structure for the aggregates was proposed based on which protons exhibited changes upon complexation with probe molecules. The researchers also published counter explanations for some of the early work done in solution by Small et al. in support of the primary and secondary aggregation model.[19,58] In reality, the NMR data alone cannot give conclusive evidence for either model because explanations for the shifts of various protons can be made to support either of the two models.

In another major contribution in support of the helical model from the same research group, circular dichroism (CD) measurements were performed.[55] In this study CD experiments on the optical probe (+)-*trans*-2-chloro-5-methylcyclohexanone, in the

presence of sodium deoxycholate were performed. Supported by NMR measurements, the researchers found that the probe was incorporated within a hydrophilic binding site consistent with the proposed helix; however, based on the CD signal alone, the optical probe was also interacting with the hydrophobic side of the bile salt monomer. Thus, NMR and CD gave rise to signals which were interpreted as the interaction of the probe with a polar environment, while CD also gave signals indicative of an interaction with a non-polar environment.

The statement in this article[55] (as well as in an earlier review of the helical model[59]) that, "one aggregation model may not suffice to explain the structure of bile salts," is probably at the heart of the debate that continues in the literature. In the solid state, the crystal structure gives a clear picture of the aggregate structure, although the researchers only present the unit cell with the solvated cavity in the middle. Showing the interactions occurring with the hydrophobic backbones of the bile salts may shed more light on the true structure of the aggregates.

1.3.2.3 Effect of ionic strength on the aggregation pattern of bile salts

Kratohvil and co-workers do not discuss an aggregation model within their study; however, they do present interesting observations for the effect of changing the ionic strength on the aggregation of bile salts.[28] This group's research used light scattering to show that below certain bile salt concentrations, depending on the NaCl concentration (or ionic strength), there was an absence of bile salt aggregation. The research was conducted on sodium taurodeoxycholate, and compared the light scattering of solutions containing different concentrations of bile salt. As the intensity of scattered light is increased, so is

the size of the aggregates being studied. On changing from solutions in the absence of NaCl to solutions containing 0.6 M of NaCl, the required concentration of bile salt in order to detect aggregate formation decreased from 4.0 mM to 0.96 mM.[28]

In light scattering work carried out by Mazer and co-workers, a different dependence on the ionic strength was studied.[48] The researchers found that the aggregates were unaffected at low ionic strengths (0.16 M of NaCl) with an increase in the concentration of bile salt, whereas in the presence of 0.6 M of NaCl, the aggregation changed dramatically with increasing bile salt concentration.[48] This means that at low concentrations of NaCl, the aggregation pattern for the bile salts was the same at all bile salt concentrations studied. In the presence of an ionic strength of 0.6 M, the size of aggregates was observed to increase as the bile salt concentration was increased. This study was conducted on bile salt solutions with the concentration ranging from 0 mM to 11 mM of taurodeoxycholate (primary aggregates only). Work done by McGown and co-workers agrees with the findings that at a high ionic strength (3.0 M NaCl) the size of NaTC aggregates increases with increasing bile salt concentration.[49]

In a different study to the one discussed above by McGown and co-workers, the effect of ionic strength was investigated by using Na^+, Mg^{2+}, Al^{3+}, and Tb^{3+}, with NaTC aggregates.[43] The effect of the size of the metal ion on the aggregation of NaTC was being investigated; however, the data obtained helps understand the effect of ionic strength on bile salt aggregation. The researchers investigated the effect of ionic strength up to a NaTC concentration of 45 mM. For all of the metal cations, a large increase in light scattering, indicating a change in aggregation, was observed when the NaTC concentration was increased from 1 mM to 5 mM. A drop in the scattering intensity was

noted when the concentration was increased to 10 mM of NaTC. As the concentration of bile salt was increased above 10 mM, the results varied drastically for the various counter-ions. Sodium and magnesium had very little effect on the aggregation above 10 mM, while aluminum and terbium showed a large increase of the aggregate size in the presence of 20 mM to 40 mM of NaTC.[43] These data suggest that primary aggregation is effected by counter-ions of all sizes and valencies, while secondary aggregation is only effected by large, multi-valent metal counter-ions.

1.4 Probe molecules for the studies within NaCh aggregates

Probe molecules are used to report on the properties of their surroundings when placed within a supramolecular system. The lifetime of the excited state of the molecule is key in determining what information may be gained by the use of the probe. As information is only recovered during the excited state lifetime of the probe, it is only possible to explore the system until the excited state decays back to the ground state. As such, if the probe has a shorter lifetime than the dynamic processes under investigation, the probe will only report on the local environment. In order to extract dynamic data on the system, the lifetime of the probe must be of the same order of magnitude as the rates of the processes being investigated.[8] There are many different types of molecules that may be used as probes: some may be reactive in nature, while others may be unreactive. Some species commonly used to probe supramolecular structures are singlet excited states, triplet excited states, radical pairs, and radical ion pairs.

Singlet excited states of most organic molecules have short lifetimes; therefore, most fluorescent probes are used to explore the local environment within a

supramolecular system. Singlet excited states are often used in quenching studies in order to gain an understanding of the quencher access from the aqueous phase to the site where the probe resides. This is an indirect method of determining the nature of binding sites as the probe is used to report on the mobility of an undetectable molecule (the quencher).

Triplet excited states of organic molecules are generally longer-lived than their singlet counterparts. This longer lifetime of triplet states is of the same order of magnitude as the dynamic interactions between probe and host and allows the investigation of the dynamic processes occurring within the organized system.[8]

Radicals or radical pairs can also be used in the study of supramolecular systems.[8] It is most common for these reactive species to be deactivated by encountering another radical within the system. Thus, by studying the decay of the radicals inferences may be made on the location of these species within the host system.

1.4.1 Benzophenone and 4,4'-dimethylbenzophenone

Upon excitation, benzophenone (Bp) (Fig. 1.14) undergoes an n to π^* transition from the ground state to the first excited singlet state.[2] Aromatic ketones are known to have a small singlet-triplet energy splitting, with the difference in energy for Bp being 30 $kJmol^{-1}$.[2] The intersystem crossing efficiency of Bp for the transition from the excited singlet state to the excited triplet state is close to unity.[2] As such, upon excitation of Bp (and its derivatives), the first transient detected on the nanosecond time scale is the triplet excited state. The lifetime of triplet Bp in a non-polar aromatic solvent is normally 7 μs, while in a polar solvent the lifetime is extended to 50 μs.[69]

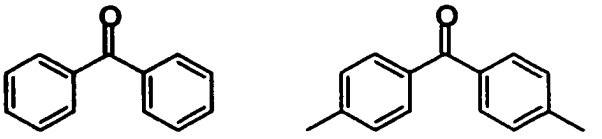

Figure 1.14 Probe molecules: benzophenone (Bp, left) and 4,4'-dimethylbenzophenone (DMBp, right).

The photochemistry of Bp is well documented[2,3] and was one of the key factors in selecting this probe for studies within bile salt aggregates. Due to its n,π* lowest excited state configuration, triplet excited Bp (and its derivatives) will undergo a hydrogen abstraction reaction, known as Norrish Type II (Scheme 1.4) in the presence of a hydrogen donor. The hydrogen abstraction rate constant (k_H) of triplet excited benzophenone has been previously determined from the following donor molecules: cyclohexane, ethanol, and 2-propanol with the k_H values being $3.63 \times 10^5\ M^{-1}s^{-1}$, $5.62 \times 10^5\ M^{-1}s^{-1}$, and $1.26 \times 10^6\ M^{-1}s^{-1}$, respectively.[2]

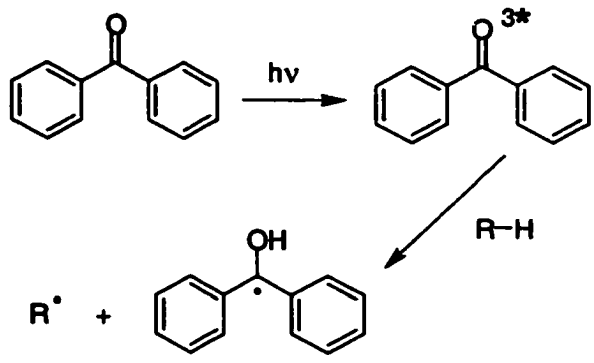

Scheme 1.4 Photochemistry of Bp: Excitation to the triplet excited state and Norrish type II reaction (hydrogen abstraction) to form the ketone ketyl radical.

4,4'-Dimethylbenzophenone was studied in order to test the effect of increased hydrophobicity on the interaction within the bile salt aggregates. The intersystem crossing quantum yield for DMBp is close to unity because it has been reported to be similar to that of Bp.[70] In a study done by Turro and coworkers, the rate of formation of excited triplet states was measured on the picosecond time scale. It was found that time constants representing the appearance of triplet excited states for Bp and DMBp were identical with a value of 18 ps (at a monitoring wavelength of 532 nm).[70] Thus it was concluded that, "the trends observed are consistent with direct singlet to triplet ISC from the S_1 to T_1 state".[70] The triplet energy of DMBp has a similar energy to the triplet energy level of Bp in a non-polar solvent, and the excited triplet state has a lifetime of 11 μs in non-polar solvent.[69]

1.4.2 Naphthalene and derivatives

Naphthalene is a small aromatic hydrocarbon (Fig. 1.11), and derivatives of this common photophysical probe were studied in this work by photophysical techniques. The fluorescence lifetime for the singlet excited state is known to be ca. 96 ns, and the fluorescence quantum yield of the excited singlet state is 0.19 in non-polar solvents.[69] In polar solvents, the singlet lifetime increases slightly to 105 ns, and the fluorescence quantum yield is 0.21.[69] In non-polar solvents, the intersystem crossing quantum yield for the transition from the singlet excited state to the triplet state is 0.75, and the lifetime of the triplet excited state has been reported to be ca. 175 μs.[69] In polar solvents, the intersystem crossing quantum yield is increased to 0.80, while the triplet lifetime is substantially increased to 1200 μs.[69]

Upon excitation, naphthalenes undergo a π to π^* transition from the S_0 to the S_1 state. For Np, the first singlet excited state lies at an energy of ca. 410 $kJmol^{-1}$, while the first triplet excited state lies well below at an approximate energy of 250 $kJmol^{-1}$. [2]

Figure 1.15 shows the series of naphthalene derivatives that were chosen for this study in order to investigate the interaction of probe molecules with NaCh aggregates. Two main features were studied with respect to the Np probes: the effect of the hydrophobicity of the probe, and probe shape. The probes were chosen so that the hydrophobicity decreased upon progressing from ethylnaphthalene (EtNp), to naphthylethanol (NpOH), and finally to acetonaphthone (NpO). In order to test the effect of the shape of the probe molecules on the incorporation within NaCh aggregates, substituents were placed in both the 1- and the 2- positions on the Np ring. Substituents at the 2-position led to more linear molecules. The substituents being placed at the 1-

position gave rise to a bulkier molecule, which may have exclude its incorporation within a tight or rigid binding site.

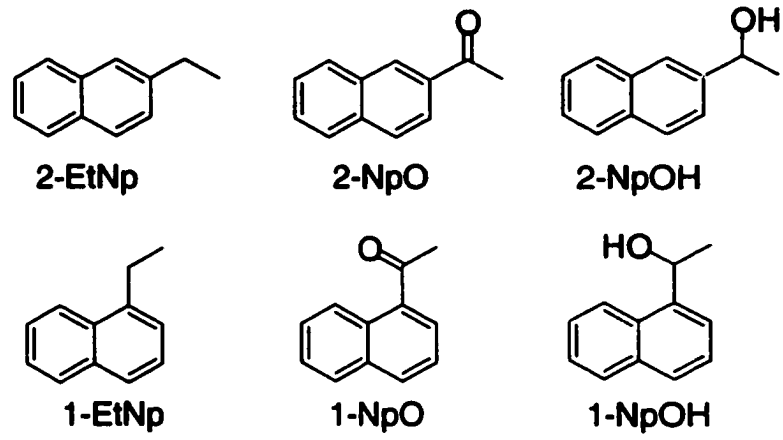

Figure 1.15 Probe molecules: 1-ethylnaphthalene (1-EtNp), 2-ethylnaphthalene (2-EtNp), 1-acetonaphthone (1-NpO), 2-acetonaphthone (2-NpO), 1-naphthyl-1-ethanol (1-NpOH) and 2-naphthyl-1-ethanol (2-NpOH).

Naphthalene derivatives have been widely used in photophysical studies.[69,71-73 74,75] A previous study in our group[74] showed that the singlet lifetimes for 1-NpOH and 2-NpOH in water were ca. 24 and 25 ns, respectively. The singlet lifetimes have been previously reported for numerous substituted Nps.[69] The triplet excited states of all of the derivatives chosen for this research have been previously studied.[69] The acetonaphthones were used by Hayon and co-workers in an extensive quenching study for inorganic ions in order to determine the differences in energy transfer and charge transfer mechanisms.[73] Baugher and co-workers studied the transient absorption spectra of 1-EtNp and a series of dinaphthylalkanes in order to identify the photochemical transient species present upon

excitation.[71] Previous work in our group studied the triplet naphthylethanols complexation to cyclodextrins.[74] This study found that the lifetime of the triplet excited states of the naphthylethanols was long, with lifetimes greater than 30 μs. Thus, there is ample evidence in the literature supporting the use of substituted naphthalenes for photophysical investigations.

1.5 Project Proposal

There is a wealth of information in the literature on the probing of microheterogeneous media by photophysical methods. Bile salts have been used in a limited number of these studies.[32,33,38,40,42,44,46,47,51,52,54] In an effort to further the knowledge of the aggregation of bile salts in solution, the photochemical and photophysical behavior of various probe molecules within NaCh aggregates will be studied. Benzophenone and 4,4'-dimethylbenzophenone will be studied to gain an understanding of chemical reactivity within the host aggregates; while a series of Np derivatives will be used to provide evidence for the existence of two different binding sites.

Benzophenone and 4,4'-dimethylbenzophenone are chosen as probe molecules for one series of experiments. The goal for this study is to examine the differences in the photochemistry of the triplet excited state of these ketones within the various binding sites of the NaCh aggregate system. In the presence of a hydrogen donor, such as NaCh, the triplet excited state of the ketones can abstract a hydrogen to form the corresponding ketone ketyl radical. Following the photochemistry of Bp (and its derivative), while varying the concentration of NaCh, will give valuable information on the reactivity of probe molecules within the different binding sites of bile salt aggregates.

A second group of probe molecules, based on the naphthalene parent compound, will be used to study the effects of probe hydrophobicity and shape on the binding dynamics with NaCh aggregates. The objectives of this work are to provide conclusive evidence in support of the existence of two distinct binding sites within the aggregate system, and to investigate the effect of probe structure on the binding dynamics with NaCh aggregates. Further, the effect of ionic strength on the aggregation of bile salts will also be examined using the substituted naphthalenes.

2 Experimental

2.1 Materials

Sodium cholate (NaCh, 98%, Aldrich, or 99%, Sigma), sodium chloride (NaCl, 99%, BDH), sodium iodide (NaI, 99%, BDH, or 99+%, Aldrich), 4,4'-dimethylbenzophenone (DMBp, >99%, Acros, purity checked by GC), 1-ethylnaphthalene (1-EtNp, 99+%, Aldrich, checked by GC, >99%), 2-ethylnaphthalene (2-EtNp, 99+%, Aldrich, checked by GC, >99%), (±)-1-naphthyl-1-ethanol (1-NpOH, >99%, Fluka, checked by GC, >99%), (±)-2-naphthyl-1-ethanol (2-NpOH, >99%, Fluka, checked by GC, >99%), 1-acetonaphthone (1-NpO, 98%, Aldrich, checked by GC, >99%), 2-acetonaphthone (2-NpO, 99%, Aldrich, checked by GC, >99%), methanol (MeOH, spectrograde, Aldrich), 2-propanol (spectrograde, Aldrich), dichloromethane (CH_2Cl_2, reagent grade, Aldrich), nitrous oxide (N_2O, USP, Praxair), and oxygen (O_2, Praxair) were used as received. Benzophenone (Bp, 99+%, Aldrich) was recrystalized from methanol/petroleum ether, and its purity was checked by GC (>99%). Sodium nitrite ($NaNO_2$, 97+%, Aldrich) was recrystalized from water. Water was deionized through a SYBRON Barnstead system.

2.2 General sample preparation

Most of the experiments described in this work were carried out at a NaCl concentration of 0.2 M. It is known that ionic strength plays a role in the aggregation of bile salts.[28,41,48] A concentration of 0.2 M NaCl was chosen in order to work close to physiological conditions.

In the study which used naphthalene derivatives as guests, the effect of the ionic strength (μ) on the host-guest complexation was investigated. The ionic strength was kept constant by taking into account the concentrations of NaI, $NaNO_2$ and NaCl in the solutions. The sample preparation for these experiments was different than when the ionic strength was not kept constant. The first section of the experimental describes the general sample preparation used for most of the work in this thesis where the ionic strength was not kept constant. In the Np project, where there are two different types of experiments, and when discussing experiments in which the data were collected without keeping the ionic strength constant, the experiments are referred to as having been done at "varying ionic strength."

Solutions used for fluorescence experiments were kept as aerated solutions because signals were sufficiently strong even in the presence of oxygen. Solutions used on the laser flash photolysis system were deoxygenated due to the fact that oxygen is a known quencher of many transient species, including excited triplet states and ketyl radicals. DMBp was deoxygenated by bubbling with N_2O, because of the formation of solvated electrons (vide infra), while all other solutions were bubbled with N_2.

2.2.1 Sodium cholate solutions

The sodium cholate solutions were prepared by dissolving the appropriate amount of sodium cholate into 25 or 50 mL of water. The appropriate amount of NaCl was also added to reach the desired 0.2 M NaCl concentration. All solutions containing NaCh were heated for 0.5 h at 50 °C prior to performing any experiments in order to avoid gel formation of the bile salts.[76] The solutions were then allowed to equilibrate at room

temperature for 30 min. No gel formation re-occurs within the 8 h that it takes to complete the experiments.[76] The solutions were not buffered to maintain a constant pH; however, it is know that a variation of pH from 6 to 8 does not significantly influence the aggregation behavior of bile salts.[17]

2.2.2 Benzophenone and 4,4'-dimethylbenzophenone solutions

Both Bp and DMBp are hydrophobic probes and therefore special care has to be taken to prepare the aqueous solutions for these ketones. The following two methods were employed to prepare the ketone solutions for all experiments. The samples in this study contained 0.2 M NaCl as described in the previous section.

In order to solubilize Bp in aqueous solutions, a film technique was employed. The Bp was initially deposited on the walls of the sample vial by dissolving the Bp in methanol and slowly evaporating the solvent with a stream of air, while the flask was manually rotated. NaCh solutions were then added to the sample vials and the solutions were stirred overnight. In the case of DMBp, adding the solid to the aqueous solutions and stirring overnight achieved the best results, with concentrations that were high enough for performing the experiments. For both ketones, the excess solid was removed by gravity filtration and the concentration of probe was determined by UV-vis spectroscopy.

2.2.3 Solutions for naphthalene derivatives

2.2.3.1 Probe and NaCh solutions

A 0.02 M methanolic probe stock solution was prepared for each of the six probes. For fluorescence experiments, the required amount of probe stock solution was injected into the aqueous NaCh solutions described above using gastight glass syringes. For 1-EtNp and 2-EtNp it was found that 20 μM gave the desired absorbance at the excitation wavelength (ca. 0.08). For 1-NpOH, 2-NpOH, 1-NpO, and 2-NpO, 10 μM was sufficient to reach the desired absorbance of ca. 0.08 at the excitation wavelength. The same concentrations were used when performing time-resolved single photon counting experiments. In the case of LFP experiments, the solutions were made identically to the fluorescence experiment solutions, except that the probe concentration for all probes was 80 μM. The 80 μM solution gave an absorbance between 0.2 and 0.5 at 266 nm. An absorbance below 0.1 was desirable for the fluorescence experiments in order to ensure that a linear relationship existed between the fluorescence intensity and the ground state absorption of the probes. Fluorescence is a more sensitive technique than LFP, allowing for lower absorbances to produce reliable results.

2.2.3.2 Quencher solutions

The quencher solutions were made fresh daily with the following guidelines being used for the concentrations required. It should be noted that the exact quencher concentration was always calculated for each new solution and the calculated value was used in further analysis. A 2.0 M stock solution of sodium iodide was used for fluorescence quenching experiments. For LFP experiments, sodium nitrite solutions were

used at concentrations of 0.03 M, 0.1 M and 0.6 M. All of the salt quencher solutions were made by dissolving the salt in water at the desired concentration. 2-propanol was used as a source of abstractable hydrogens in the Bp project in order to form the Bp ketyl radicals. In all experiments the final 2-propanol concentration was 0.62 M. Oxygen quenching experiments were performed by bubbling the solutions with N_2/O_2 mixtures, using a calibrated flow mixing system from Airgas. Alternatively, estimates of the quenching rate constants were arrived at by taking kinetic decays in the presence of nitrogen, air and oxygen. The amount of oxygen can be calculated[69] and a three-point plot (Equation 1.11) gave an estimate of the quenching rate constant.

2.3 Sample preparation for experiments conducted at constant ionic strength

As mentioned previously, testing the effect of ionic strength on the aggregation of bile salts was a goal of this project. The solutions for the varying ionic strength experiments were prepared so that the ionic strength varied with the addition of ionic quenchers. In a second study, care was taken during sample preparation to keep the ionic strength of the solutions constant. This was achieved by altering the NaCl concentration with the amount of ionic quencher added throughout the experiment. For this reason, experiments carried out with this sample preparation method are referred to as experiments done at "constant ionic strength".

The three ionic strengths chosen for this study were 0.03 M, 0.2 M and 0.4 M. An ionic strength of 0.03 M was the lowest possible in the study, as this is the maximum ionic strength reached in an experiment due to the addition of quencher. An ionic strength of 0.2 M was chosen to replicate the experiments carried out in the varying ionic strength

experiments. Experiments at an ionic strength of 0.4 M were done to test the effect of increasing the ionic strength.

In the experiments done at varying ionic strength, only one sample was used for fluorescence quenching measurements, and usually only two samples were used in the quenching studies of the triplet states. In the constant ionic strength experiments, each emission spectrum on the fluorimeter used a separate solution, and multiple solutions were required for the laser quenching experiments (vide infra).

2.3.1 Preparation of NaCh/NaCl solutions for quenching experiments

Sodium cholate solutions were prepared by dissolving the appropriate amounts of bile salt in water, with no addition of NaCl. Probe stock solutions were added in the same manner as described above (Section 2.2.3.1). NaCl was prepared as a concentrated stock solution, in a similar fashion to NaI. The NaCh solutions were heated once both salts were added, with the heating procedure described above (Section 2.2.1). Deoxygenation of the samples was also carried out as described previously (Section 2.2).

2.3.2 Sample preparation for fluorescence quenching experiments

For experiments carried out at an ionic strength of 0.03 M the stock solution concentrations for NaCl and NaI were 1.03 M, while for experiments carried out at ionic strengths of 0.2 M or 0.4 M, the stock solution concentrations were 4.2 M.

Initial aliquots of 2 mL of the probe/NaCh solution were used for a series of solutions. The appropriate amount of quencher (NaI) was added to the solutions in order to span a concentration range of 0 to 0.03 M. The appropriate amount of the sodium

chloride stock solution was added in order to keep the ionic strength constant throughout the experiment. The stock solutions were prepared so that the concentration of the bile salt would not be altered by more than 10%. Table 2.1 shows the solution preparation for a series of experiments.

Table 2.1 Sample preparation for fluorescence quenching experiments performed at a constant ionic strength (μ). (a) μ = 0.03 M (top), (b) μ = 0.2 M (middle) and (c) μ = 0.4 M (bottom) (blank refers to solutions with no probe added that were used for baseline readings)

μ = 0.03 M	blank	1	2	3	4	5	6	7
mL of NaCl	30	60	50	40	30	20	10	0
mL of NaI	30	0	10	20	30	40	50	60

μ = 0.2 M	blank	1	2	3	4	5	6	7
mL of NaCl	50	100	97	94	91	88	85	82
mL of NaI	50	0	3	6	9	12	15	18

μ = 0.4 M	blank	1	2	3	4	5	6	7
mL of NaCl	105	210	207	204	201	198	195	192
mL of NaI	105	0	3	6	9	12	15	18

2.3.3 Sample preparation for laser flash photolysis quenching experiments

For the nitrite quenching experiments of the triplet excited state of the probe molecules, stock solutions of 0.1 M and 2 M $NaNO_2$ were prepared. NaCl stock solutions

of 0.06 M and 2 M were used to keep the solutions at a constant ionic strength with varying quencher concentrations.

In order to maintain a constant ionic strength and span the necessary quencher concentration range, five separate solutions were required for each experiment. The first sample was prepared with probe, bile salt and NaCl in solution. During the course of the experiment two solutions were added for each kinetic trace. One solution contained $NaNO_2$ in water to quench the excited triplet state. The other contained probe and bile salt to assure that the probe and bile salt concentrations were not being diluted. Data at very low quencher concentrations were collected using this sample.

The rest of the experiment was carried out using a series of four samples. Each of these samples contained a different concentration of quencher that was diluted over the course of the experiment. The solutions contained probe, bile salt, NaCl and $NaNO_2$ in water. Again, two solutions were added prior to acquiring each trace. In this case, the first solution contained probe, bile salt and NaCl while the second contained only probe and bile salt. The reasoning for the addition is the same as in the case for the first sample. This was the most efficient design possible to span the concentration range of quencher solution needed while keeping the ionic strength constant. All additions were made with gastight glass syringes.

2.4 Instrumentation

2.4.1 UV-Vis absorption spectroscopy

UV-vis (ultraviolet and visible) absorption spectra were recorded on a Varian Cary 5 or Cary 1 spectrophotometer at room temperature. In order to obtain a corrected

absorbance spectrum, a baseline (of air) had to be run at the start of each day. The absorbance of a solution was then taken with the Cary correcting for the baseline that had been collected. The absorbance of the sample was obtained by subtracting the absorbance reading at a wavelength where the probe does not absorb from the reading at the desired wavelength. The scan rate was either 200 or 400 nm/min, and the bandwidth was always 2.0 nm. Samples were measured in 10 mm x 10 mm quartz cells or in 7 mm x 7 mm Suprasil cells. For the benzophenone solutions, absorbance values were always taken in 10 mm x 10 mm cells to assure the pathlength remained constant. This was necessary in order to calculate the concentration of the solutions using the Beer-Lambert law (vide supra).

2.4.2 Fluorescence spectroscopy

2.4.2.1 Steady-state experiments

Steady-state fluorescence measurements were carried out using a PTI QM-2 (Photon Technology International QuantaMaster) Luminescence spectrophotometer. The excitation source was a Xenon-arc lamp (75 W), and all experiments were carried out at room temperature (20 ± 0.2 °C). The emission and excitation slits were set such that the bandpass was between 2 and 5 nm. The slits were adjusted in order to maximize the emission intensities for different probes. A stepsize of 0.5 nm and an integration time of 1 s were employed. For all the naphthalene probes, the excitation wavelength was 290 nm, and the emission scans were recorded from 300 nm to 500 nm for 1-EtNp, 2-EtNp, 1-NpOH, and 2NpOH, and from 300 nm to 600 nm for 2-NpO. In all cases, a solution containing water, bile salt, NaCl and NaI (50 mM) was run as a baseline. The corrected

emission scan was obtained by subtracting the baseline scan from the acquired emission spectra. All solutions were run in 10 mm x 10 mm quartz fluorescence cells.

The spectra were corrected using FeliX™ software. Further analysis of the data, including generation of quenching plots, was performed using the Kaleidagraph™ (Synergy Software version 3.08d) fitting program, which employs a least square error analysis fitting routine.

2.4.2.2 Time-resolved experiments

Time-resolved measurements were performed on a PTI LS-1 time-correlated single photon counter at room temperature (20.0 ± 0.1 °C). The excitation source was a nanosecond hydrogen arc-lamp. The excitation wavelength was 290 nm, while the emission wavelength was set at 333 nm. The slit width was adjusted so that the decay curve was simulated in as short a time as possible while maintaining the conditions necessary for a Poisson distribution (Section 1.2.3). The maximum number of counts was set at 10 000 for the channel of maximum intensity. The instrument response function was measured using an aqueous silica gel solution in order to give the finite lamp profile. The excitation and emission wavelengths that were used to collect the scattered light were set to 290 nm, which was the same as the excitation wavelength for the sample. Collection of the lamp profile is important as it was deconvoluted from the decay curve upon analysis (Section 1.2.3). All solutions were contained in homemade 10 mm x 10 mm Suprasil quartz cells.

Lifetime analysis and fitting of the decay traces were done using the PTI software. Statistical analysis was performed by the program and allowed for determination of the

goodness of the fit, based on χ^2, Durbin-Watson (D-W) and Run test Parameter (Z). A χ^2 value close to unity indicates no deviation between the experimental data and the fit of the program, based on an assumed kinetic model. χ^2 values between 0.9 and 1.2 were considered acceptable. The D-W parameter should be greater than 7, 7.5 or 8 for single, double and triple exponential decays, respectively. The Z value has to be greater than -1.96 in order to achieve a confidence level of 95%. Visual inspection of the weighted residuals and the autocorrelation function were also taken into account.

2.4.3 Laser flash photolysis

The basic setup for the laser flash photolysis system is shown in Scheme 2.1.[11] One of the following two excitation sources was used throughout the study. A Lumonics excimer laser (2) model EX-510 operated with a Xe/HCl gas mixture, 308 nm, $\leq$ 40 mJ/pulse. The second excitation source was a Spectra Physics Quanta-Ray GCR-12 Nd: YAG laser (1) (or GCR-3 (21-which is actually located directly below 1)), 266 nm, $\leq$ 40 mJ/pulse; 355 nm, $\leq$ 70 mJ/pulse. If necessary, the laser pulse energies can be attenuated to less than 20 mJ/pulse by either the use of neutral density filters (3)(63, 40, 25 and 10 %) in the case of the excimer laser, or by decreasing the energy of the pulse on the YAG lasers.

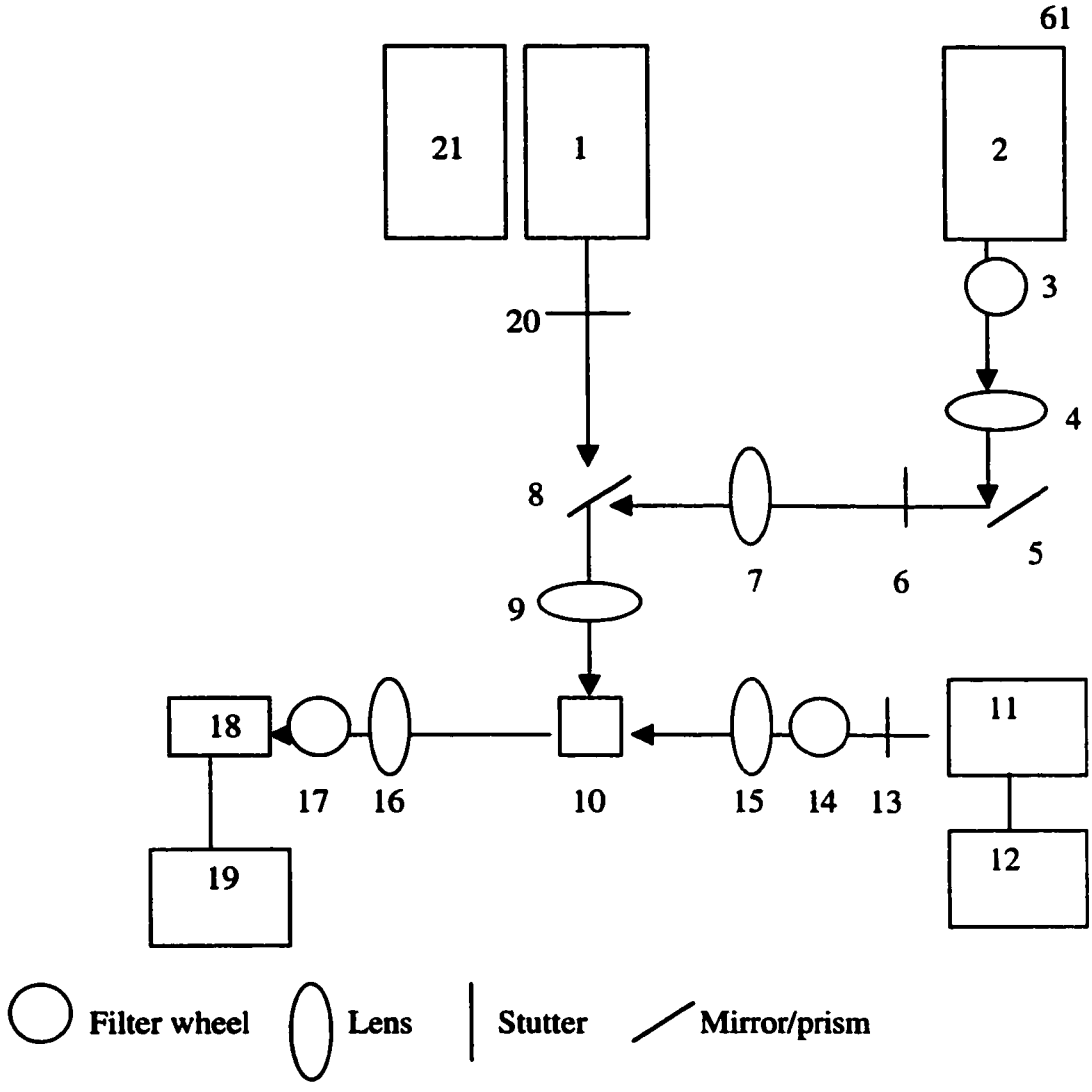

Scheme 2.1 Schematic for the LFP system

The YAG GCR-12 laser beam is aligned directly onto the sample holder. The second harmonic (532 nm) of the laser generates unwanted laser light; therefore the beam passes through a broad band interference filter (not in diagram) that blocks out the residual light of this wavelength from the sample holder. The YAG GCR-3 laser beam must be brought up to the monitoring table by deflection through 2 prisms, after which it is aligned to hit the sample holder in the same fashion as the GCR-12 YAG. It should be

noted that for both the YAG lasers, the prism (8) and the lens (9) were removed from the experimental set-up. In the case of the excimer laser, the laser beam is passed through a lens (4), and is then reoriented using a mirror (5), and concentrated using a spherical lens (7). Next, it passes through a prism (8) that is used to alter the beam direction so that it strikes the sample holder (10) at 90 degrees relative to the monitoring beam; after passing through one final spherical lens (9).

The monitoring system consists of a 150 W Xenon-arc lamp (11) (Oriel housing model 66057, PTI power supply model LPS-220) as a light source. The Xenon-arc lamp can maintain a high intensity output for 4 ms, when triggered by a pulser (12) (custom built, University of Victoria). The monitoring beam passes through a cutoff filter (14) (no filter, 320 nm, 375 nm, 435 nm or 590 nm) to reduce degradation of the sample by the Xenon-arc lamp. The beam is then focused with a lens (15), in such a way that the focal point of the beam lies beyond the sample holder. The monitoring beam passes through the sample holder through a slit with a diameter of 1 mm. After passing through the sample holder, the beam goes through a second focusing lens (16) and through another cutoff filter wheel (17), which is set to the same wavelength as (14). The second cutoff filter is in place to assure that only the desired transients are detected, and to avoid interference from scattered laser light. The cut-off wavelengths are set by the computer and are always no less than 20 nm below the wavelength being monitored.

The detection system begins with a monochromator ((18), CVI Digikrom 240) which selects the wavelength of light to be monitored. The light intensity is then detected by the photomultiplier (PMT, Hamamatsu R446). The signal from the photomultiplier tube is directed to a baseline compensation unit, which offsets the light intensity before

the laser pulse. After the laser pulse, the baseline compensation unit holds the light intensity constant. The signal is then transferred to a digital oscilloscope (Tektronix, TDS 520) and to the computer (19).

Experiments in the benzophenone project made use of a two-oscilloscope set-up.[77] This allows for two kinetic traces to be collected simultaneously on two different time-scales. This type of experiment was necessary when non-exponential decay traces were observed. One oscilloscope collects the non-exponential decay. The second oscilloscope is set to a much longer time scale and collects the final baseline reading. This final baseline reading is critical for two reasons. First, it can then be said whether the species present decayed or whether there is a residual absorption from one or more transients. Second, a precise value of the baseline is used in Equation 2.2 as the final A_3 value (vide infra).

Timing is a critical component of the laser flash photolysis system, as the excitation by the laser must occur while the pulse from the monitoring lamp is stable. This occurs within a few ms after the lamp is pulsed. The timing for the lamp, laser, baseline compensation unit and oscilloscope are controlled by a custom-built pulse generator coupled to a delay generator (Stanford Research System, model DG535). The time sequence begins with the triggering of the lamp pulser. Shutters in front of the appropriate laser (20 and 6) and the monitoring beam (13) are opened prior to the triggering of the lamp pulser. This is important in the case of the two YAG lasers in order to avoid prolonged exposure of the sample to irradiation. Exposing the solutions to a constant irradiation of laser light could cause decomposition of the sample. This is not a

concern with the Excimer, as the laser is triggered for each decay trace and is not continuously firing.

When a transient with a lifetime longer than 2 μs was monitored, the kinetic trace had to be corrected for baseline shifts. A baseline correction shot was taken immediately following the signal shot, where the lamp was pulsed, but the sample was not excited by the laser. The baseline correction shot was subtracted from the signal after the data were transferred to the computer but before the ΔA value was calculated.

Absorbance values were calculated according to Equation 2.1. The absorbance values (ΔA) are related to the ratio of light intensities being detected by the PMT in the absence and presence of transients. Equation 2.1 assumes a linear response function between the signal measured at the PMT and the light intensity irradiating the detector. Since the response of the PMT is not linear, only small changes in light intensity are measured, which correspond to ΔA values ≤ 0.2.

$$\Delta A = -\log\{1 - (\frac{(V_t)_{corrected}}{(V_o)})\}$$

Equation 2.1

In most cases, 6 different kinetic traces were averaged to give the final decay, and when collecting transient spectra. The naphthalene data were collected using mainly the 266 nm YAG laser, and the monitoring wavelength used was 420 nm. The exceptions were experiments with 1-NpO and 2-NpO, where the samples were excited with the 308 nm laser. The ground state absorbance for the Np samples at the laser wavelength of interest was kept between 0.2 and 0.5 (pathlength = 0.7 cm). The Bp data were collected

using the 308 nm excimer laser with the key monitoring wavelengths being 540 nm and 600 nm. The Bp data were collected at the maximum concentration possible, which in certain cases (vide infra) only gave absorbance values of approximately 0.1 (pathlength = 1.0 cm). A single cell was not exposed to more then 60 laser shots, in order to avoid decomposition of the probes. Taking UV-vis absorption spectra before and after laser irradiation confirmed that no significant decomposition had taken place. The temperature for the laser flash experiments was kept constant at 20 ± 2 °C.

All kinetic data were collected using 7 mm x 7 mm Suprasil cells. Transient absorption spectra were collected using a 7 mm x 7 mm Suprasil flow cell to ensure that fresh solution was irradiated for each laser shot. In the flow system, the cell connects to a reservoir which contains the solution and this reservoir is continuously bubbled with nitrogen to assure proper deoxygenation. In the case of the benzophenone spectrum in the presence of 2-propanol, a flow system could not be employed due to the fact that the constant bubbling of nitrogen altered the 2-propanol concentration. For this set of data a series of static cells, all deoxygenated, was employed. For each cell, the spectrum was taken at a wavelength of interest (between 640 nm and 400 nm) and at 530 nm. All the data points were then normalized at 530 nm in order to take into account the slightly different lifetimes that may arise due to different extents of deoxygenation for each sample. For DMBp the spectrum was collected using static cells purged with nitrous oxide.

The software for the LFP system was written using the Labview 6 environment (National Instruments, Dr. L. Netter) and it performs a multitude of tasks including: controlling all experimental settings, subtracting baseline correction shots, transforming

voltage to absorbance, averaging sets of measurements, fitting the kinetic traces, and saving all the data. Further analysis was carried out using the non-least square fitting routine in Kaleidagraph™ (Synergy Software, version 3.08d).

Kinetic traces that did not follow mono-exponential decays were fitted to the sum of two exponentials using Equation 2.2.

$$\Delta A = A_1 e^{-k_1 t} + A_2 e^{-k_2 t} + A_3$$

Equation 2.2

The parameters A_1 and A_2 represent the pre-exponential factors for the two species; these have associated decay rate constants of k_1 and k_2. A_1 and A_2 are related to the total absorbance ΔA of each trace and A_3 is the final ΔA value. A_3 may be different from the baseline before laser excitation for one of two reasons: either an offset in the baseline of the instrument is present or the absorbance is due to the presence of a long lived transient. If the value of A_3 is not determined correctly, the lifetime of the slower process cannot be determined accurately. This was the main reason experiments with two oscilloscopes, measuring two time scales, were performed. The A_3 value was then fixed within the fitting routine in order to extract the rate constants of the two decay processes.

2.5 Procedures

2.5.1 Determination of molar absorptivities for Bp and DMBp

Due to the insolubility of benzophenone and its derivative in water, a method had to be devised to determine the exact concentration of the ketones in the NaCh solutions. When the data were analyzed it was apparent that the concentration of Bp greatly

influenced the outcome of the experiments. Thus the concentration of the ketones had to be determined from the ground state absorption spectra, using the molar absorptivities (ε) of the ketones.

The ε for Bp and DMBp was found by initially determining the ε values for both ketones in dichloromethane (CH_2Cl_2). Next, to find the ε of the aqueous systems, the ketones were extracted from aqueous and NaCh solutions using dichloromethane. A series of extractions were performed until no further ketone absorption was observed in the extracted CH_2Cl_2 fraction. All dichloromethane fractions were combined; the absorbance of the solution was measured and the ketone concentrations in the aqueous system were back-calculated using the Beer-Lambert law (Equation 1.4).

2.5.2 Detection of solvated electrons

Photoionization of ketones is a concern when laser studies are performed.[78] It has previously been shown that this photoionization process occurs readily in the presence of supramolecular systems.[79,80] Often, when the presence of solvated electrons is detected, the corresponding radical cations are not observed.[81] An absorption band in the 650 nm to 800 nm (with a max at 720 nm) region of the transient spectrum characterizes solvated electrons in water.[82] For all probes studied, a kinetic trace was taken at 650 nm to assure no signal was present due to solvated electrons. In the Bp study, no solvated electrons were detected in either aqueous solutions or in the presence of bile salts. DMBp showed a relatively strong solvated electron signal in the presence of bile salts, and for this reason all solutions of DMBp / NaCh were bubbled with N_2O, a known quencher of solvated electrons.[83] In the naphthalene study, occasionally a weak solvated electron signal was detected that could be eliminated by decreasing the energy of the laser pulse.

3 Photochemistry of benzophenone and 4,4'-dimethylbenzophenone in sodium cholate

3.1 Results

3.1.1 Molar absorptivities of Bp and DMBp in water and sodium cholate aggregates

Knowing the concentration of Bp and DMBp throughout the study proved to be of importance. Due to the insolubility of the ketones in water, it was not possible to determine the concentration by weight when preparing the solutions. The alternative was to measure the ground state absorption spectra and calculate the ketone concentration using the Beer-Lambert Law (Equation 1.4). It was observed that the Bp and DMBp ground state absorbance spectra changed significantly in solvents of different polarities. A similar solvent effect has been previously observed.[3] The π to π^* absorption band below 300 nm is red-shifted on going from a solvent of lower polarity to higher polarity as the excited state is more polar than the ground state. The opposite effect is observed for the n to π^* absorption band centered at ca. 350 nm, as the excited state is less polar than the ground state. In the current study, the spectra of the ketones in water and those in the presence of bile salts could not be superimposed (Fig. 3.1). Thus, the molar absorptivities of the compounds in aqueous solution and at all NaCh concentrations were determined.

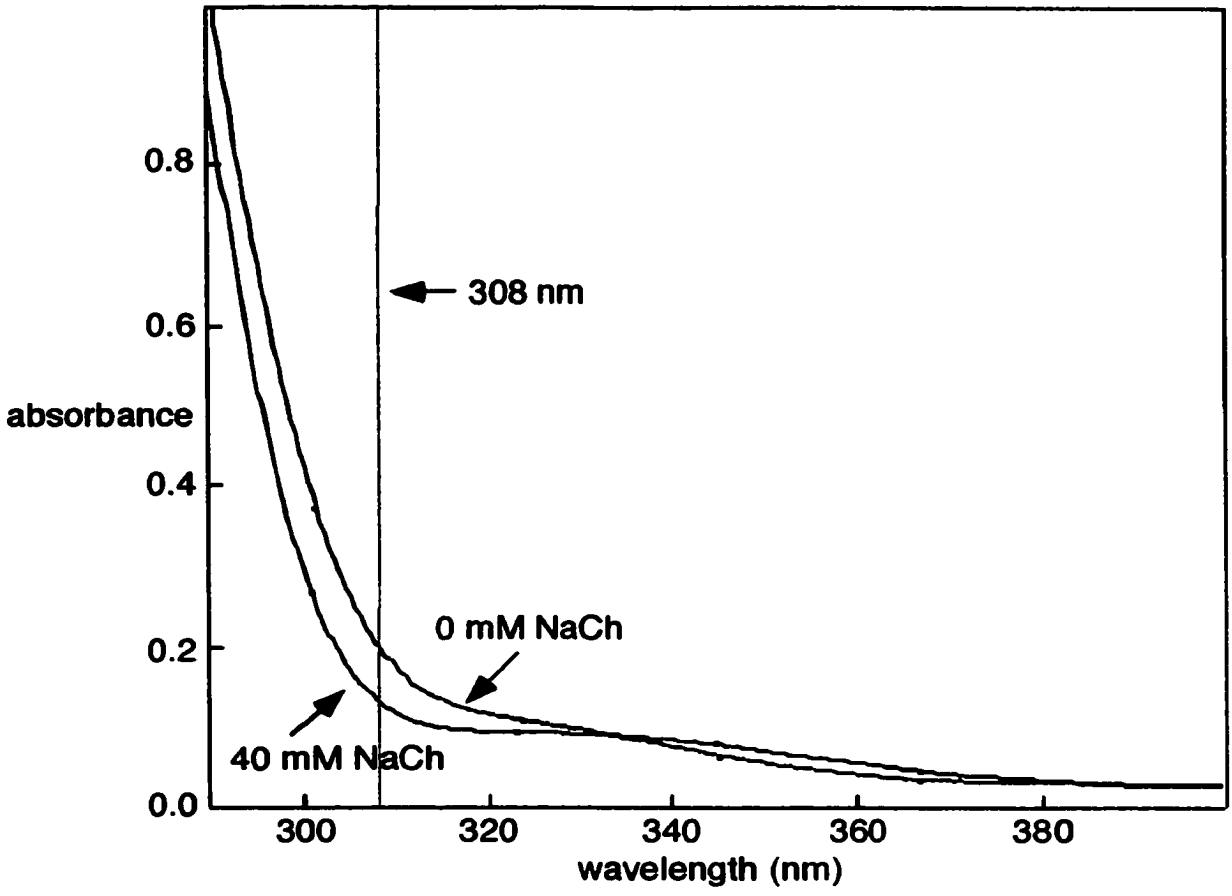

Figure 3.1 Ground state absorption spectra of Bp in the absence of NaCh and in the presence of 40 mM of NaCh, to show the difference in the absorption of Bp ([Bp] = 0.6 mM) due to the presence of NaCh, at the excitation wavelength, 308 nm.

All molar absorptivity (ε) values were determined at 308 nm because the data for this study were collected using the excimer laser (λ_{ex} = 308 nm). The ε for Bp in CH_2Cl_2 was found to be 89 ± 2 $M^{-1}cm^{-1}$ (2 determinations), while that of DMBp was found to be 180 ± 3 $M^{-1}cm^{-1}$ (2 determinations). In aqueous solutions, the molar absorptivities were determined to be 280 ± 30 $M^{-1}cm^{-1}$ and 280 ± 40 $M^{-1}cm^{-1}$ for Bp and DMBp, respectively (2 determinations each).

When extracting the ketones from the bile salt solutions, problems arose with the DMBp solutions. In the presence of NaCh, the solutions of DMBp became cloudy upon the addition of dichloromethane, and an emulsion formed that was very difficult to separate. In the presence of NaCh, the values determined for the ε of DMBp were similar to the values obtained for Bp. The errors associated with the values for DMBp were much larger than those for Bp. Consequently, the values obtained for Bp were used for both ketones and were determined to be the following: in the presence of 10 mM of NaCh and 40 mM of NaCh, the ε values recovered were 310 ± 10 $M^{-1}cm^{-1}$ (2 determinations) and 210 ± 10 $M^{-1}cm^{-1}$ (3 determinations), respectively.

3.1.2 Photochemistry of Bp and DMBp in water

The excitation of Bp in the presence of a hydrogen donor leads to the formation of both triplet excited states as well as ketyl radicals (Scheme 1.4). As sodium cholate has abstractable hydrogens, both of these transient species were followed in this study.

3.1.2.1 Transient absorption spectra

The transient absorption spectra of Bp and DMBp were acquired in order to determine the wavelengths of interest for the kinetic studies for both the triplet excited species, as well as the ketyl radicals. The triplet absorption spectrum had a maximum at 525 nm, with the absorbance extending into the 600 nm region (Fig. 3.2). Ketyl radicals were generated by the addition of 2-propanol (0.62 M) to Bp in water. The maximum absorption of the ketyl radical was shifted to 540 nm, with little absorbance at 600 nm (Fig. 3.2).

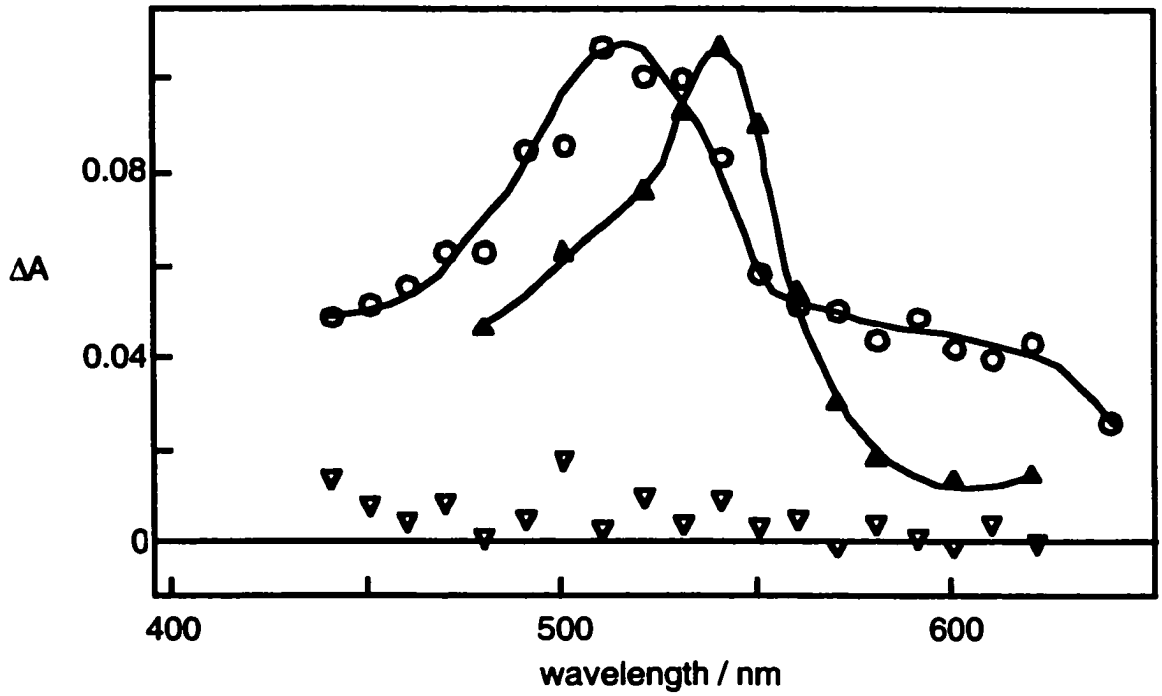

Figure 3.2 Transient absorption spectra for Bp in water (0.2 M NaCl), in the absence (0, delay = 9.9 μs) and in the presence (▲, delay = 12 μs) of 0.62 M of 2-propanol. The two spectra were normalized at the peak maximum in order to emphasize the shift in the spectrum upon the formation of ketyl radicals. The third spectrum (▽, delay = 30 μs) is the signal for Bp in water observed for a long delay after the laser pulse. The solid lines were included to guide the eye.

The same transient spectra were observed at all time delays after the laser pulse for Bp in water, indicating that only one species was present. At long delays after the laser pulse, no absorption was observed due to a complete decay of the transient species (Fig. 3.2). The species present in water was the benzophenone triplet excited state, as the spectrum was similar to those spectra reported previously in the literature.[84,85] The triplet excited state and ketyl radical spectral features for DMBp were similar to those observed for Bp, which was expected since it has been shown that mono-substituted triplet Bp derivatives give rise to similar transient spectra.[86]

3.1.2.2 Transient kinetics of Bp and DMBp in water

The kinetics for triplet Bp (and DMBp) in aqueous medium followed a first order decay, and the lifetime was ca. 5 μs for both ketones. The lifetime was seen to decrease with an increasing concentration of ketone due to self-quenching. Self-quenching occurred when a ground state ketone molecule encountered a triplet excited state, and the two interacted resulting in the deactivation of the excited state. This quenching process followed the same quenching equation used when nitrite or oxygen were introduced as quenchers (Equation 1.11, with [Q] = [ketone]).

Due to the fact that self-quenching was a factor in the deactivation of the excited triplet species, the self-quenching rate constant for Bp was determined, and the value recovered was $(1.2 \pm 0.3) \times 10^8$ $M^{-1}s^{-1}$ (Fig. 3.3). This value is comparable to the value previously reported in the literature for Bp in water $(1.7 \pm 0.2) \times 10^8$ $M^{-1}s^{-1}$.[87] DMBp was less soluble than Bp in water, and therefore only an estimate of the self-quenching rate constant was obtained (2×10^8 $M^{-1}s^{-1}$).

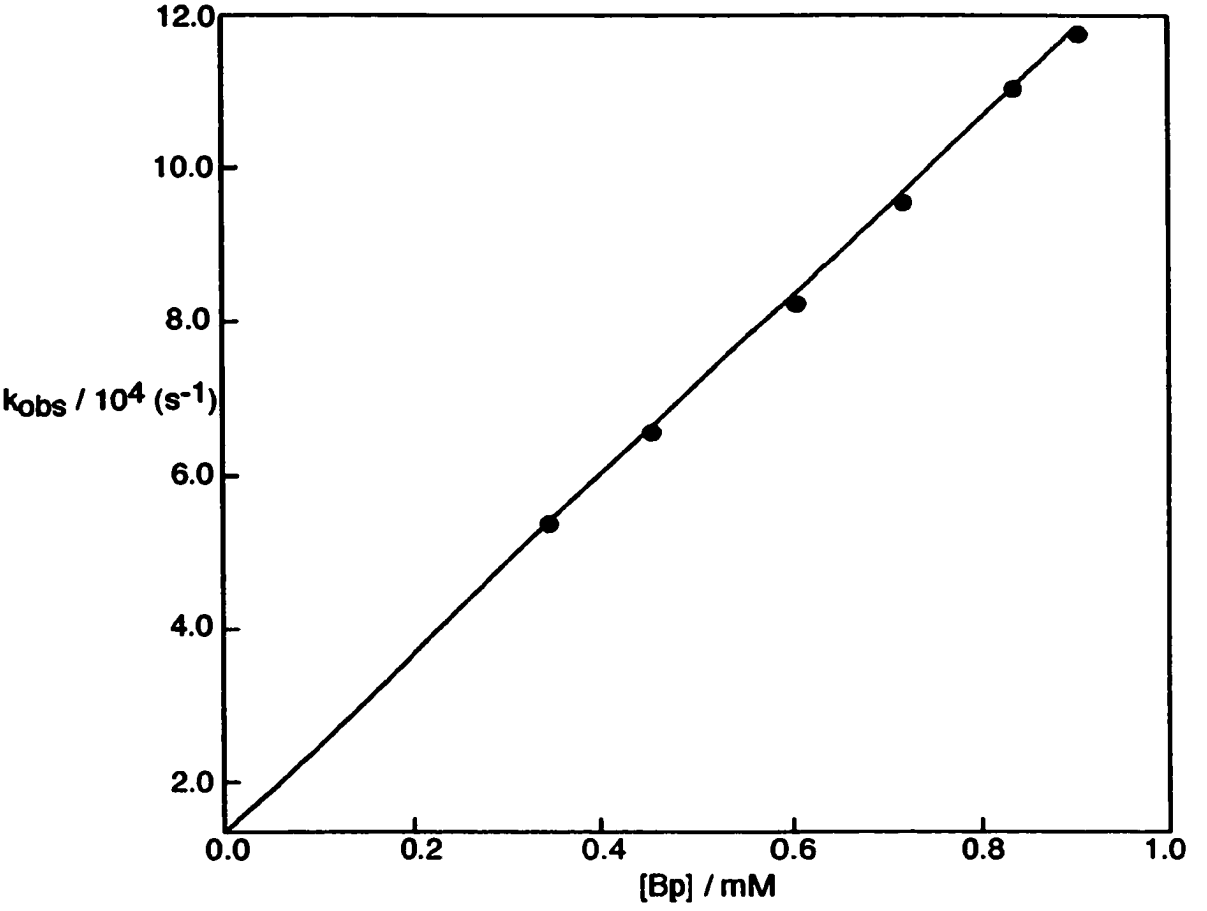

Figure 3.3 Self-quenching plot for the triplet excited state of Bp in water, with a self-quenching rate constant of 1.2×10^8 $M^{-1}s^{-1}$.

3.1.2.3 Quenching studies

3.1.2.3.1 Nitrite as a triplet excited state quencher

Nitrite is a known quencher of triplet excited states,[51,73] and it led to a decrease in the observed triplet lifetime for Bp and DMBp in aqueous solutions. For both ketones the quenching plots in water were linear and the quenching rate constants were comparable with an average value of $(4.0 \pm 0.6) \times 10^9$ $M^{-1}s^{-1}$ (2 determinations) (Fig. 3.4).

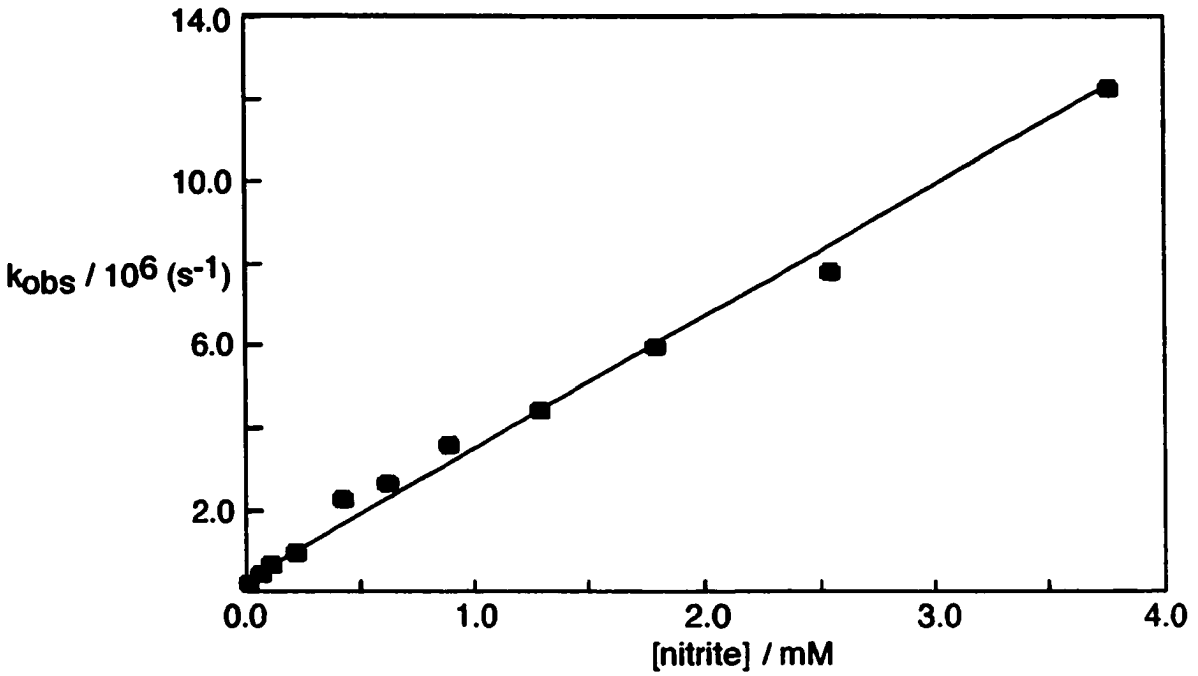

Figure 3.4 Quenching plot for the triplet excited state of Bp in water quenched with sodium nitrite. A quenching rate constant of 3.4 x 10^9 $M^{-1}s^{-1}$ was recovered.

3.1.2.3.2 Oxygen as a triplet excited state quencher

Oxygen quenches the triplet excited states and the ketyl radicals of Bp and DMBp. For the experiments in water, where only the triplet excited state was present, the quenching rate constant was determined by collecting kinetic traces in the presence of nitrogen, air and oxygen. The oxygen concentration was then calculated[69] and an estimate of the quenching rate constant of 2 x 10^9 $M^{-1}s^{-1}$ was obtained.

3.1.2.3.3 2-propanol as a triplet excited state quencher

In water, 2-propanol was used to determine the hydrogen abstraction rate constant for the triplet excited states of Bp and DMBp. The most likely hydrogens to be abstracted

from NaCh are the alcohol methine hydrogens (see below); thus 2-propanol was used to mimic this structure in the absence of bile salts. The hydrogen abstraction rate constant could not be measured directly using NaCh as the different aggregate structures at varying concentrations would affect the ability of the triplet excited Bp to reach the abstractable hydrogens.

Upon the addition of 2-propanol to Bp in water, the kinetic decays were no longer mono-exponential. The value for the triplet lifetime in the presence of 2-propanol (0.62 M) was found to be approximately 500 ns, while the decay for the ketyl radical was slower, with a half-life longer than 35 μs. The hydrogen abstraction rate constants (or quenching rate constants) for triplet Bp and DMBp from 2-propanol were determined to be (2.9 ± 0.6) x 10^6 $M^{-1}s^{-1}$ and (5.5 ± 0.8) x 10^5 $M^{-1}s^{-1}$, respectively (2 determinations each). These rate constants were determined by following the quenching of the triplet excited state at 600 nm. The values obtained represent an estimate of the hydrogen abstraction rate constant for the ketones in water by 2-propanol. These values were of the same order of magnitude as values previously reported in the literature.[86,88]

3.1.3 Photochemistry of Bp and DMBp when complexed to NaCh aggregates

3.1.3.1 Transient absorption spectra of Bp and DMBp in presence of NaCh aggregates

The Bp triplet excited state and ketyl radical were both observed in the transient spectra of Bp in the presence of 10 mM and 40 mM of NaCh. Both transients were formed within the pulse of the laser (ca. 10 ns). At short delays after the laser pulse, the spectrum was broad with a significant absorption in the 600 nm region (Fig. 3.5). At

longer delays after the laser pulse, the signal in the 600 nm region decreased relative to the signal in the 525 - 550 nm region (Fig. 3.5). As was seen in the spectrum of Bp in water, in the absence of 2-propanol, the triplet excited state absorbs significantly in the 600 nm region. Upon addition of 2-propanol to form the ketyl radical, the absorption in the 600 nm region was drastically decreased. The absorption at 540 nm was present at a time delay of 4.9 μs while the absorbance at 600 nm was not. Therefore, the ketone ketyl radical (monitored at 540 nm) is longer lived than the ketone triplet excited state (monitored at 600 nm).

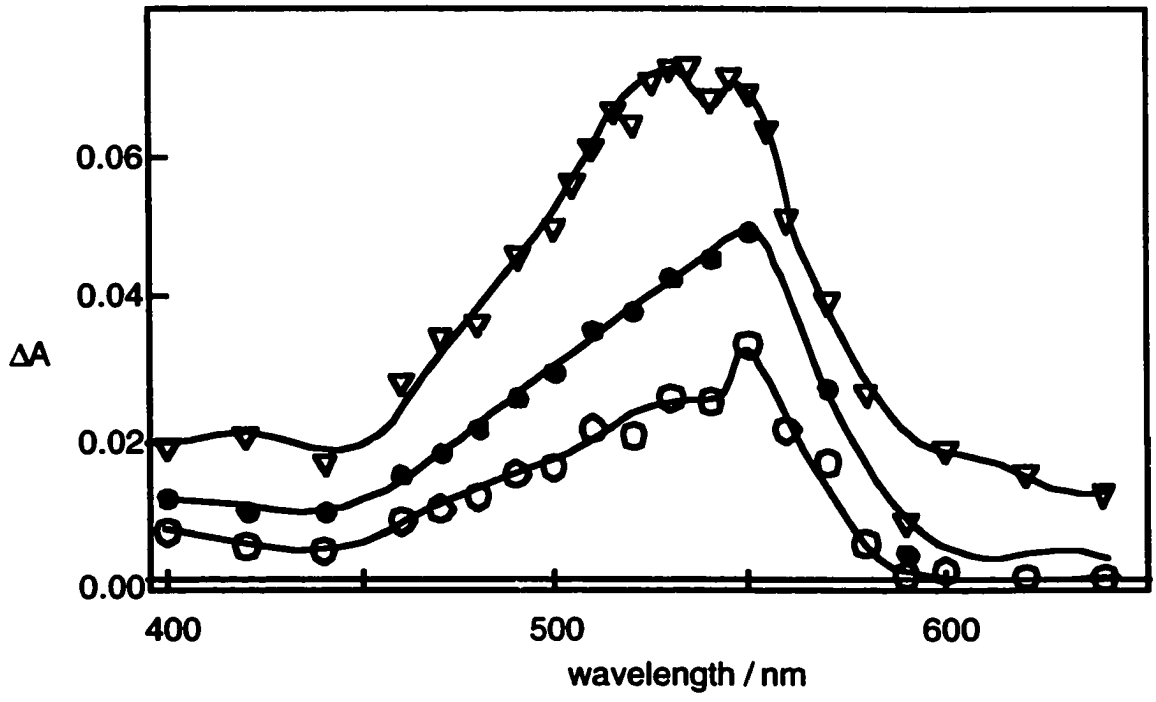

Figure 3.5 Transient absorption spectra of Bp in the presence of 40 mM of NaCh at varying time delays after the laser pulse (0.07 μs (▽), 0.3 μs (●), 4.9 μs (O)). The solid lines were included to guide the eye.

3.1.3.2 Kinetic processes for Bp and DMBp in NaCh aggregates monitored in the 600 nm region

The kinetic decays at 600 nm in the presence of NaCh, for both ketones, were not mono-exponential. All decay traces were therefore fitted to the sum of two exponentials (Equation 2.2) (Fig. 3.6) in order to extract the lifetimes as well as the pre-exponential factors for both processes. In order to obtain reliable data from Equation 2.2, the value of A_3 (the final absorbance) was needed. This being the case, these experiments were always carried out with two oscilloscopes and the second oscilloscope was used to determine the value of A_3 (inset in Fig. 3.6).

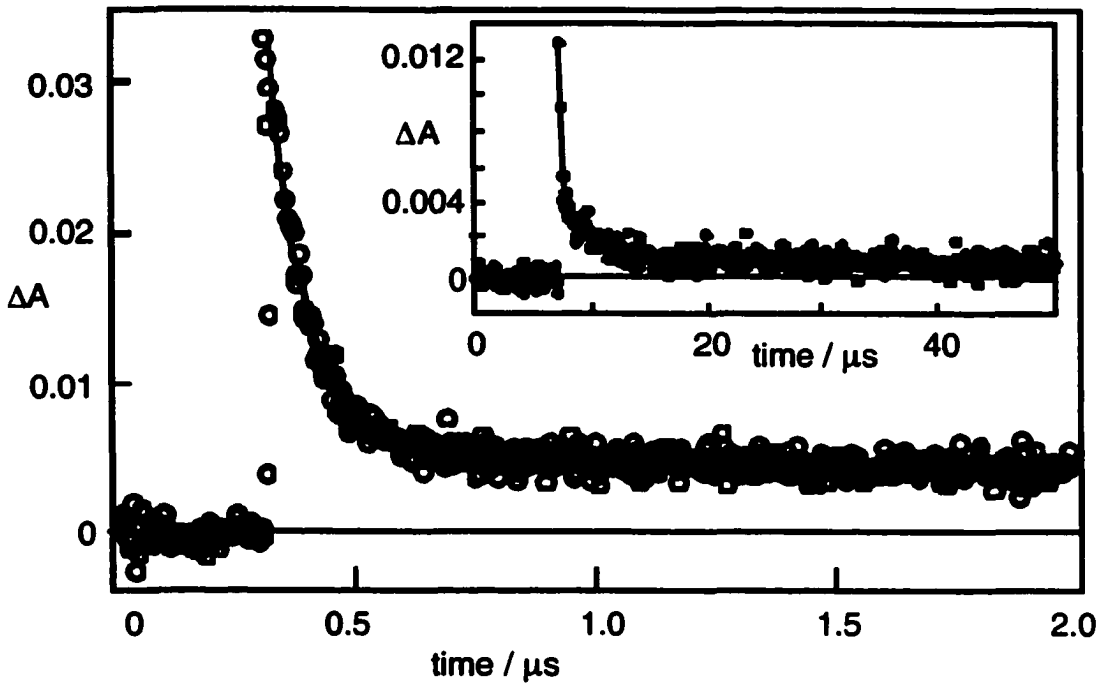

Figure 3.6 Decay at 600 nm fitted to the sum of two exponentials (τ_1 = 0.07 μs, τ_2 = 5.6 μs) for the transients formed when irradiating Bp in the presence of 40 mM of NaCh. The inset shows the decay on a long time scale in order to determine the values for τ_2 and A_3.

The contribution of the fast component was determined by the ratio of A_1/A_t. A_1 was the absorbance of the first transient and was obtained from the fit to the sum of two exponentials (Equation 2.2). A_t was the total absorbance for both transients and was equal to ΔA_{max} minus the residual absorption (A_3). The fast component was the major transient contributing to more than 75 % of the total signal present for Bp (Table 3.1) and more than or equal to 80 % of the total signal for DMBp (Table 3.2). The only exception to this trend was at a low concentration of Bp in the presence of 40 mM of NaCh. In this case, the fast component only comprised 40 % of the signal. For Bp, the lifetime of the fast component in the presence of 10 mM of NaCh was found to be 320 ± 30 ns, while the

lifetime of the fast transient in the presence of 40 mM of NaCh was found to decrease significantly with increasing Bp concentrations (vide infra). The lifetime of triplet DMBp in the presence of 10 mM and 40 mM of NaCh was found to be 850 ± 70 ns and 90 ± 20 ns, respectively. The lifetime values of DMBp did not decrease significantly with an increase in DMBp concentration.

Table 3.1 Dependence of the relative triplet concentration, measured in terms of the absorbance at 600 nm, and the relative contribution of the initial fast decay (A_1 / A_t) on the NaCh and Bp concentrations. Errors are average deviations of two independent experiments.

[NaCh] / mM	[Bp] / mM	Relative absorbance of Triplet	A_1/A_t
10	0.9 - 1.0	1.0	0.84 ± 0.02
10	0.55 - 0.6	0.59 [a]	0.83 ± 0.01
10	0.2 - 0.3	0.32 ± 0.02	0.86 ± 0.01
10	0.03 - 0.05	0.09 ± 0.02	b
40	2.7 - 3.0	1.0	0.87 ± 0.01
40	1.1 - 1.2	1.0 ± 0.1	0.86 ± 0.01
40	0.6 [a]	0.7 [a]	0.78 [a]
40	0.14 - 0.15	0.35 ± 0.01	0.4 ± 0.2

(a) Data from only one experiment; (b) the decay had only one component.

Table 3.2 Dependence of the relative triplet concentration, measured in terms of the absorbance at 600 nm, and the relative contribution of the initial fast decay (A_i / A_t) on the NaCh and DMBp concentrations. Errors are average deviations of two independent experiments.

[NaCh] / mM	[DMBp] / mM	Relative absorbance of Triplet	A_i/A_t
10	0.35 - 0.45	1	0.84 ± 0.04
10	0.09 [a]	0.37 [a]	b
40	2.2 [a]	1.0 [a]	0.87 [a]
40	1.3 - 1.4	0.73 [a]	0.85 [a]
40	0.78 - 0.88	0.52 ± 0.06	0.84 ± 0.04
40	0.26 [a]	0.23 [a]	0.80

(a) Data from only one experiment; (b) the decay had only one component.

For both ketones, at 600 nm, a second decay was present. For Bp, the lifetime for the slower decay varied between 2 μs and 13 μs, while for DMBp the lifetime varied between 10 μs and 20 μs. The second, slower decay at 600 nm comprised ca. 15 to 25 % of the signal. It was difficult to reproduce the value of the lifetime for the long lived component because of its minor contribution to the decay and the variation in the signal-to-noise ratio.

3.1.3.2.1 Effect of Bp or DMBp concentration on the kinetic processes at 600 nm

The amount of triplet excited state formed was measured as the ΔA value right after the laser pulse at 600 nm (ΔA_{max}). Examining the relative absorbance for the triplet excited states with changing ketone (Bp or DMBp) concentration showed that the triplet

concentration decreased with decreasing ketone concentration (Table 3.1 and 3.2). For Bp in the presence of 10 mM of NaCh, the ΔA_{max} appeared to decrease proportionally with a decrease in the Bp concentration, excluding the data at an extremely low concentration of Bp (0.03 - 0.05 mM). A direct relationship was not noted for Bp in the presence of 40 mM of NaCh or for DMBp at any of the NaCh concentrations observed.

As mentioned previously, the lifetime for Bp in the presence of 40 mM of NaCh varied when the ketone concentration was altered (Fig 3.7). As the benzophenone concentration was increased, the lifetime of the transient was observed to decrease. For DMBp, similar trends were not observed in the presence of 40 mM of NaCh. In the presence of 10 mM of NaCh, neither ketone showed an effect on the triplet excited state lifetime with a decrease in ketone concentration.

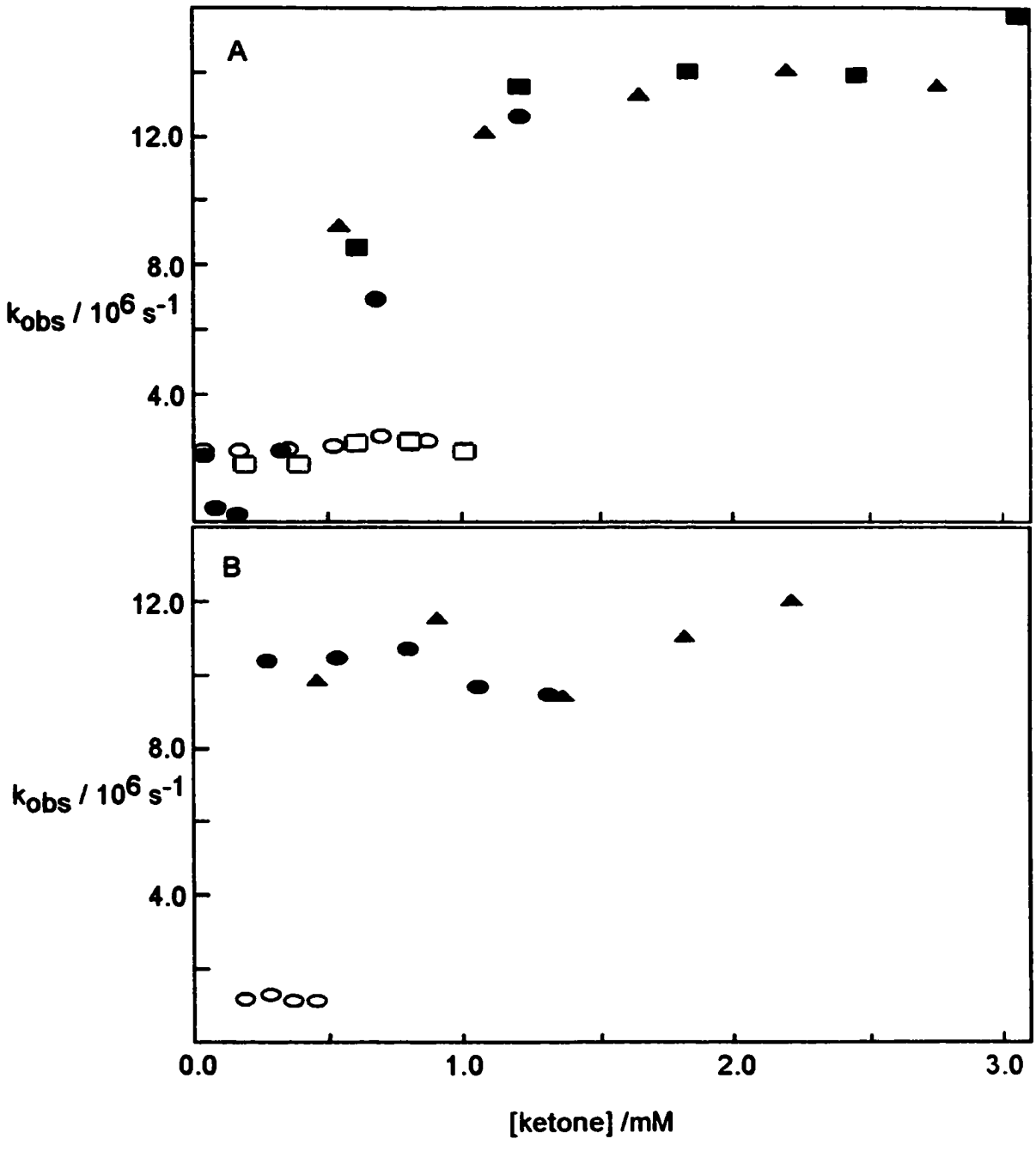

Figure 3.7 Dependence with ketone concentration of the observed rate constant for the fast triplet decay at 600 nm, of Bp (A) and DMBp (B) in the presence of NaCh. The open symbols are solutions in the presence of 10 mM of NaCh while closed symbols are solutions in the presence 40 mM of NaCh. The different symbols correspond to independent experiments.

3.1.3.3 Kinetic processes for Bp and DMBp in NaCh aggregates in the 540 nm region

The kinetics for the ketyl radical for both ketones were followed at a monitoring wavelength of 540 nm. Although both the triplet excited state and ketyl radical absorb in this region, the kinetics for the ketyl radical could still be studied because the transient spectra showed that the Bp ketyl radical was longer lived than the triplet excited state. Initially, a fast decay was detected (Fig. 3.8), followed by a much slower decay. The lifetime for the fast decay at 540 nm was always comparable to the lifetime of the fast decay at 600 nm, and both of these were the decay of the excited triplet states of the ketones.

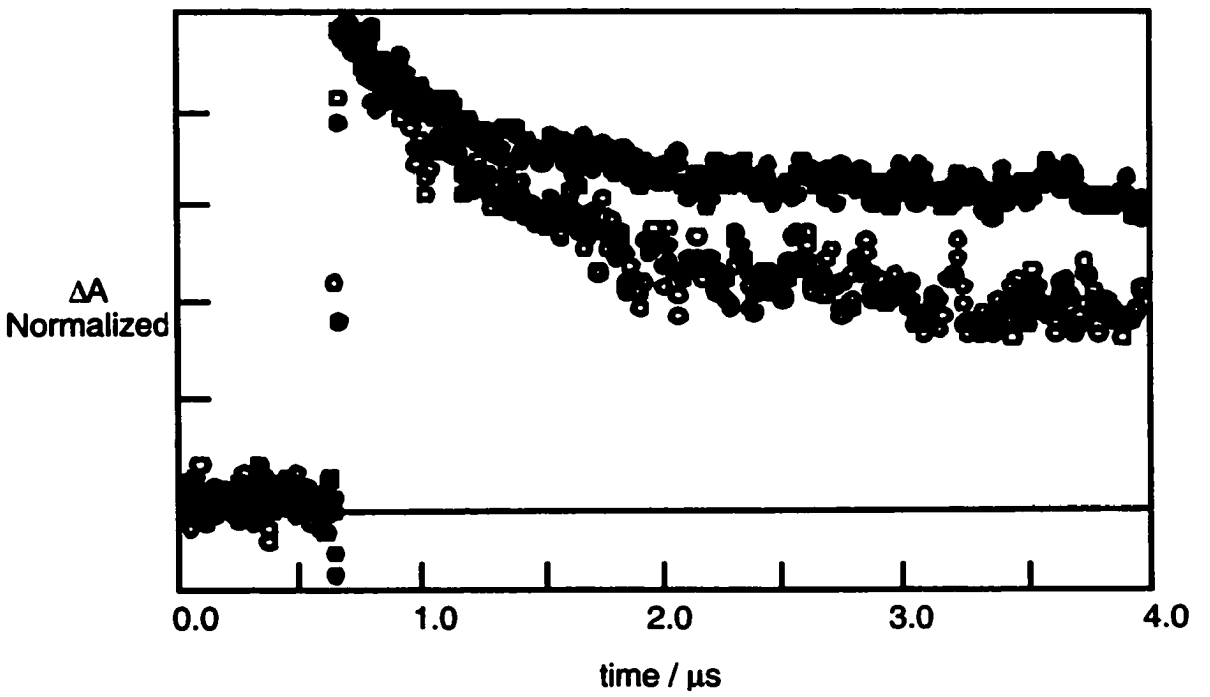

Figure 3.8 Transient kinetics at 540 nm in the presence of 10 mM of NaCh for Bp (●, 1.0 mM) and DMBp (O, 0.44 mM)

At high concentrations of Bp (> 2.0 mM) and in the presence of 40 mM of NaCh, the kinetics for the system were much more complex. The initial fast decay was still present, but it was no longer followed by the slow decay. In this case, a growth followed the initial fast decay (Fig. 3.9 (A)). The species growing was then observed to decay over a long time scale (Fig. 3.9 (B)).

The growth accounted for 15 to 30 % of the total ketyl radicals present at 540 nm. The growth was most predominant when the Bp concentration was high; in these cases, the lifetime of the growth at 540 nm, was observed to correspond to the lifetime of the long lived species decaying at 600 nm, to within 20 %. At lower Bp concentrations, the growth and the slow decay at 600 nm were comparable within a factor of 2. The larger error in the second case arose from the poor signal-to-noise ratio when measuring the small amplitude of the growth. The growth was not observed for Bp at concentrations lower than 2 mM, or when the NaCh concentration was lower then 40 mM. There was no growth observed for any of the experiments carried out using DMBp, whereas in all cases the kinetic traces showed the fast decay of an initial species, followed by a second much slower bimolecular decay.

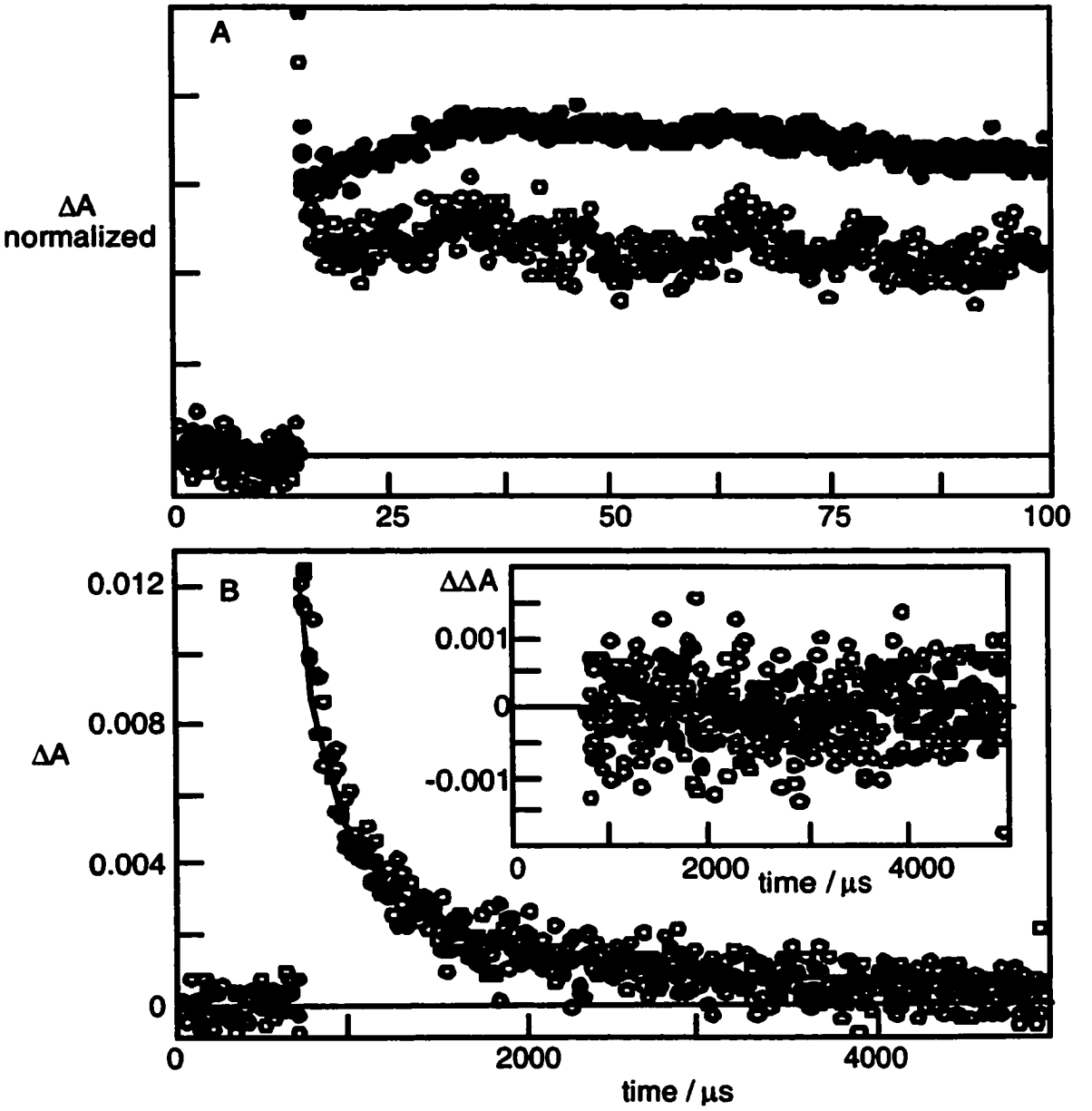

Figure 3.9 Kinetics at 540 nm in the presence of 40 mM of NaCh. (A) Normalized transient decays for Bp (●, 2.7 mM) and DMBp (O, 2.2 mM) illustrating the growth observed for Bp. (B) Decay of the Bp ketyl radical after the growth shown in A. The solid line represents the fit to a bimolecular decay and the residuals for the fit are shown in the inset.

The relative amount of ketyl radical was calculated for the signal at 540 nm. The value for the amount of ketyl radical, A_{ketyl} was taken as the absorbance value after the decay of the triplet (the initial fast decay). The absorbance maximum immediately after the laser pulse represented the total absorbance of all transients, which were monitored (A_t). The ratio of A_{ketyl}/A_t gave the relative amount of ketyl radicals with respect to the total species (ketyl radicals and triplet excited states) observed. When a growth was observed, the amount of ketyl radical present was taken before the onset of the growth. As can be seen in Table 3.3, the relative amount of Bp ketyl radical formed was higher in the presence of 10 mM of NaCh than in the presence of 40 mM of NaCh. The decay of the ketyl radical was always second order in ketyl, meaning that the decay of the ketyl radicals occurred via the recombination of two ketyl radicals. It was also noted that the relative amount of ketyl radical formed was lower for DMBp than for Bp when comparing similar ketone and NaCh concentrations (Tables 3.3 and 3.4).

Table 3.3 Dependence of the relative ratios of ketyl absorption to the total absorption and the $2k/\varepsilon l$ values on varying concentrations of NaCh and Bp at 540 nm. Errors are average deviations of two independent experiments.

[NaCh] / mM	[Bp] / mM	A_{ketyl} / A_t	$2k/\varepsilon l / 10^5\ s^{-1}$
10	0.9 - 1.0	0.60	15 ± 1
10	0.55 - 0.6	0.60 ± 0.02	17 ± 6
10	0.2 - 0.3	0.56 ± 0.08	19 ± 6
10	0.03 - 0.05	0.36 ± 0.02	---
40	2.7 - 3.0	0.43 ± 0.01	3.3 ± 0.9
40	1.1 - 1.2	0.41 ± 0.01	4.8 ± 0.2
40	0.6 [a]	0.36 [a]	5.4 [a]
40	0.14 - 0.15	0.30 ± 0.05	---

(a) data from only one experiment.

Table 3.4 Dependence of the relative ratios of ketyl absorption to the total absorption and the $2k/\varepsilon l$ values on varying concentrations of NaCh and DMBp at 540 nm. Errors are average deviations of two independent experiments.

[NaCh] / mM	[DMBp] / mM	A_{ketyl} / A_t	$2k/\varepsilon l / 10^5\ s^{-1}$
10	0.35 - 0.45	0.34 ± 0.02	---
10	0.09	0.22[a]	---
40	2.2	0.23[a]	3.1[a]
40	1.3 - 1.4	0.22 ± 0.03	3.7[a]
40	0.78 - 0.88	0.23 ± 0.01	4.4[a]
40	0.26	0.16[a]	---

(a) data from only one experiment.

As can be seen in Table 3.3, the apparent first order rate constant for the recombination of ketyl radicals ($2k/\varepsilon l$) for Bp decreased with an increase in the concentration of NaCh. For Bp at concentrations below 0.2 mM reliable data for the value of $2k/\varepsilon l$ was not recovered. For DMBp, values for $2k/\varepsilon l$ obtained at 40 mM of NaCh were found to be similar to those recovered for Bp in the presence of 40 mM of NaCh (Tables 3.3 and 3.4).

Diluting the ketone (Bp or DMBp) concentration did not have an effect on the apparent first order rate constant for the decay of the ketyl radicals. Further, in most cases, the ratio of ketyl radical to total species decaying did not change when the Bp concentration was decreased. The exception was at very low ketone concentration where the ratio was observed to decrease.

3.1.3.4 Deactivation of ketone transient species with quenchers

Quenching is a useful technique for studying the interactions between a supramolecular system and a photophysical probe. In this work, choosing two different quenchers that would target the different transients was key in understanding the dynamics of Bp and DMBp with NaCh aggregates. Nitrite was used to study the quenching of the triplet excited states. Oxygen was used because it quenches both the triplet excited state as well as the ketone ketyl radical. By comparing the different outcomes for the quenching experiments with nitrite and oxygen, assignments could be made for all the transients observed in this study.

3.1.3.4.1 Nitrite quenching

As mentioned previously, nitrite quenches triplet excited states[51,73] but not ketyl radicals. Studying the kinetics at 540 nm, it was found that nitrite quenched the initial fast decay effectively but not the long-lived signal. The initial fast decay corresponded to the fast decay at 600 nm and is assigned to a triplet excited state. The pursuing longer-lived decay was believed to be a ketyl radical and thus it was expected that the long-lived decay would be unaffected by the addition of nitrite. The lifetimes of both decays at 600 nm were shortened with the addition of nitrite.

Quenching studies can be used to determine characteristics other than the quenching rate constant of an excited state probe. In previous work, it was shown that quenching of the triplet states in the presence of a supramolecular system led to curved quenching plots.[9,51] In these plots, the observed rate constant was plotted against quencher concentration. When a downward curvature was present the interpretation was such that

the dynamics of the system had reached a stage where exit of the excited state probe from the host system had become the rate determining step (Section 1.1.3.1.1).[8,89,90] This stage was reached when the quencher concentration was high enough to have quenched the excited state molecules in the aqueous phase. Thus, quenching studies may be used as evidence to support the location of the probe based on the shape of the quenching plot generated, as well as by using the quenching rate constants determined.

For Bp, the quenching of the fast component at 600 nm gave rise to linear quenching plots (Fig. 3.10) at all NaCh concentrations. The quenching rate constant was always the same, within experimental error, regardless of the ketone or bile salt concentration. The average value recovered was $(3 \pm 1) \times 10^9$ $M^{-1}s^{-1}$ (9 determinations). This value was the same as the quenching rate constant of triplet Bp in water by nitrite.

The second component in the kinetics at 600 nm, at all host concentrations, was also quenched by nitrite, although less efficiently (Fig. 3.10). The quenching rate constant recovered was less than 6×10^7 $M^{-1}s^{-1}$, and the plots were also linear. The fact that the transient was quenched by nitrite suggests that this transient is a triplet excited state.

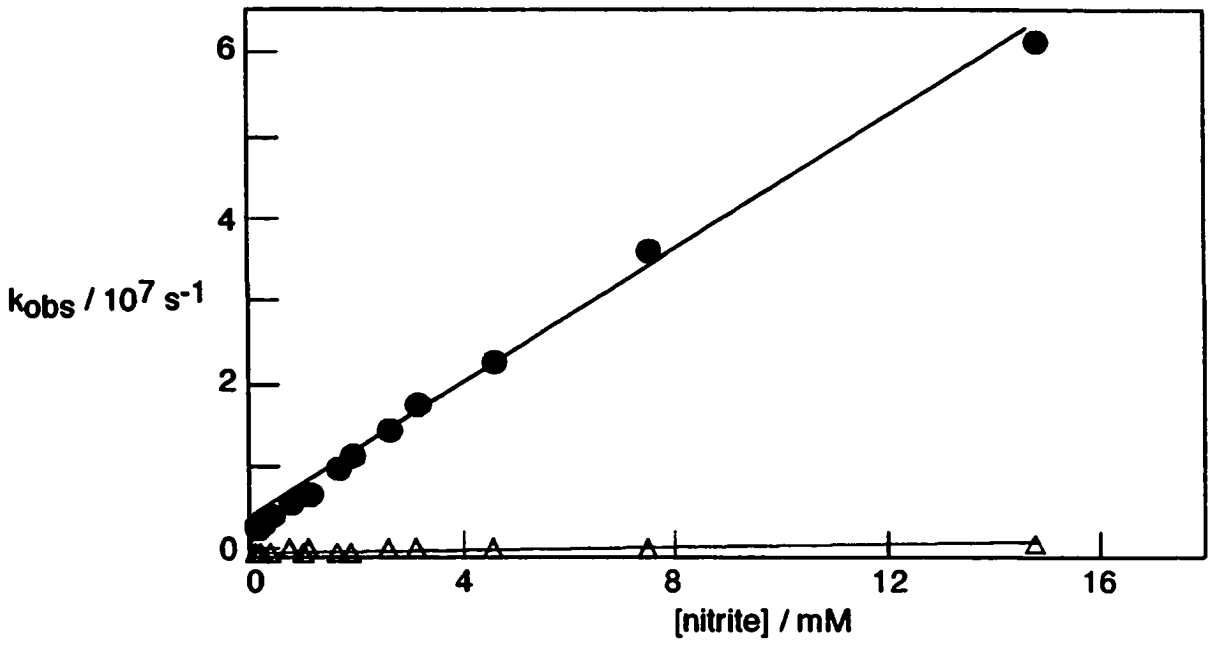

Figure 3.10 nitrite quenching plot, for one of the independent experiments, for the triplet excited state of Bp at 600 nm. Fast (●) and slow (Δ) triplet components in the presence of 10 mM of NaCh.

For DMBp, the results for the quenching of the initial fast component in the presence of 10 mM of NaCh were similar to those described above for Bp. The plots were linear (Fig. 3.11), with a quenching rate constant of (4.9 ± 0.5) x 10^9 $M^{-1}s^{-1}$ (2 determinations). In the presence of 40 mM of NaCh, a curved quenching plot was observed for the fast component (Fig. 3.11). Data from two separate experiments were combined and the curved quenching plot was fitted using Equation 1.16. The k_o value (decay in water) was determined by substituting the DMBp concentration, k_{sq}, and k_{obs} into the self-quenching equation (Equation 1.11, with Q = DMBp) and calculating the value of k_o to be equal to 4.3 x 10^5 s^{-1}. The value for k_q was fixed at 4.9 x 10^9 $M^{-1}s^{-1}$, as was determined independently (see above). The value for k_{NaCh} was determined from the

decay in the absence of quencher, and was fixed to the average value between the two experiments of $1.07 \times 10^7\ s^{-1}$.

The parameter k_q (H) can often span a wide range of values and still provide an adequate fit for the data; thus, often only ranges are reported for this parameter. Using the minimum and maximum values for this range, the other parameters recovered were relatively constant. For DMBp in the presence of 40 mM of NaCh, the range for k_q (H) was determined to be from 0 to $1 \times 10^7\ M^{-1}s^{-1}$. The values recovered for k_- and k_+/N were $(1.2 \pm 0.1) \times 10^7\ s^{-1}$and $(4 \pm 1) \times 10^8\ M^{-1}s^{-1}$, respectively. The errors for these parameters correspond to the error between the values recovered when using the low and high values stated for the range of k_q (H) values.

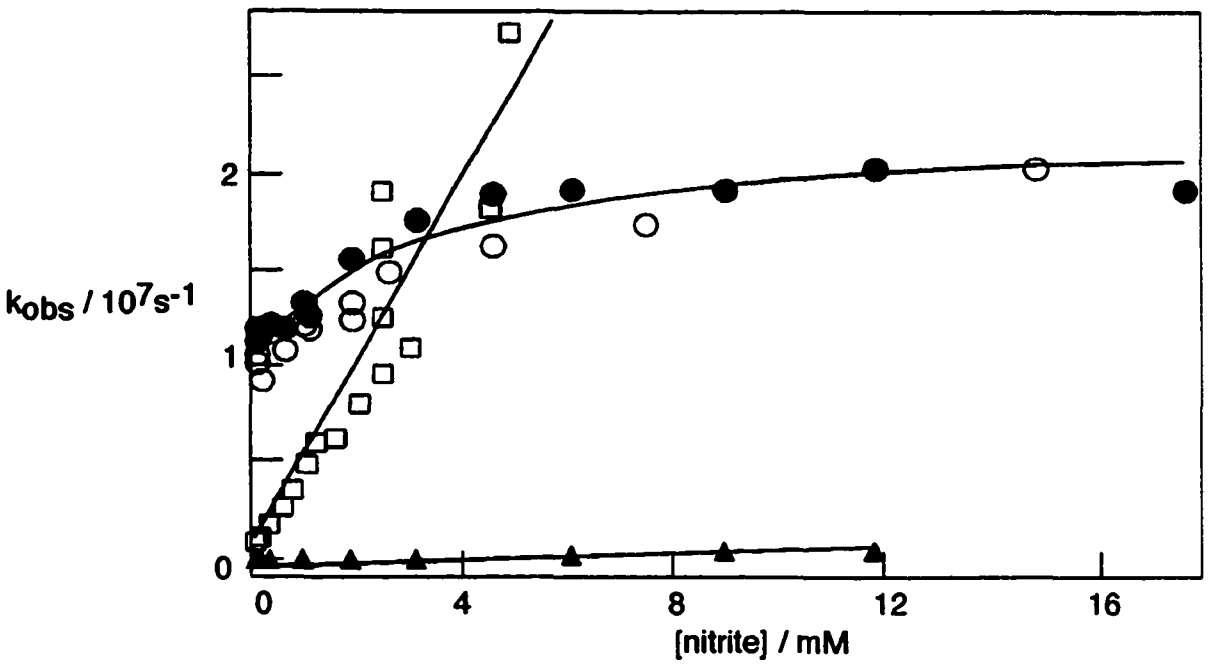

Figure 3.11 Nitrite quenching plot for the fast component of the triplet excited state decay of DMBp in the presence of 10 mM of NaCh(□) and 40 mM of NaCh (○,●, two independent experiments), and the slow component of the decay in the presence of 40 mM of NaCh(▲).

For DMBp the slower component at 600 nm was quenched by nitrite, and the plots were linear (Fig. 3.11). The only data that could be studied with any reliability for the slow decay at 600 nm was at high ketone and bile salt concentrations. At all other conditions the signal-to-noise ratio was too poor to perform adequate analysis. The quenching rate for DMBp in the presence of 40 mM of NaCh was 4 x 10^7 $M^{-1}s^{-1}$.

3.1.3.4.2 Oxygen quenching

In order to test the hypothesis that the two transients present in this study were the triplet excited state and the ketyl radical of the ketones, oxygen was used as a second quencher. Oxygen quenches both the triplet excited state as well as the ketone ketyl radical. It was found that oxygen did shorten the lifetimes of all the transients observed at both 600 nm and 540 nm for both ketones. For Bp, the quenching rate constant for the fast component of the decay at 600 nm was found to be high. A range for the quenching rate constant for this component of (3 – 7) x 10^9 $M^{-1}s^{-1}$ was recovered from data in the presence of 10 mM and 40 mM of NaCh. Oxygen was also efficient at quenching the slower component for the triplet Bp decay at 600 nm, with a quenching rate constant range of (0.8 – 2.0) x 10^9 $M^{-1}s^{-1}$.

3.2 Discussion

3.2.1 Bp and DMBp in aqueous solution

As mentioned in Chapter one, this study used the model of primary and secondary aggregation to explain the chemistry under investigation. The important feature of this model is that two regions of different hydrophobicities are present for binding of the probe molecules at high bile salt concentrations. At low bile salt concentrations (10 mM) only primary aggregates are present with a hydrophobic binding site. At higher bile salt concentrations ($\geq$ 20 mM), secondary structures form by the combination of primary aggregates that yield additional hydrophilic binding sites.

It was of interest to determine which hydrogen(s) on the bile salt aggregate was (were) most likely being abstracted by the triplet excited state of Bp and DMBp. There

are five chemically different hydrogens present on the bile salt molecule: the hydrogen of the alcohol group, primary alkane hydrogens on the methyl groups, secondary and tertiary alkane hydrogens on the ring structure, and alcohol methine hydrogens. In order to understand which hydrogen may be abstracted, the bond dissociation energies were critical. Table 3.6 lists appropriate values for the bond dissociation energies for the five types of bonds mentioned above. The bond dissociation energies were not measured for bile salt molecules; however, using base hydrocarbons as models gave an understanding of the relative bond strengths. The alcohol hydrogen was modeled with methanol, while the primary, secondary and tertiary hydrogens were modeled with ethane, propane, and 2-methylpropane, respectively. The alcohol methine hydrogen was modeled using various alcohols including ethanol and 2-propanol.

Table 3.6 Bond dissociation energies (BDE) for the various hydrogens present on bile salt molecules.

Species	Bond dissociation Energy
Alcohol hydrogen	102 kcal mol^{-1} [91]
Primary alkane hydrogen	100 kcal mol^{-1} [92]
Secondary alkane hydrogen	96 kcal mol^{-1} [92]
Tertiary alkane hydrogen	93 kcal mol^{-1} [92]
Alcohol methine hydrogen	88-91 kcal mol^{-1} [93]

As can be seen from the values in Table 3.6, the weakest bond is the alcohol methine hydrogen. A comparison of the difference in rate constants for hydrogen

abstraction between the tertiary alkanes and alcohol methine hydrogens was calculated. Using the highest value for the BDE of the alcohol methine hydrogens, it was found that abstraction of the alcohol methine hydrogen would be at least 78 times faster than abstracting the tertiary hydrogen. It was, therefore, assumed that the hydrogens that were the most likely to be abstracted were the alcohol methine hydrogens. The carbon atoms bearing the abstractable hydrogens are highlighted in Scheme 3.1.

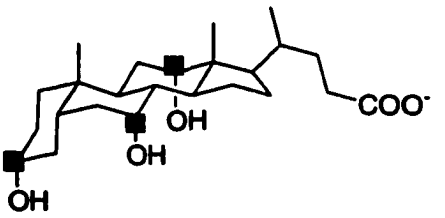

Scheme 3.1 Location of hydrogen atoms most likely to be abstracted from a NaCh molecule.

3.2.2 Reactivity of ketones in NaCh primary aggregates

Primary aggregates are formed by the aggregation of the hydrophobic backbones of the NaCh monomers leading to a hydrophobic binding site.[19,42,52] At 600 nm, two transients with different lifetimes were observed at all bile salt concentrations, and at low and high ketone concentrations. Both transients were quenched by nitrite; thus, two different triplet species were detected in the presence of primary aggregates. For Bp, the quenching rate constant by nitrite for the first transient ($(3 \pm 1) \times 10^9$ $M^{-1}s^{-1}$) was similar to that of Bp in water ($(4.0 \pm 0.6) \times 10^9$ $M^{-1}s^{-1}$). Thus, this excited triplet state was located within the aqueous bulk, and not within the NaCh aggregates. The quenching rate constant, by nitrite, for the second transient was found to be significantly smaller, with $k_q = 6 \times 10^7$ $M^{-1}s^{-1}$. As this rate constant was almost two orders of magnitude smaller than

the rate constant in water, it was reasonable to assume that the transient was less accessable to the aqueous quencher, and thus located within a binding site of NaCh. In the presence of 10 mM of NaCh, only primary aggregates are present, and as such, this triplet was assigned to being located within the primary aggregate.

For DMBp in the presence of 10 mM of NaCh, quenching studies were only carried out on the initial fast decay at 600 nm because the signal to noise ratio for the slower decay was poor, and reliable data were not obtained. The quenching rate constant recovered in the nitrite quenching experiments for the initial fast decay was similar to that in water, with an average k_q of $(4.9 \pm 0.5) \times 10^9$ $M^{-1}s^{-1}$. This transient was assigned to the decay of DMBp in the aqueous bulk.

The lifetime of the ketone triplet excited state corresponding to the fast decay at 600 nm was much shorter (hundreds of nanoseconds) than that of the triplet excited state of Bp or DMBp in water. The triplet lifetime was therefore affected by the presence of the NaCh. The second decay at 600 nm had a much slower decay lifetime, of several microseconds. Other possible assignments for the slow decay were considered for the transients and discarded based on the following observations. The ketyl radical can be ruled out as it would not be quenched by nitrite. The ketone radical cation and anion were also not possible. Bp radical cations have been shown to react readily with water, and the absorption of this transient is at shorter wavelengths.[78,81] The solvated electron that was needed to form the radical anion would have been quenched by nitrous oxide.[83] Thus, if the signal was due to radical anions, in the presence of nitrous oxide there were no solvated electrons and thus, the anion would not form. The only assignment possible for these transients, therefore, was the triplet excited state of the ketones.

There were two possible bimolecular deactivation pathways for the triplet excited state of the ketones to undergo in the absence of quencher: hydrogen abstraction from the NaCh molecules or self-quenching if the triplet excited state entered the aggregate and encountered another (ground state) ketone. To test for the self-quenching hypothesis, dilution experiments were performed to determine whether the lifetime of the excited state ketone changed with a decrease in the overall concentration of the ketone, as self-quenching is dependent upon the ground state ketone concentration. For solutions in the presence of 10 mM of NaCh, no effect of ketone concentration was observed. As the ketone concentration did not affect the lifetime of the transients, it can be assumed that an excited triplet state entering a primary aggregate did not encounter another ketone molecule within the aggregate. If this were the case, as the concentration of ketone was increased a self-quenching effect would have been noticed. Self-quenching can also take place in the form of static quenching. Static quenching takes place within a binding site and cannot be ruled out in this study; however, when discussing self-quenching, the process being described is the encounter of a triplet excited state ketone molecule with a ground state molecule upon entering a binding site.

Each monomer of NaCh has three alcohol methine hydrogens. It was assumed that the rate constant for hydrogen abstraction would be similar to that determined for the hydrogen abstraction from 2-propanol (above). In such a case, the upper limit for the rate constants for hydrogen abstraction from NaCh would be 8.7×10^6 $M^{-1}s^{-1}$ and 1.7×10^6 $M^{-1}s^{-1}$ for Bp and DMBp, respectively (i.e. three times the determined rate constants for 2-propanol). The product of the rate constant for hydrogen abstraction and the concentration of NaCh yields the upper limit for the observed rate constant for the

formation of ketyl radicals from triplet excited states in the aqueous phase. This is due to the fact that the formation of ketyl radicals will depend upon how easily a ketone triplet excited state encounters the NaCh aggregate (depends on [NaCh]) and how quickly it reacts with the NaCh to form the ketyl radical. Calculating this limit in the case of 10 mM of NaCh yields values of $8.7 \times 10^4\ s^{-1}$ and $1.7 \times 10^4\ s^{-1}$ for Bp and DMBp, respectively. The reciprocal value for the duration of the laser pulse is $10^8\ s^{-1}$. Since the reciprocal value for the laser pulse is higher than the calculated formation of ketyl radicals, and a signal from ketyl radicals was seen directly after the laser pulse, it can be concluded that ketyl radicals were formed within the laser pulse. Furthermore, they were formed by the reaction of Bp triplets that were solubilized within the bile salt aggregate.

Although the most extractable hydrogens on the NaCh monomer are the alcohol methine hydrogens, it must be pointed out that these hydrogens are located in an equatorial position on the bile salt backbone, and are not oriented towards the center of the primary aggregate. Thus, when discussing hydrogen abstraction within the primary aggregate, it is not possible that the alcohol methine hydrogens are involved. As such, the most likely hydrogens abstracted within the primary aggregate are the tertiary alkane hydrogens.

It was observed that hydrogen abstraction occurred in the presence of primary aggregates to a greater extent than in the presence of secondary aggregates; as can be seen in Tables 3.3 and 3.4 when looking at the ratio of A_{ketyl} / A_t. In the presence of primary aggregates, triplet excited states of the ketone were located within the primary binding site and within the aqueous bulk. If the hydrogen abstraction reaction was occurring between the excited triplet ketone in the aqueous bulk and the outside of the

primary aggregate, than a decrease in the hydrogen abstraction rate constant in the presence of secondary aggregates would not be expected. Thus, the hydrogen abstraction reaction observed in the presence of primary aggregates was occurring within the primary binding site.

A final point of interest, when the probe molecules were in the presence of primary aggregates, was to see how the structure of the probe would affect the binding to this rigid sight. It was of interest to note that the lifetime of the slow decay at 600 nm was shorter for Bp in comparison with DMBp. There are two possible reasons for this observation. The hydrogen abstraction rate constant for Bp is higher than for DMBp; thus, as Bp ketyl radicals were formed faster than DMBp ketyl radicals, the lifetime for triplet Bp would be shorter. The residence time of the probe within the aggregate would also affect the lifetime of the transient. If the triplet lifetime was determined only by the exit process, then the exit rate constant for DMBp ($(0.5 - 1) \times 10^5\ s^{-1}$) would be slightly lower than that for Bp ($(0.8 - 5) \times 10^5\ s^{-1}$), as would be expected for the more hydrophobic probe. It is of interest to note that the exit rate constant for Np from the primary site was previously reported as being $(1.0 \pm 0.4) \times 10^6\ s^{-1}$;[51] thus, there is at least a factor of two difference in the exit rate constant between the Bps and Np from the primary site. This observation suggests that the binding to the primary site is sensitive to the structure of the probe molecule, whereas it was determined that binding to the secondary site was much less selective (vide infra).

3.2.3 Reactivity of ketones in NaCh secondary aggregates

With the formation of secondary aggregates, the system was more complex because two possible binding sites were available for probe molecule interactions. At high concentrations of NaCh the primary aggregates interacted to form secondary aggregates with a hydrophilic binding site.[51-53,94] The results at higher bile salt concentration were consistent with an increased level of complexity. Having two distinct binding sites of varying hydrophobicities within the NaCh aggregates allowed for an examination of the effect of hydrophobicity of the guest on the binding dynamics with the NaCh aggregates.

As was mentioned in Chapter one, data on the size and aggregation number for NaCh aggregates is disputed in the literature.[28-30,48,66,67] This study presents the first estimates of the aggregation number based on triplet excited state investigations of probe molecules within these aggregate systems.

3.2.3.1 Triplet excited state reactions

One of the first differences observed when secondary aggregates were present was a decrease in the lifetime of the triplet excited Bp, with an increase in the Bp concentration. The nitrite quenching rate constants for the initial fast decay were similar to those obtained for the ketones in water, suggesting that either the triplet was located within the aqueous phase or the dynamics with the secondary aggregate were extremely fast. The data recovered in this study suggested that the process was not taking place entirely in the aqueous phase. At all concentrations studied, the lifetime of triplet Bp in water was much longer than Bp in the presence of NaCh. At high Bp concentrations (ca.

2.5 mM), the lifetime determined for the triplet in water was found to be ca. 2.8 μs. In the presence of 40 mM of NaCh, the triplet lifetime of Bp (2.5 mM) was 70 ns. Thus, the decrease in the triplet lifetime must be related to processes taking place within the NaCh aggregates.

The most likely explanation for the kinetic data observed was that the dynamics (entry and exit) involving the secondary site were extremely fast. In other words, there was interaction between the triplet excited state ketones and NaCh aggregates; however, the interaction occurred on a time scale that was too fast to be detected using the nitrite quenching methodology. The residence time for the excited state probe within the aggregate system would need to be greater than 25 ns, in order for the exit of the probe from the site to be detected by the quenching methodology because of the time resolution for the kinetic measurement. The fact that a linear quenching plot was observed, as opposed to a curved plot suggested that the dynamics involving the secondary aggregate, for Bp, were extremely fast. It was assumed that association with secondary aggregates was very fast, in fact, close to the diffusion limit. An exit rate constant of 4×10^7 s^{-1} corresponds to the minimal residence lifetime of 25 ns mentioned above. Since the exit of the probe was not detected by the methodology the rate constant must be greater than 4×10^7 s^{-1}. This was not the case for DMBp where a curved quenching plot was observed in the presence of 40 mM of NaCh. The residence time for DMBp was longer than for Bp (83 ns, vide infra); thus, the entry and exit of DMBp were detectable by nitrite quenching experiments, and led to the curved quenching plot observed (vide infra).

The oxygen quenching rate constant for Bp in water was determined to be 2×10^9 $M^{-1}s^{-1}$; thus, it appeared that the fast component of the decay in the presence of NaCh was

quenched with a higher rate constant than in water. This may be explained by the fact that oxygen may be present in somewhat higher concentrations due to a higher solubility in the presence of NaCh aggregates. It must be noted that this change in solubility was not accounted for in the calculations, as the values for the oxygen concentration in water[69] were used in calculating the quencher concentration in the presence of bile salt.

All experiments were carried out with the bile salt aggregate concentration (when secondary sites are present) in excess of the ketone concentration; therefore, the entry rate constant for Bp (k_e[secondary sites]) did not vary with varying Bp ground state concentration. Once the triplet Bp entered the NaCh aggregate there were three possibilities: the triplet could exit back to the aqueous phase, it could undergo hydrogen abstraction, or if it encountered a ground state ketone, it would be self-quenched.

At low Bp concentrations, the probability of a triplet excited state finding a ground state Bp in the secondary site was low. This is due to the fact that the encounter of the two Bp molecules depends upon the concentration of Bp as well as the association of the excited state molecule with the aggregate. Consequently, self-quenching did not compete with the other two processes, at low Bp concentrations.

At low Bp concentrations, the observed rate constant was approximately 1×10^6 $M^{-1}s^{-1}$. This value was lower than the observed rate constant when only primary aggregates were present, indicating a decrease in the hydrogen abstraction efficiency. One hypothesis may be that the decrease in hydrogen abstraction efficiency was due to the change in polarity of the two binding sites. It has been shown in the past that polarity does not affect the hydrogen abstraction rate constant;[86,88] thus, an alternative explanation must exist. The most likely explanation is that the likelihood of the triplet excited state

accessing an abstractable hydrogen was decreased in the secondary site compared to the primary site.

A decrease in the triplet lifetime was observed at high Bp concentrations. The most likely explanation was self-quenching of the triplet excited states by ground state Bp molecules located within the bile salt aggregates. Self-quenching was a more efficient process than hydrogen abstraction, so when the ketone concentration was high, self-quenching competed with the exit of the probe to the aqueous phase. To quantitatively analyze this data the concentration of secondary sites and the partition equilibrium constant between Bp and the secondary sites must be known. Neither of these parameters is known, so a quantitative analysis was not performed. These data were used to determine an estimate for the aggregation number of bile salts presented in section 3.2.4 below.

The slower exit rate for the triplet DMBp led to curved quenching plots when using nitrite as a quencher in the presence of 40 mM of NaCh. This was not observed for Bp, and this observation was consistent with the fact that DMBp is more hydrophobic than Bp. The exit rate constant recovered was 1.2×10^7 s^{-1}, which yields a residence lifetime of 83 ns for the triplet DMBp.

In contrast to the data for Bp, the lifetime for triplet DMBp did not vary when the concentration of the probe was decreased. For Bp, the decrease in lifetime was attributed to an increase in self-quenching when the ketone concentration was increased. There are two possibilities for the lifetime of DMBp not changing with an increase in the ketone concentration: the self-quenching rate constant for DMBp was higher than that of Bp,[95] making the process more efficient, or DMBp resided in the secondary aggregate for a

longer period of time. The longer residence time could have allowed the triplet excited probe to intra-aggregate migrate to a different secondary site, as opposed to exiting to the aqueous phase. If this occurred, and the triplet excited state encountered a ground state DMBp, then self-quenching would occur. Therefore, at lower concentrations of DMBp, the excited state probe molecule would have a longer period of time to encounter a ground-state molecule and self-quench. For these reasons, self-quenching would not vary with a change in DMBp concentration, and the lifetime would remain unaltered.

From the curved quenching plot of DMBp in the presence of 40 mM of NaCh, the value recovered for k_q/N was 4×10^8 M^{-1} s^{-1}. The estimated value of N for secondary sites is between 6 and 13 (vide infra), thus giving an association rate constant between (2.4 - 5.2) x 10^9 M^{-1} s^{-1} for the interaction of DMBp with the secondary aggregate. This result shows that the entry and exit dynamics of guests from the secondary site were fast. Furthermore, the data support the claim that the exit of a probe from the secondary site is dependent on the probe polarity.

3.2.3.2 The formation and reaction of the ketone ketyl radicals

In Tables 3.3 and 3.4, the ratio of ketyl absorption to total absorption at 540 nm gave an indication of how much ketyl radical was formed within the laser pulse. In this section, data for the secondary aggregates is compared with data in the presence of primary aggregates (10 mM) in order to gain a full understanding of the results. It was observed that the ratio of ketyl radicals to total species decaying remained fairly unaffected while varying the ketone concentration (for both Bp and DMBp). This observation suggests that the partitioning of Bp or DMBp between the aqueous phase,

primary site, and secondary site was not affected by altering the probe concentration. At very low ketone concentration a decrease was observed that suggested that the amount of ketyl radical formed within the aggregate was decreased.

One of the most interesting results in the study was the fact that the yield of ketyl radicals was higher when only primary aggregates were present (10 mM of NaCh), rather than when secondary aggregates were present. This result suggests that the main source for ketyl radicals was hydrogen abstraction by triplet Bp or DMBp from within the primary aggregate. At a higher bile salt concentration, there were two binding sites present in the NaCh aggregates where the probes were located. As the bile salt concentration was increased, there was an increase in the amount of ketone solubilized. Although more molecules of Bp/DMBp were solubilized within the aggregate at higher host concentration, the percentage of molecules located within the secondary site, as opposed to the primary site, could have been increased. If it is assumed that ketyl radical formation occurred mostly within the primary site, it is then clear why the value for the ratio of ketyl radicals formed decreased in the presence of secondary sites.

At both 10 mM and 40 mM of NaCh, it was observed that the ketyl radical yield for DMBp was lower than that for Bp. The hydrogen abstraction rate constant from 2-propanol, was lower for DMBp than for Bp; therefore, it is understandable that the yield of ketyl radicals would be lower for the more hydrophobic probe.

Another interesting finding of the study was the growth of ketyl radicals observed in the kinetics, in the presence of 40 mM of NaCh, and when the concentration of Bp was high. This growth was not observed when the concentration of the host or the guest were decreased, and it was absent in the kinetics for DMBp. The lifetime of the growth was

found to be between 2 to 13 μs, which was comparable to the lifetime of the slow decay at 600 nm. Hence, it would appear that the triplet state formed within the primary aggregate (vide supra) was responsible for the ketyl radical which was formed on a slow time scale at high Bp and NaCh concentrations.

It is probable that the slow formation of ketyl radicals occurs at all concentrations of Bp and DMBp, but may only be detectable when the total amount of ketyl radical being formed is high. This would explain the absence of a growth with DMBp, as the amount of this ketone solubilized was lower than that of Bp. Another possible explanation for the absence of the growth for DMBp was, once again, the lower hydrogen abstraction rate constant for this ketone when compared to Bp. It is impossible at this time to distinguish between the two explanations for the absence of a growth with the DMBp data.

The decay of the ketyl radicals was second order in ketyl radicals. For Bp, the apparent first order rate constant for the decay of ketyl radicals was observed to be larger in the presence of 10 mM of NaCh than in the presence of 40 mM of NaCh, by a factor of 3. The value for the molar absorptivity coefficient for the Bp ketyl radical in water was reported in the literature as 3000 $M^{-1}cm^{-1}$.[85] Using this value and assuming homogeneous irradiation of the sample over the entire 7 mm cell pathlength, the bimolecular rate constant was estimated. The values for the bimolecular rate constants for the decays of the Bp ketyl radical, in the presence of 10 mM and 40 mM of NaCh, were 1.8×10^9 $M^{-1}s^{-1}$ and 5.3×10^8 $M^{-1}s^{-1}$, respectively. The value at 10 mM of NaCh was similar to the rate constant for a diffusional process in water of two radicals. The diffusional rate constant in water has a value of 6×10^9 $M^{-1}s^{-1}$;[69] however, due to the fact that only 25 % of all

encounters for radicals will have singlet multiplicity, the expected rate constant for the encounter of two radicals in water is $1.5 \times 10^9 M^{-1}s^{-1}$. As the value for the bimolecular rate constant in the presence of 10 mM of NaCh was found to be similar to that in water, the ketyl radicals were recombining in the aqueous phase, after exiting the primary aggregate. In the presence of 40 mM of NaCh, the rate constant was substantially lower, indicating that the ketyl radical reactions may be occurring in a more restricted environment. Recombining within the secondary site would lead to a lower bimolecular rate constant, as the encounter of the radicals would be slowed by the presence of the supramolecular system. In this case, it is reasonable to assume the radical recombination reactions were taking place within the secondary aggregate, as well as in the aqueous phase. The ketone ketyl radical may recombine with another ketone ketyl radical or with a bile salt radical.

3.2.4 Size of primary and secondary aggregates

Using the competing reactions of self-quenching and exit of the ketone probes in the presence of secondary aggregates (mentioned above), the aggregation number for the primary and secondary aggregates was estimated. A schematic representation of the competing processes is shown in Scheme 3.2.

$$Bp^{3*} + Agg(Bp) \underset{k_-}{\overset{k_+}{\rightleftharpoons}} [Agg(BP^{3*}/Bp)] \xrightarrow{k_{sq}} Agg(2\,Bp)$$

Scheme 3.2 Reaction of triplet Bp with a ground state molecule of Bp located within the NaCh aggregates, leading to two possible deactivation pathways: self-quenching or exit of the Bp molecule, from the secondary site.

Assuming a scenario where k_{aq} is much larger than k_-, the ratio of rate constants is reduced to unity and leaves only the product of the fraction of occupied sites and the secondary site concentration. Dividing the 40 mM of NaCh by the combined aggregation number of 6 leads to a secondary site concentration of 6.7 mM. Therefore, when the secondary site concentration is 6.7 mM the fraction of occupied sites is 0.21.

To justify the validity of the secondary site concentration estimated above, the partition equilibrium constant for the system under the above conditions was calculated. In order to carry out this calculation, it was assumed that the distribution of Bp molecules within the secondary sites of NaCh followed a Poisson distribution, as was previously seen for micelles.[97] In order to use this mathematical analysis, it was assumed that to a first approximation the secondary sites can be viewed as micelles. The following characteristics of micelles were assumed: it was possible to bind more than one solute per secondary site, and the presence of a solute did not change the binding efficiency. As has been mentioned, the binding dynamics to the secondary site is very fast, and it appears that binding is not dependent on guest size; thus these assumptions were considered acceptable. The key information the Poisson distribution provides is the ratio of the concentration of incorporated guests with respect to the secondary site concentration (n) when the fraction of occupied sites (f) is known. (Equation 3.2)

$$f = (1 - e^{-n})$$

Equation 3.2

Using Equation 3.2 with f = 0.21, a value of n = 0.24 was recovered. Again, when the secondary site concentration was taken as 6.7 mM the concentration of bound Bp was

1.58 mM. The partition equilibrium constant of Bp when the total ketone concentration was 2 mM was calculated to be ca. 750 M^{-1}. (Equation 3.3) Values of 2040 M^{-1} and 6300 M^{-1} have been reported for acetophenone and xanthone, respectively, with SDS micelles;[98] thus the partition equilibrium constant (k_p) for Bp under the conditions used in this analysis was reasonable.

$$k_p = \frac{(Bp_{bound})}{(Bp_{unbound}) * (ss - Bp_{bound})}$$

Equation 3.3

where, Bp_{bound} represents the concentration of Bp bound within the aggregate system, $Bp_{unbound}$ represents the concentration of Bp not bound within the aggregate system, and ss represents the concentration of secondary sites.

The lower limit for the secondary site concentration, leading to an upper limit for the combined aggregation number, was estimated using reasonable values for f and the partition equilibrium constant. Assuming an f value of unity would assume that all the Bp was bound; however in the experiments aqueous Bp was observed, thus this would be unreasonable. If an upper limit of 0.5 was assumed for f, which was reasonable in conjunction with the observation of unbound Bp present, a lower secondary aggregate concentration of 2.8 mM was calculated. This led to a partition equilibrium constant of 3.8×10^4 M^{-1}. This value appears to be high suggesting that the secondary site concentration is probably higher than 2.8 mM. An upper limit of ca. 1.5×10^4 M^{-1} was considered more appropriate, based on the literature values mentioned above. Using this partition equilibrium constant a secondary site concentration of 3 mM and the fraction of occupied sites of 0.47 were calculated. A value of 0.47, for the fraction of occupied sites,

seems reasonable based on the amount of unbound Bp that was observed in this study. Thus, it was assumed that 3 mM was close to the lower limit for the secondary site concentration. Assuming a secondary site concentration of 3 mM (of a 40 mM NaCh solution) leads to an upper combined aggregation number (N_1N_2) of 13.

Thus, it can be stated that $6 \leq N_1N_2 \leq 13$. This means that, at most, 6 monomers can make up a primary site, as it must be assumed that at least 2 primary aggregates are needed to make up a secondary site. Conversely, it is also reasonable that, at most, a secondary site is defined by 4 primary aggregates, assuming that at least 3 monomers are necessary to define a primary aggregate. This finding does not contradict the possibility of larger aggregate structures existing with multiple secondary binding sites. Our findings would be consistent with a model in which one structure had many secondary binding sites; however, the intra-aggregate mobility would be too slow to compete with exit of triplet Bp from the secondary site into water.

3.2.4.1 Model for the Bp and DMBp reactivity in NaCh

It is evident throughout the work that the concentration of NaCh and thus the type of binding sites present affected the chemistry being observed. The reactivity of the ketones also appears to vary with varying hydrophobicities. In the presence of only primary aggregates, Bp and DMBp reacted similarly. In both cases there were various triplet states present. There were two triplet states located within the primary aggregate: one that formed a ketyl radical within the laser pulse, and another that was unreactive within the laser pulse and existed as a long lived triplet. There were also triplet states present in the aqueous solution. It was noticed that ketyl radicals located in the primary

aggregates recombined at rates that were diffusion controlled. This suggests that the ketyl radicals exited the primary aggregates into the aqueous phase, and then recombined.

When secondary aggregates were present, a layer of complexity was added to the system. All the processes present in the primary aggregate were still occurring; however, the introduction of a second binding site allowed for more chemical processes to take place. The exit of the probe from the secondary site was fast compared to the exit from the primary site. The reaction of the ketyl radicals was slowed in the presence of secondary sites. This observation suggests that the recombination reaction was likely occurring in the secondary sites as well as in the aqueous phase.

The triplet excited states of the ketones were also observed to exist in the secondary site. In the secondary site, three pathways were in competition with one another: self-quenching, hydrogen abstraction, and exit of the probe to the aqueous phase. As the residence time of the ketones was short in the secondary site, it was found that hydrogen abstraction did not compete with exit of Bp into the aqueous phase. Self-quenching was found to be a more efficient process than hydrogen abstraction, and as such was able to compete with the exit of triplet Bp to the aqueous phase. DMBp was found to have a longer residence time (83 ns) in the secondary site than Bp (the upper limit estimated was 25 ns), most likely due to the fact that the hydrophobicity is increased for DMBp as compared to Bp.

The aggregation number of bile salts has been previously hypothesized.[28,30,48,66,67] In work done by Tato and co-workers, the aggregation number for the primary aggregate was found to be between 3 and 5.[66] The researchers varied the concentrations of NaCl and NaCh, and determined the aggregation number based on freezing point determinations

and by measuring the sodium concentration, leading to measurements for the values of pNa. The same researchers determined similar aggregation numbers for other commonly studied bile salts: sodium taurocholate (2.59 ± 0.59), sodium deoxycholate (5.82 ± 0.04), and sodium deoxytaurocholate (5.42 ± 0.47) using the same techniques.[67] In light scattering work by Kratohvil and co-workers, aggregation numbers for sodium taurodeoxycholate and sodium deoxycholate were also estimated.[28] These researchers found that the aggregation number for primary aggregates varied from 3.5 to 13.6 as the NaCl concentration was increased from 0 M to 0.6 M for sodium taurodeoxycholate, and the value for sodium deoxycholate varied from 8.0 to 11.6 at NaCl concentrations of 0.15 to 0.6 M. In work done by Mazer and coworkers using light scattering, the researchers estimated the aggregation number of primary aggregates to lie between 4 and 10.[48] All the above research was carried out at concentrations of bile salts where only primary aggregates are present. In the current study the aggregation number is based on the incorporation of the Bp guest within the secondary aggregates. At these NaCh concentrations both primary and secondary aggregates are present and thus the amount of Bp bound is the amount bound to either the primary aggregates or the secondary aggregates. Thus, using the qualitative analysis above a value for the aggregation number of the primary aggregates was determined. The value calculated in this study of 3 to 6 monomer of NaCh for an aggregation number of the primary site seems reasonable.

The above data and explanations further validate the existence of two different and unique binding sites within sodium cholate aggregates in solution. The qualitative analysis carried out on the Bp self-quenching data also provides the first estimates on aggregation size from a dynamic study. It was shown that only a small number of

monomers of NaCh are actually required to define the primary and secondary binding sites.

4 Naphthalenes as probes in NaCh aggregates: effect of hydrophobicity and shape of a probe molecule on the binding dynamics

The naphthalene series of probes (1-EtNp, 2-EtNp, 1-NpOH, 2-NpOH, 1-NpO and 2-NpO, Fig. 1.15) was used to study two main features of complexation with sodium cholate aggregates. The effect of varying the probe hydrophobicity, as well as the effect of the shape of the probe, was investigated. From previous studies it was known that naphthalene resides in the primary aggregate site, while xanthone resides in the secondary site.[51] Based on this information, the series of Np probes was chosen with the intention of probing both complexation sites of NaCh aggregates.

4.1 Results of experiments at varying ionic strength

The experiments done in the first half of this chapter are the experiments that have been described as being carried out at varying ionic strengths (Section 2.2). The solutions contained 0.2 M NaCl; however, in the presence of ionic quenchers the ionic strength of the solution was increased. The ionic strength varied from 0.20 M to 0.25 M.

4.1.1 Steady-state fluorescence: a qualitative analysis of the binding location for the probe molecules

In most cases, the lifetime of a fluorescent probe molecule is much shorter than the lifetime of the dynamic processes occurring between the probe and the host aggregates. This being the case, the probe fluorescence reports on the environment in which the probe is located. Dynamic data for the system are obtained from triplet decay kinetics because triplet states have longer lifetimes. Fluorescence quenching experiments

gave an indication of the probe incorporation within the aggregate, as the quenching rate constant is a measure of the accessibility of the quencher to the probe molecule within the aggregate.

4.1.1.1 Emission spectra of probes in the presence of NaCh aggregates

The emission spectra of 2-NpOH, 1-NpOH, 2-EtNp, and 1-EtNp were all similar, with the emission spanning the spectral region of 315 nm to 400 nm. Figure 4.1 shows that the spectra had some fine structure with multiple peak maxima. For the alkane-substituted probes, a sharpening in the peaks was noted when the concentration of bile salt was increased, as well as a slight red-shift. The alcohol substituted Nps displayed slight red shifts in the emission spectra upon incorporation within the NaCh aggregate, but sharpening of the emission spectra was not noted (Fig. 4.1).

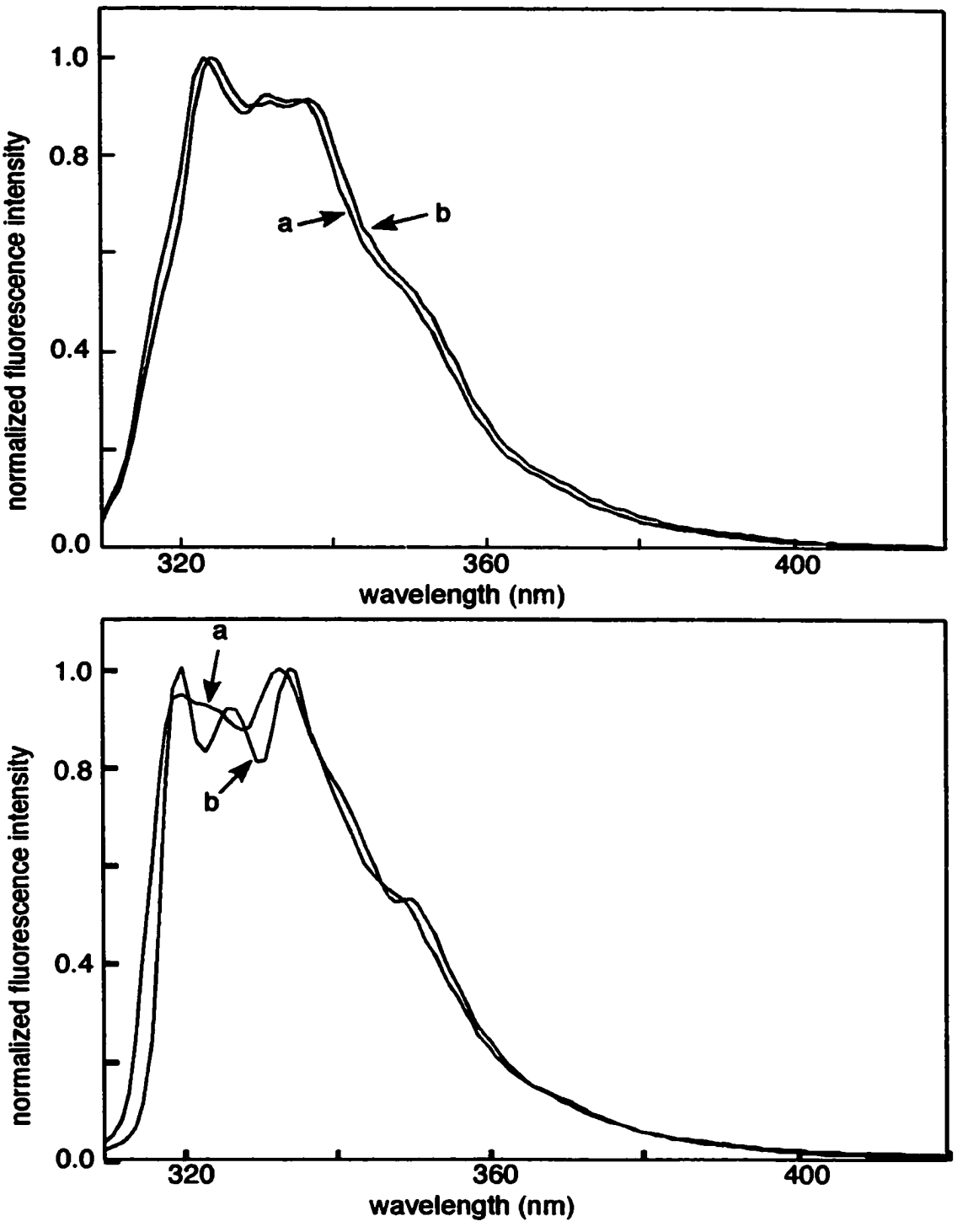

Figure 4.1 Normalized fluorescence emission spectra for the singlet excited states of 2-NpOH (top) and 2-EtNp (bottom) in the absence of NaCh (a) and in the presence of 40 mM of NaCh (b).

The emission spectrum of 2-NpO had different spectral features than those observed for the four previous probes. The emission was red shifted, and located between 375 nm and 550 nm. The peak did not show fine structure in the presence of NaCh, as was observed for the ethylnaphthalenes. No shift was noted upon the addition of 40 mM of NaCh, as was noted for the hydroxyl and alkyl substituents. 1-NpO did not fluoresce.

4.1.1.2 Quenching of the singlet excited states of the Np probes by sodium iodide

Deactivation of the singlet excited state of the various Np derivatives was studied using sodium iodide (NaI) as a quencher.[69] Upon the addition of NaI, the fluorescence emission intensity of all the probes was observed to decrease. Figure 4.2 shows an example for the fluorescence spectra of 2-NpEt, when the quencher concentration was increased.

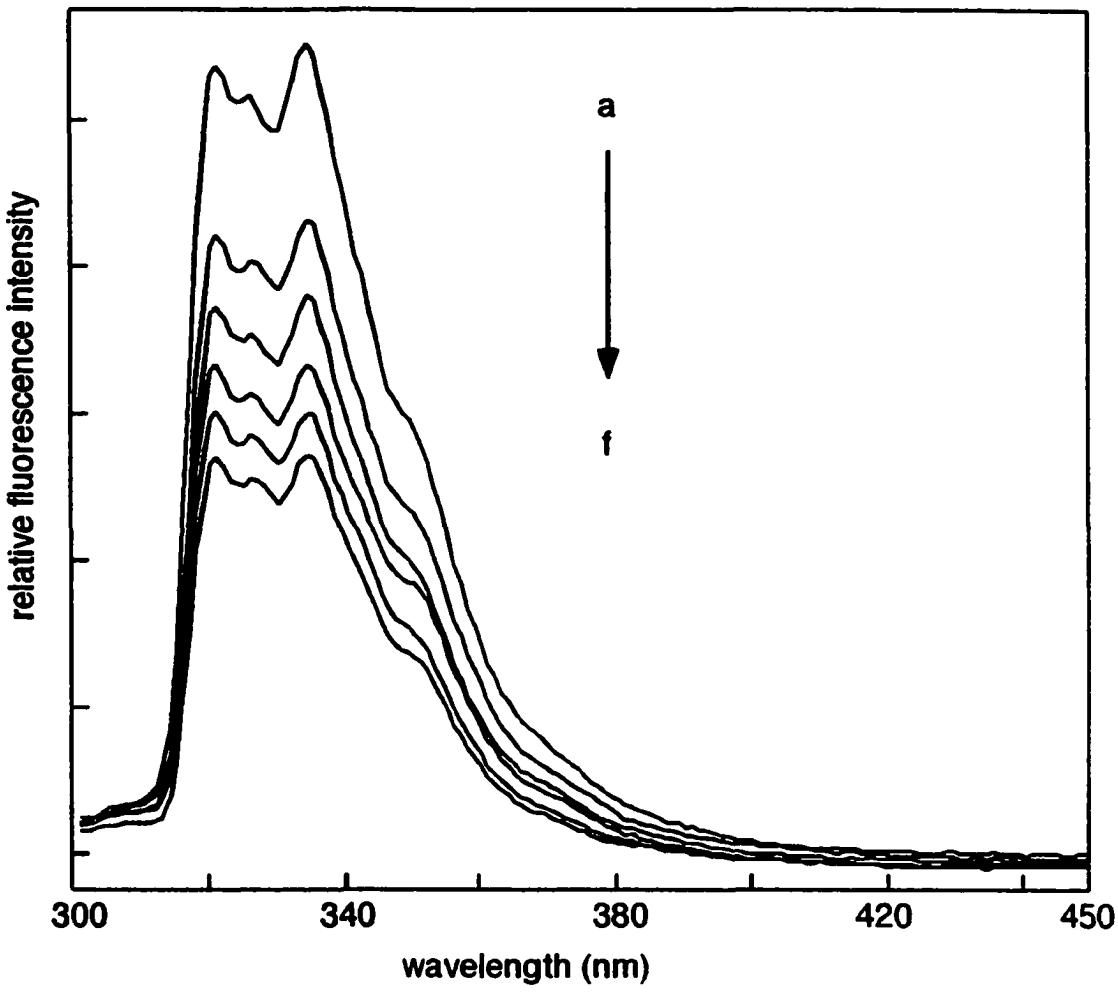

Figure 4.2 Quenching of the fluorescence emission spectra of 2-EtNp in the presence of 10 mM of NaCh with the following NaI concentrations: a = 0 mM, b = 10 mM, c = 20 mM, d = 30 mM, e = 40 mM and f = 50 mM.

The data from these emission spectra were analyzed in order to extract the Stern-Volmer constants (K_{SV}) for the probes in the presence of varying concentrations of NaCh. The K_{SV} values were obtained by plotting the ratio of the area of the emission spectrum in the absence of quencher divided by the area of the spectrum in the presence of quencher, against quencher concentration. The areas used in the integration were from 305 nm to 495 nm for the ethyl and hydroxyl substituted probes, and from 380 to 545 nm for the

carbonyl substituted probes. Following Equation 1.13 the Stern-Volmer constant was obtained from the slope of the plot (Fig. 4.3).

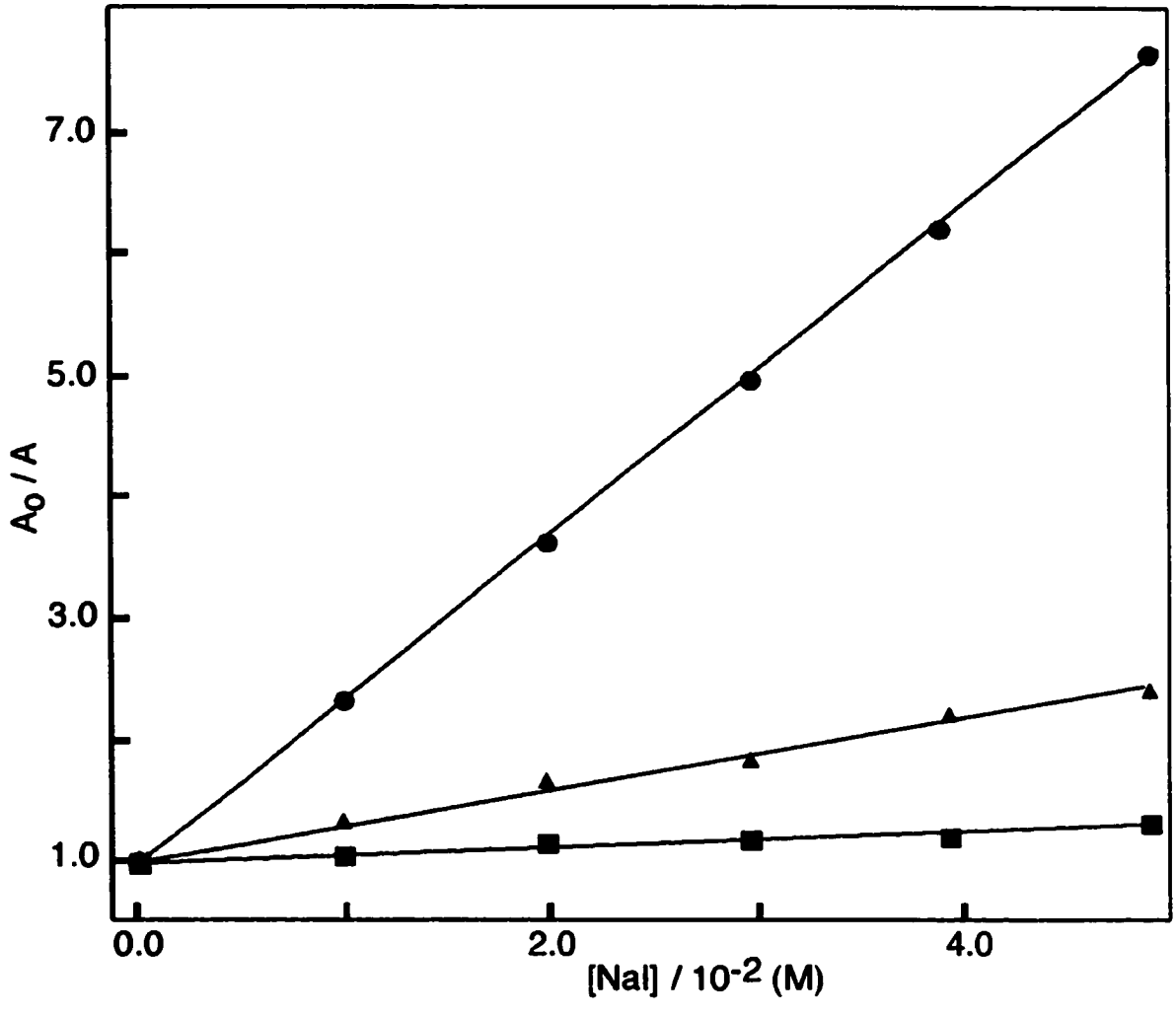

Figure 4.3 Stern-Volmer plots for the quenching by iodide of the singlet excited state of 2-EtNp in the presence of 0 mM (●), 10 mM (▲) and 40 mM (■) of NaCh.

Table 4.1 Stern-Volmer constants obtained from steady-state fluorescence quenching of the Np probes in the presence of varying concentrations of NaCh. The numbers in parentheses indicate the number of independent experiments performed to arrive at the average value.

[NaCh] / mM	$K_{sv}/10^1\ M^{-1}$				
	1-EtNp	2-EtNp	1-NpOH	2-NpOH	2-NpO
0	14.2 ± 0.5 [b] (2)	14.6 ± 0.6 [b] (2)	14.5 ± 0.9 [a] (2)	13.6 ± 0.2 [a] (2)	1.78 ± 0.09 [b] (2)
3	14.1 ± 0.5 [b] (2)	14.3 ± 0.4 [b] (2)	14.6 ± 0.6 [b] (2)	11 ± 1 [a] (3)	2.1 ± 0.2 [a] (2)
5	13.8 ± 0.9 [a] (2)	14.3 ± 0.7 [a] (2)	15 ± 2 [a] (2)	13.9 ± 0.4 [b] (2)	1.7 ± 0.1 [a] (2)
10	curved [c] (3)	2.2 ± 0.6 [a] (3)	13 ± 1 [a] (2)	11.1 ± 0.7 [a] (3)	2.0 ± 0.2 [a] (2)
20	0.78 ± 0.03 [a] (3)	0.7 ± 0.1 [a] (3)	9 ± 2 [b] (3)	6 ± 1 [a] (2)	2.0 ± 0.3 [a] (3)
30	0.71 ± 0.02 [b] (2)	0.58 ± 0.08 [a] (3)	6.0 ± 0.7 [b] (3)	3.2 ± 0.2 [a] (2)	2.0 ± 0.3 [a] (3)
40	0.69 ± 0.01 [b] (2)	0.56 ± 0.06 [a] (4)	4.6 ± 0.5 [a] (2)	3.0 ± 0.1 [a] (2)	1.7 ± 0.2 [b] (2)

a) The errors correspond to average deviations (when two experiments were performed) and standard deviations (when more than two experiments were performed). b) Errors of individual values from the independent experiments were taken into account. c) A non-linear plot was obtained.

From Table 4.1 it can be stated that the K_{sv} for 2-NpO did not change with an increase in the NaCh concentration. For all the other probe molecules, large jumps in the K_{sv} values were observed at different "critical concentrations" and are described below.

For both probes with the hydroxyl substituent, a significant decrease was noted in the K_{sv} value upon progressing from a 10 mM NaCh solution to a solution containing 20 mM of NaCh. A smaller decrease was then noted upon increasing the NaCh concentration from 20 mM to 30 mM. For the ethylnaphthalenes, two concentration changes had a large effect on the Stern-Volmer constant. For 2-EtNp, when the NaCh concentration was increased from 5 mM to 10 mM a large decrease occurred in the K_{SV} values. The value for the K_{SV} then decreased by a factor of two when the NaCh concentration increased from 10 mM to 20 mM. For 1-EtNp a large decreased was noted in the K_{SV} value between NaCh concentrations of 5 mM and 20 mM. The plots in the presence of 10 mM were curved; therefore no K_{SV} could be determined. No further decrease was observed for the K_{SV} values at higher bile salt concentrations.

4.1.2 Single photon counting: time-resolved fluorescence results

Single photon counting is a more time consuming technique than steady-state fluorescence, so experiments were only carried out at key NaCh concentrations (determined in Section 4.1.1). 2-NpO was omitted as its fluorescence signal was weak and no conclusive results were obtained from the steady-state data.

The SPC decay traces in the absence of NaCh were fitted to a monoexponential decay (Equation 1.7) (Fig 4.4). In the presence of NaCh, the decay traces were fitted to the sum of two exponentials (Equation 2.2) (Fig 4.5). The fits for the decays were considered acceptable, based on the statistical parameters described in Section 2.4.2.2, as well as a visual inspection of the residuals. Probe molecules, with different lifetimes, located in different environments within the aggregates gave rise to separate decays.

Thus, the number of species with different singlet excited state lifetimes was determined using the statistical parameters and the residuals.

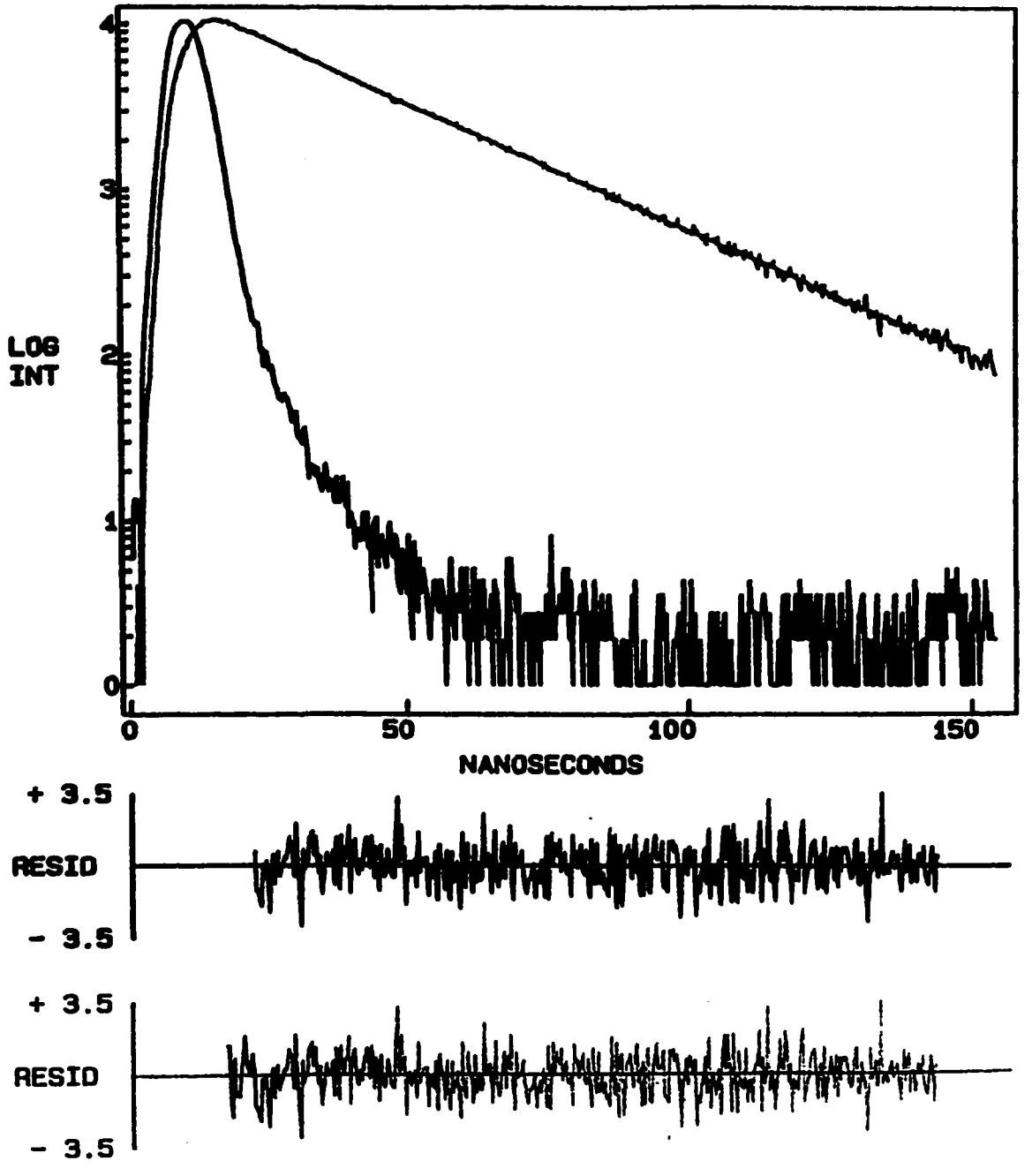

Figure 4.4 Single exponential fluorescence decay for 2-EtNp in water (top). The residuals for the fit of the experimental data for a single exponential decay (middle). The residuals for the fit of the experimental data for to the sum of two exponentials (Equation 2.2) (bottom).

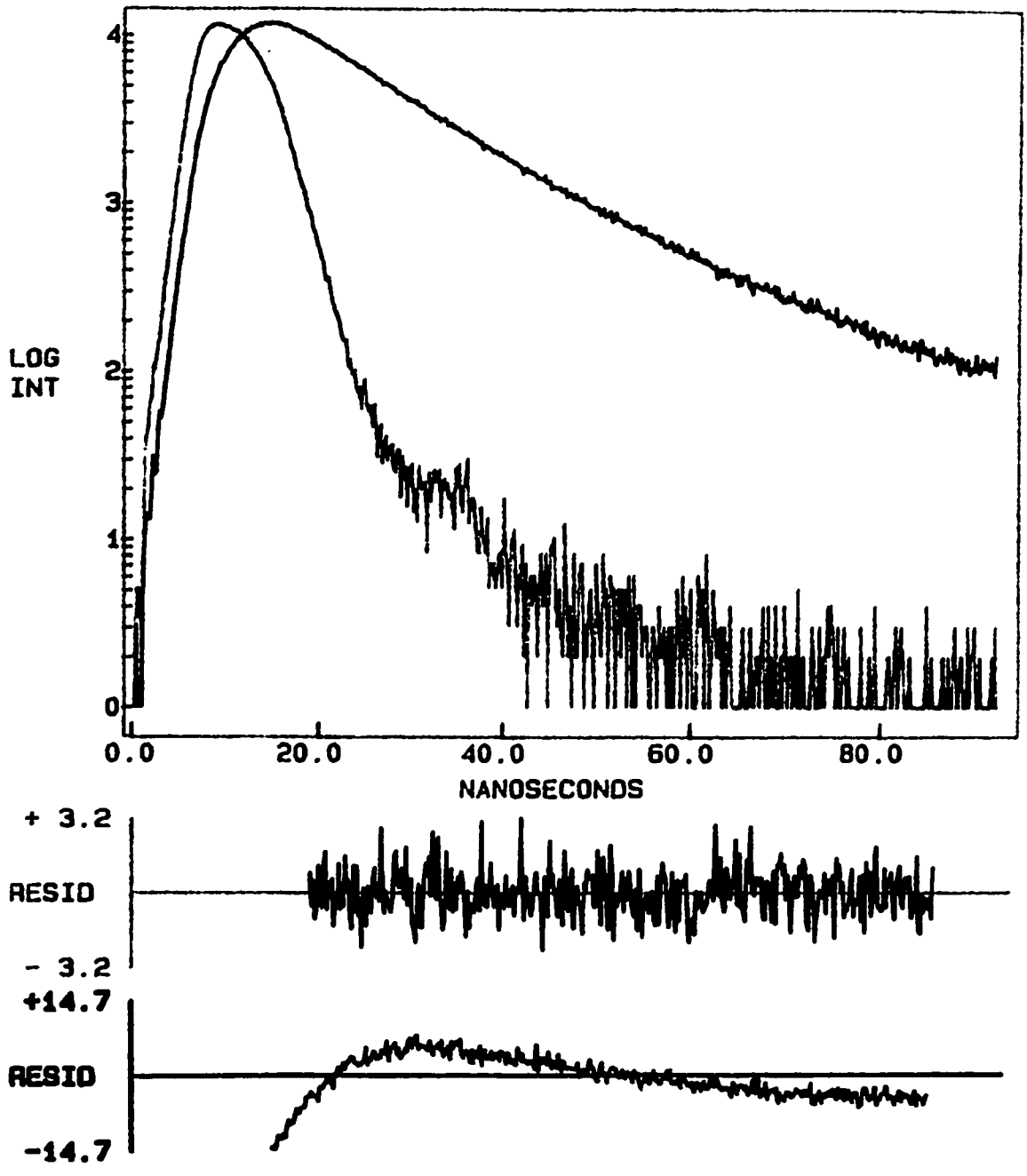

Figure 4.5 Fluorescence decay for 1-NpOH in the presence of 10 mM of NaCh, and 30 mM of NaI, fitted to the sum of two exponentials (top). The residuals for the fit of the experimental data for the sum of two exponentials (Equation 2.2) (middle). The residuals for the fit of the experimental data for a single exponential decay (bottom).

In Figure 4.5, the residuals for the decay trace fitted to a single exponential decay were unacceptable. The residuals for the fit of the decay trace for the sum of two exponentials, along with the statistics recovered, suggested that two singlet species of 1-NpOH with different lifetimes were present. In the case of the monoexponential decay (Fig. 4.4), a visual inspection of both residuals was acceptable. It must be pointed out that, although the program fit was acceptable for the sum of two exponentials, the pre-exponential factors were 0.01 and 0.99. As the pre-exponential factors give an idea of the relative abundance of each species, the data recovered suggests that only species with the lifetime corresponding to the pre-exponential factor 0.99 exists. The lifetime of the component with a pre-exponential factor of 0.99 had the same lifetime as that obtained when the data were fitted to a monoexponential decay. Thus, in this case, it was assumed that only one singlet species of 2-EtNp was present.

The lifetime data obtained from the decays in the SPC experiments were then plotted (Fig.4.6) to obtain the Stern-Volmer constants (Equation 1.13) for the probe molecules. When more then one component was present, the average lifetimes (Equation 1.14) were used. Average lifetimes were needed to determine whether static quenching, dynamic quenching, or a combination of the two was occurring (as described in Section 1.1.3.1).

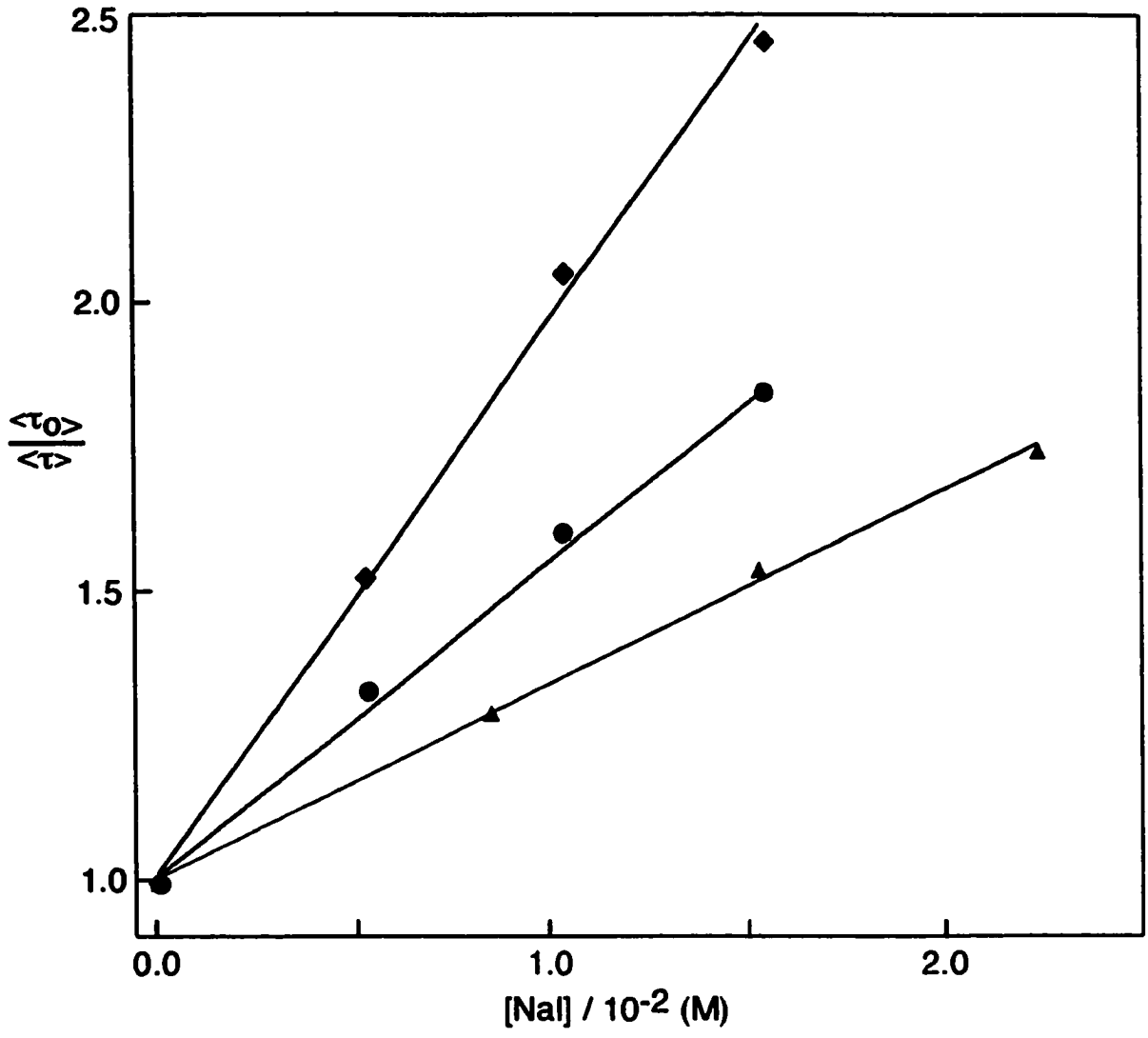

Figure 4.6 Stern-Volmer plot for 2-NpOH in the presence of 10 mM (◆), 20 mM (●) and 40 mM (▲) of NaCh, data using average lifetimes obtained from single photon counting experiments.

In a study done previously using naphthalene, anthracene, and pyrene, as fluorescent probes, in the presence of NaCh aggregates, a different analysis method was employed in order to deduce the mechanism for fluorescence quenching.[52] In this study

Equation 4.1 was used to determine the ratio of fluorescence intensities, which in turn was plotted to determine the Stern-Volmer constants from time-resolved analysis,

$$\frac{I_o}{I} = \frac{1}{\frac{f_1}{(\frac{\tau_o}{\tau_1})} + \frac{f_2}{(\frac{\tau_o}{\tau_2})}}$$

Equation 4.1

where f is the fraction of the intensity that corresponds to each component. The value of f is given by Equation 4.2,

$$f_i = \frac{a_i \tau_i}{\Sigma a_i \tau_i}$$

Equation 4.2.

The intensity fractions (f) are defined by Equation 4.2, and are therefore related to the intensity average lifetimes (Equation 1.15). As was explained in the introduction, basing calculations on the intensity averaged lifetimes, leads to an over estimation of the contribution due to static quenching. This is due to the fact that intensity averages take into account the area of the decay that can be attributed to each component. When there is a very fast decay the area that corresponds to the decay is difficult to measure accurately, thus leading to greater error in the overall analysis. The current study analyzes the data in a manner currently accepted in the literature.[4-6] The accepted analysis uses amplitude average lifetimes. In this method, the values for the amplitudes are extrapolated for each component, and therefore do not have the error associated with them that were noted for intensity average lifetimes. The previous study concluded that static and dynamic quenching were both occurring for the three probe molecules within the NaCh

aggregates.[53] In the previous study, for pyrene in the presence of 10 mM of NaCh, the plots of I_o/I versus quencher for steady-state and time-resolved fluorescence led to Stern-Volmer constants of (16.7 ± 2.1) M^{-1} and (10.8 ± 0.3) M^{-1}, respectively.[53] If the time-resolved data were analyzed using the equation for amplitude average lifetimes (Equation 1.14), the value of K_{SV} would be (16 ± 1) M^{-1}. Based on using the amplitude average lifetimes it is now believed that the analysis was incorrect as steady-state and time-resolved quenching experiments led to the same value for the Stern-Volmer constant.

Table 4.2 Single photon counting results: values for τ_0 (or $<\tau_0>$), K_{sv} values and k_q (or $<k_q>$) values for the hydroxy and alkyl substituted Np derivatives in the presence of 0 mM, 10 mM, 20 mM and 40 mM of NaCh. Errors were recovered from data analysis as each experiment was performed once.

Probe	[NaCh] /mM	τ_0[a],$<\tau_0>$[b] /ns	K_{SV} /M^{-1}	k_q[a],$<k_q>$[b] / 10^9 $M^{-1}s^{-1}$
1-EtNp	0	29.23 ± 0.04[a]	141 ± 1	4.82 ± 0.03[a]
	10	41.0 ± 0.5[b]	7 ± 1	0.17 ± 0.02[b]
	20	60 ± 1[b]	6 ± 1	0.10 ± 0.02[b]
	40	70.3 ± 0.1[a]	8 ± 1	0.11 ± 0.01[a]
2-EtNp	0	28.09 ± 0.04[a]	132 ± 1	4.70 ± 0.04[a]
	10	43.1 ± 0.8[b]	10 ± 1	0.23 ± 0.02[b]
	20	52 ± 2[b]	6 ± 1	0.12 ± 0.02[b]
	40	56 ± 5[b]	6 ± 1	0.11 ± 0.02[b]
1-NpOH	0	24.56 ± 0.03[a]	171 ± 4	7.0 ± 0.2[a]
	10	25 ± 1[a]	158 ± 2	6.3 ± 0.3[a]
	20	25 ± 1[b]	50 ± 3	2.0 ± 0.1[b]
	40	31.4 ± 0.4[b]	42 ± 2	1.4 ± 0.1[b]
2-NpOH	0	25.26 ± 0.03[a]	157 ± 9	6.2 ± 0.4[a]
	10	26.7 ± 0.9[b]	106 ± 1	4.0 ± 0.1[b]
	20	29.4 ± 0.3[b]	55 ± 3	1.9 ± 0.1[b]
	40	32 ± 2[b]	38 ± 3	1.2 ± 0.1[b]

a) A value from monoexponential fits. b) Average values for the fit of the decay to the sum of two exponentials.

The Stern-Volmer constants obtained from the SPC data were in close agreement with those obtained from the steady-state fluorescence experiments, within experimental error. Having obtained the $<\tau_o>$ for the systems studied by SPC it was possible to calculate the quenching rate constants for the Np probes by NaI in the presence of 0 mM,

10 mM, 20 mM, and 40 mM of NaCh. As the K_{SV} values obtained from steady-state and time-resolved fluorescence were similar, the values for the average quenching rate constant, from SPC, and the quenching rate constants, from steady-state fluorescence, were also comparable.

There are two factors that influence the trend noted in the Stern-Volmer constants. As the lifetime of the probe increased in the presence of the NaCh aggregates, the Stern-Volmer constants would increase as well. The quenching efficiency decreased (decreasing the value for k_q); therefore, the Stern-Volmer constants would decrease. The change in the quenching rate constant was always significantly larger then the change in lifetime; therefore, the K_{SV} values were observed to decrease. This led to the observation that the trends, when the concentration of NaCh was increased, of the Stern-Volmer constants were identical to those observed for the average quenching rate constants.

Further evidence for the protection due to complexation of the probes with the host system was obtained by independently examining the quenching rate constants of the two separate decays in the SPC experiments. In the presence of sodium cholate, all of the decays, except for the ethylnaphthalenes in the presence of 40 mM of NaCh and 1-NpOH in the presence of 10 mM of NaCh, were fitted to the sum of two exponentials, giving two separate lifetimes (Table 4.3 and 4.4). It was found in most cases that NaI readily quenched one of the two components while the other component was quenched to a much lesser extent or not at all (Fig. 4.7).

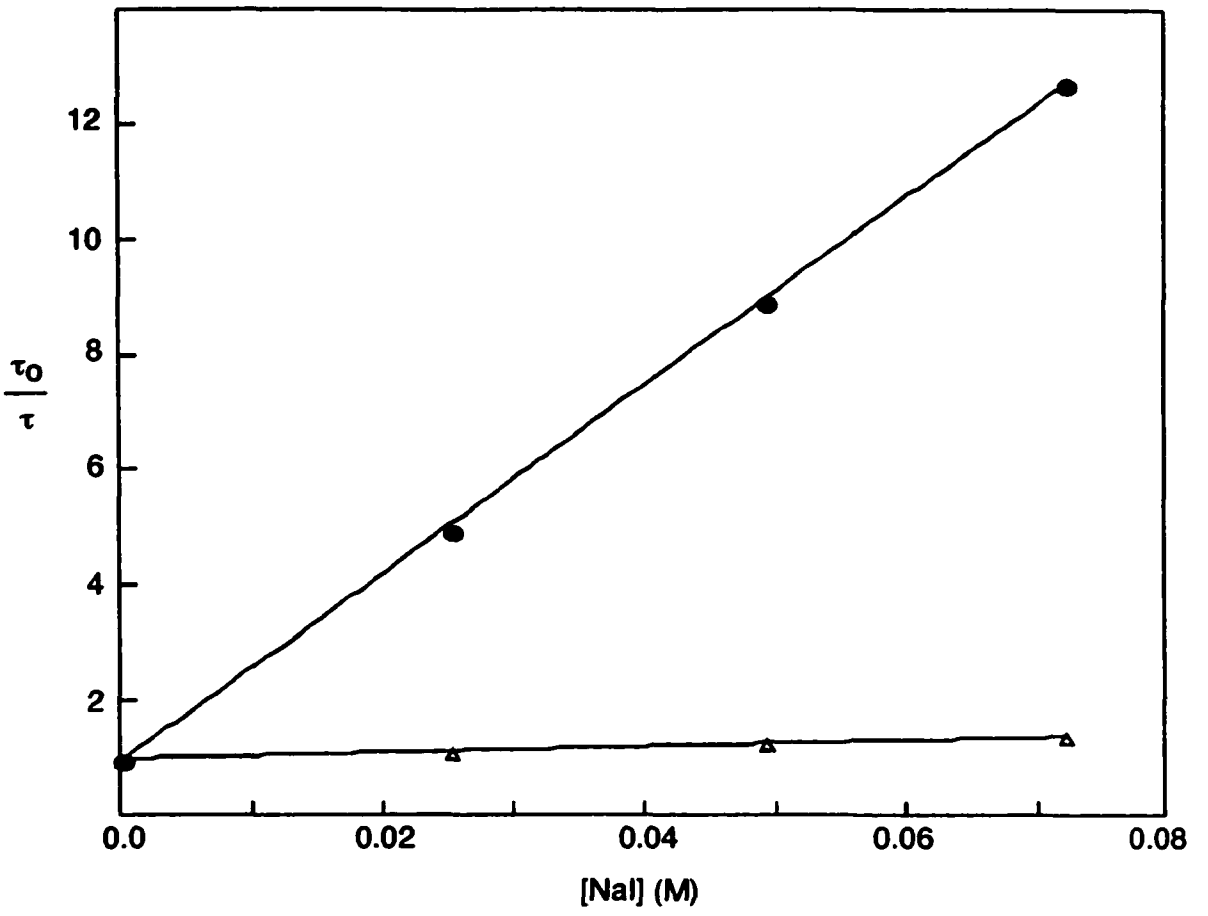

Figure 4.7 Stern-Volmer plot for the excited state species with two different lifetimes obtained from the SPC experiments; singlet excited state quenching by NaI for 1-EtNp in the presence of 20 mM of NaCh.

Table 4.3 Lifetimes in the absence of quencher, average pre-exponential factors (A), and quenching rate constants for the species with different lifetimes for 1-EtNp and 2-EtNp in the presence of various concentrations of NaCh. Data for both alkane substituted probes in the absence of NaCh gave rise to monoexponential decays; therefore, only one lifetime and one value of k_q were reported.

Probe	[NaCh] /mM	τ_0 (1) /ns	<A> (1)	$k_q(1) / 10^9$ $M^{-1}s^{-1}$	τ_0 (2) /ns	<A> (2)	$k_q(2) / 10^9$ $M^{-1}s^{-1}$
1-EtNp	0	29	1.0	4.8 ± 0.1	----	---	---
1-EtNp	10	28	0.58	2.4 ± 0.6	66	0.42	<0.06 [a]
1-EtNp	20	24	0.16	6.9 ± 0.1	68	0.84	0.078 ± 0.005
1-EtNp	40	b	b	b	70	0.94	0.09 ± 0.01
2-EtNp	0	28	1.0	4.8 ± 0.1	---	---	---
2-EtNp	10	28	0.46	4.7 ± 0.1	56	0.54	0.07 ± 0.02
2-EtNp	20	28	0.06 – 0.2	~0.40 [c]	55	0.85	0.09 ± 0.01
2-EtNp	40	b	b	b	56	0.92	0.07 ± 0.02

a) Quenching of the species corresponding to the slow component was too inefficient to be measured with precision. b) A short-lived species was observed in the presence of quencher. Its contribution to the total signal was small (A < 0.1) and for this reason could not be analyzed in the quenching experiments. c) Only an order of magnitude was determined because the pre-exponential factor of this component varied between 0.06 and 0.2.

Table 4.4 Lifetimes in the absence of quencher, average pre-exponential factors (A), and quenching rate constants for the species with different lifetimes for 1-NpOH and 2-NpOH in the presence of various concentrations of NaCh. Data for both alcohol substituted probes in the absence of NaCh gave rise to monoexponential decays; therefore, only one lifetime and one value of k_q were reported.

Probe	[NaCh] /mM	τ_0 (1) /ns	<A> (1)	$k_q(1) / 10^9$ $M^{-1}s^{-1}$	τ_0 (2) ns	<A> (2)	$k_q(2) / 10^9$ $M^{-1}s^{-1}$
1-NpOH	0	25	1.0	6.8 ± 0.2	---	---	---
1-NpOH	10	25	0.95	4.6 ± 0.2	a	a	a
1-NpOH	20	22	0.74	3.6 ± 0.1	36	0.26	0.31 ± 0.05
1-NpOH	40	25	0.51	4.0 ± 0.1	39	0.49	0.43 ± 0.03
2-NpOH	0	25	1.0	6.3 ± 0.4	---	---	---
2-NpOH	10	25	0.81	4.4 ± 0.8	35	0.07 – 0.3	~2 [b]
2-NpOH	20	25	0.63	4.5 ± 0.6	37	0.37	0.42 ± 0.09
2-NpOH	40	25	0.45	6.0 ± 0.6	37	0.55	0.5 ± 0.1

a) A long-lived species (τ of ca.30 ns) was observed in the presence of quencher. Its contribution to the total signal was small (A < 0.1) and for this reason could not be analyzed in the quenching experiments. b) Only an order of magnitude was determined because the pre-exponential factor of this component varied between 0.07 and 0.3.

Graphing the Stern-Volmer plots of the species with different lifetimes from the SPC experiments independently and then calculating the quenching rate constants (Table 4.3 and 4.4) allowed the quenching efficiency for each of the excited state components to be determined. Values spanning three orders of magnitude were recovered. The first excited state component for all decays, except 2-EtNp in the presence of secondary aggregates, gave rise to quenching rate constants with values of the same order of magnitude as the quenching of the probes in water (10^9 $M^{-1}s^{-1}$). The value for the second

excited state component of 2-NpOH in the presence of 10 mM of NaCh was also of the same order of magnitude. The value for the quenching rate constant for the first excited state component of 2-EtNp in the presence of 20 mM of NaCh appears to be an order of magnitude lower (10^8 $M^{-1}s^{-1}$) than in water.

The value for the quenching rate constant of the second excited state component at all other bile salt concentrations for the ethylnaphthalenes was two orders of magnitude lower (10^7 $M^{-1}s^{-1}$) than the quenching in aqueous solution. The values were reproducible with the average value for the k_q's being (8 ±1) x 10^7 $M^{-1}s^{-1}$. For the alcohol derivatives, the values for the second excited state components were an order of magnitude lower than in water (10^8 $M^{-1}s^{-1}$). More precisely, these values were reproducible with the average value for the k_q's being (4.1 ± 0.4) x 10^8 $M^{-1}s^{-1}$.

Analyzing the pre-exponential factors for the two excited state decays was not possible to a large extent because the molar absorptivities, at the excitation wavelength of 290 nm, for the probes in the different binding sites would be needed in order to extract any useful information. Obtaining the molar absorptivities in supramolecular systems is difficult because the equilibrium constant for the excited state must be known, or the probe must be included entirely within one binding site.[8] However, following the trend in the pre-exponential factors was of interest. In general, it was found that pre-exponential factors for the various components did not change drastically during a quenching experiment. The percent relative standard deviation (%RSD) in the pre-exponential factors varied from 1% to 14%. Therefore; if the NaCh concentration remained constant and the only variable was the quencher concentration, the pre-exponential factors for the two components observed by SPC were similar. The two exceptions to this were 2-EtNp

in the presence of 20 mM of NaCh, and 2-NpOH in the presence of 10 mM of NaCh, as previously noted in the tables.

4.1.3 Laser flash photolysis: investigation of the complexation dynamics of the triplet excited states of the Np probes with NaCh aggregates

4.1.3.1 Transient spectra and kinetics

The transient absorption spectra of all the naphthalene derivatives studied exhibited similar characteristics. The absorption band was sharp with a maximum of approximately 420 nm. In a previous study it was observed that in the presence of sodium cholate the spectrum of Np narrowed in the 410 nm to 430 nm region and was red-shift slightly.[51] The current study was not done with the same precision because the focus of the work was not on the transient spectral features. The findings within this study do not discount the possibility of the spectral changes occurring, as was previously observed. Figure 4.8 shows a representative transient absorption spectrum for the naphthalene derivatives used in this study. A wavelength of 420 nm was used as the monitoring wavelength for all of the studies described in this chapter.

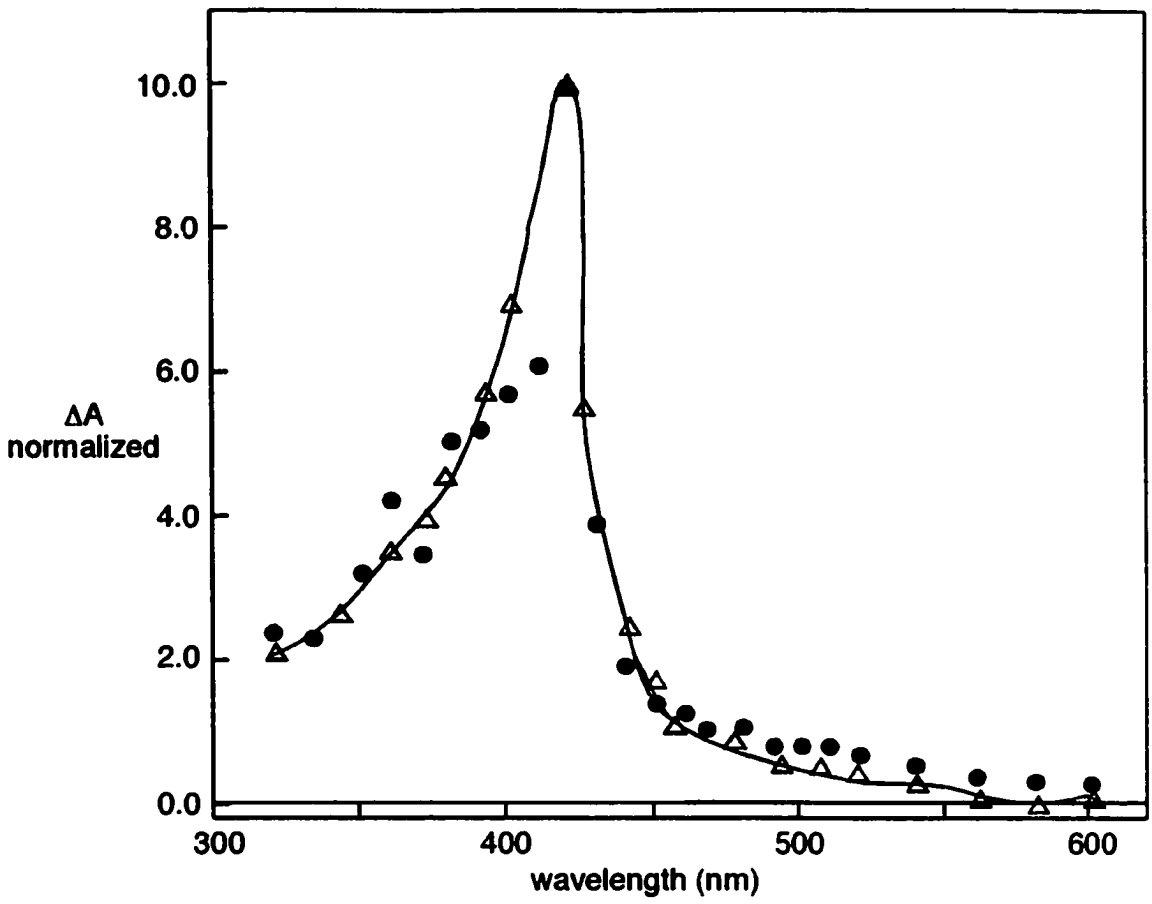

Figure 4.8 Transient absorption spectra of 2-NpOH in the absence of NaCh (●, delay = 6.5 μs) and in the presence of 40 mM of NaCh (Δ, delay = 12 μs). The spectra have been normalized at the absorption maximum at 420 nm. The solid line represents a smooth curve through the data in the presence of 40 mM of NaCh. Only one curve was shown as both sets of data gave rise to a similar spectrum.

The kinetic decay traces for all the naphthalene derivatives were mono-exponential in the presence and absence of NaCh (Fig 4.9). The lifetimes of the probes were also unaffected by the concentration of NaCh. For 1-EtNp the lifetimes in the absence of quencher were always greater than 130 μs, whereas, for 2-EtNp the lifetimes in the absence of quencher were always greater than 75 μs. For 1-NpOH, the lifetimes

were greater than 29 μs, whereas, for 2-NpOH the lifetimes in the absence of quencher were always greater than 43 μs. For 1-NpO and 2-NpO, the lifetimes were greater than 9 μs. The slight variation in lifetimes between experiments for a single probe was due to different extents of deoxygenation.

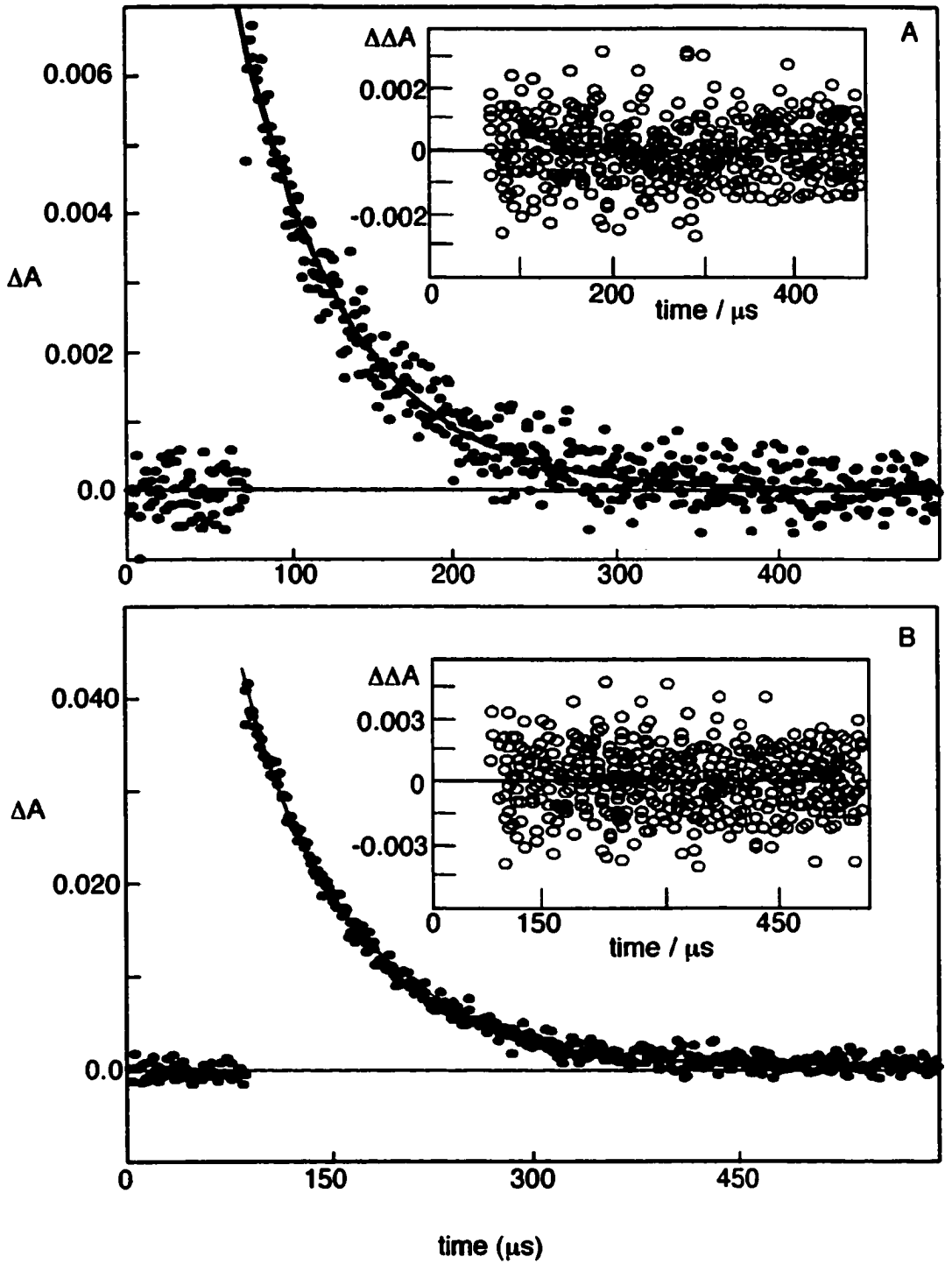

Figure 4.9 Kinetic decay traces of 1-EtNp in the absence of NaCh (A) and in the presence of 40 mM of NaCh (B). All traces were fitted to a monoexponential decay and the residuals for the fit are shown in the insets.

4.1.3.2 Quenching of the triplet excited naphthalene probes by nitrite

In order to gain information on the location of the probes within the host NaCh aggregates, quenching studies with nitrite were performed. The quenching plots for all the probes in the absence of sodium cholate gave rise to linear plots (Fig. 4.10), as did the plots for 1-NpOH in the presence of 10 mM of NaCh. The quenching rate constants are given in Table 4.5.

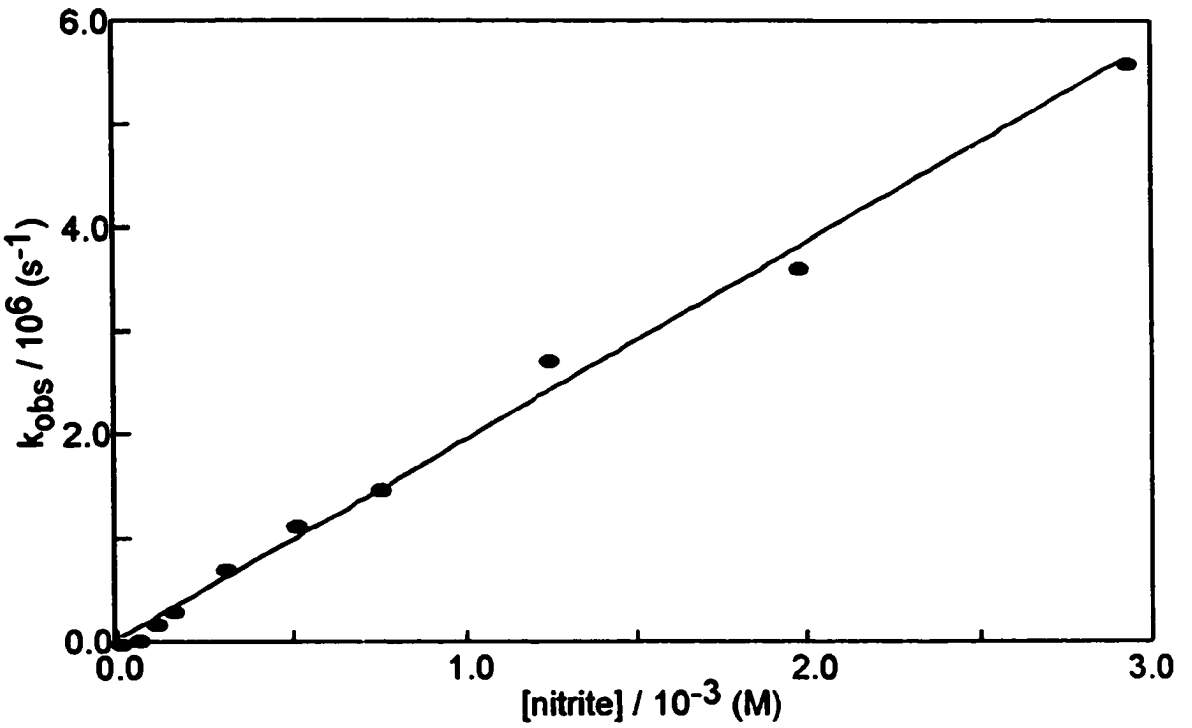

Figure 4.10 Linear quenching plot for triplet 2-EtNp in the absence of NaCh quenched by sodium nitrite.

Table 4.5 Triplet quenching rate constants for the linear quenching plots of the naphthalene derivatives in the absence of NaCh and 1-NpOH in the presence of 10 mM of NaCh. The number in parentheses represents the number of independent experiments performed.

Probe	$k_q / 10^9$ $M^{-1}s^{-1}$	
	0 mM NaCh	10 mM NaCh
1-EtNp	2.7 ± 0.2 (2) [b]	
2-EtNp	1.8 ± 0.1 (2) [a]	
1-NpOH	3.4 ± 0.2 (2) [b,c]	2.4 ± 0.2 (2) [a]
2-NpOH	3.1 ± 0.1 (2) [b]	
1-NpO	1.6 ± 0.3 (2) [a]	
2-NpO	2.3 ± 0.3 (3) [a]	

a) The errors correspond to average deviations (when two experiments were performed) and standard deviations (when more than two experiments were performed). b) Errors of individual values from the independent experiments were taken into account. c) Data were collected for μ = 0 M and μ = 0.2 M and the same values were obtained.

Nitrite quenching of the probe molecules in the presence of 10 mM (except 1-NpOH), 20 mM, and 40 mM of NaCh led to plots that were not linear (Fig. 4.11). Similar to the case of DMBp in the presence of 40 mM of NaCh (Section 3.1.3.4.1), these data were analyzed using Equation 1.16, where the dynamics of interaction between the probe molecules and the NaCh host system were investigated.

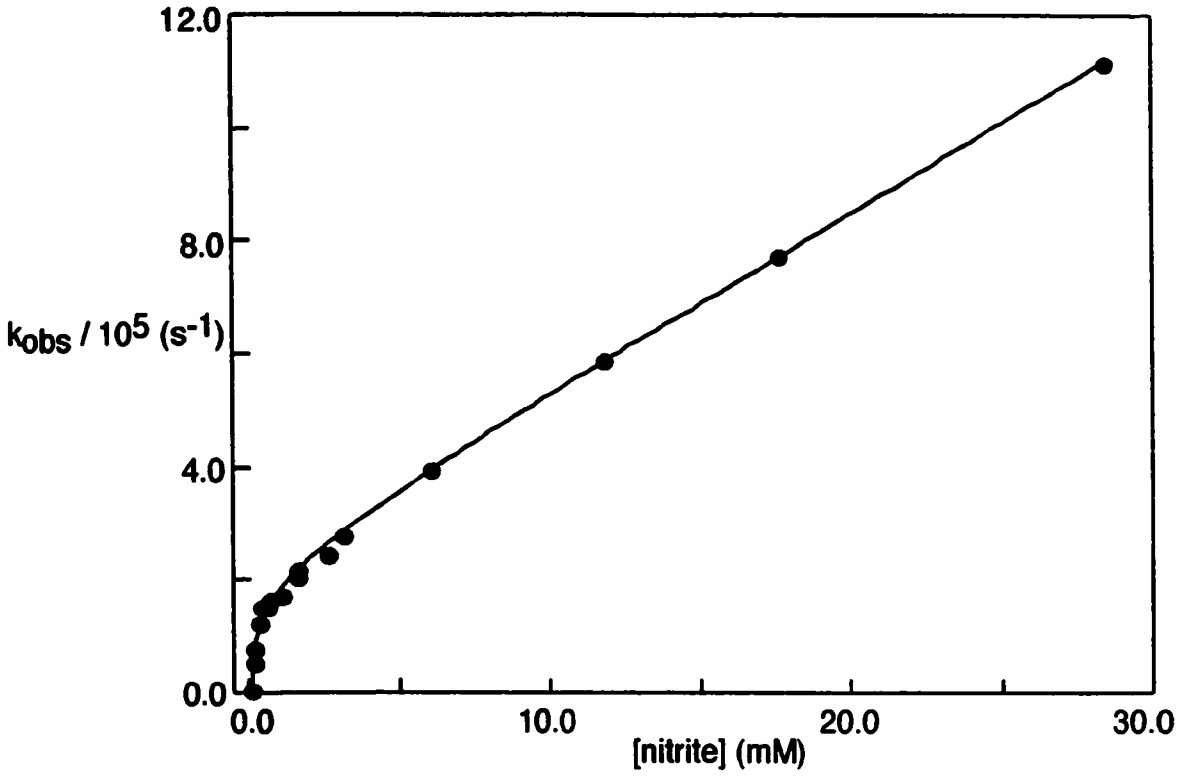

Figure 4.11 Curved quenching plot for the quenching of triplet 1-EtNp in the presence of 10 mM of NaCh by nitrite.

The quenching rate constants for the probes within the host system (k_q (H)) were obtained from the nitrite quenching data (Equation 1.16, Table 4.6). In many cases, as described in chapter three (Section 3.1.3.4.2), a wide range of quenching rate constants led to a reliable fit for the data. The reliable fit of the data was decided based on a visual inspection of the fit.

Table 4.6 Quenching rate constants (or ranges) ($k_q(H)$) for the triplet excited states of 1-EtNp, 2-EtNp, 1-NpOH, 2-NpOH, 1-NpO, and 2-NpO in the bile salt aggregates quenched by nitrite for experiments that led to curved quenching plots. The number in parentheses represents the number of independent experiments performed.

Probe	$k_q(H)$ /$M^{-1}s^{-1}$		
	10 mM NaCh	**20 mM NaCh**	**40 mM NaCh**
1-EtNp	$(3.7 \pm 0.5) \times 10^{7}$ [a] (2)	$(2.2 \pm 0.2) \times 10^{7}$ [b] (2)	$(2.38 \pm 0.08) \times 10^{7}$ [b] (2)
2-EtNp	$(4.1 \pm 0.2) \times 10^{7}$ [b] (2)	$(3.2 \pm 0.6) \times 10^{7}$ [a] (3)	$(2.1 \pm 0.2) \times 10^{7}$ [b] (2)
1-NpOH	---	$0 - 1 \times 10^{8}$ [c] (2)	$0 - 1 \times 10^{8}$ [c] (2)
2-NpOH	$0 - 1 \times 10^{9}$ [c] (2)	$0 - 1 \times 10^{8}$ [c] (2)	$0 - 1 \times 10^{8}$ [c] (2)
1-NpO	$0 - 1 \times 10^{8}$ [c] (2)	$0 - 1 \times 10^{8}$ [c] (2)	$0 - 1 \times 10^{8}$ [c] (2)
2-NpO	$0 - 1 \times 10^{9}$ [c] (2)	$0 - 1 \times 10^{8}$ [c] (2)	$0 - 1 \times 10^{8}$ [c] (2)

a) The errors correspond to average deviations (when two experiments were performed) and standard deviations (when more than two experiments were performed). b) Errors of individual values from two independent experiments were taken into account. c) Only a range of values could be reported.

As can been seen in Table 4.6, there are striking differences between the ethyl substituted naphthalenes and the other probe molecules. The ethyl substituted derivatives gave rise to precise values for the quenching rate constants, while for the other probe molecules only a range for the possible values of $k_q(H)$ was recovered. In most cases the range in quenching rate constants encompasses the range in values between two

independent experiments. The data recovered for 2-NpOH in the presence of 40 mM of NaCh was an exception to the analysis method. One of the independent experiments gave rise to a precise value of 1 x 10^8 $M^{-1}s^{-1}$ for the kq(H), while the other set of data could be fitted for a range of 0 – 1 x 10^8 $M^{-1}s^{-1}$. The most likely reason for this discrepancy was due to a different scatter of data points in the quenching graph. The precise value for the quenching rate constant was found to be at the high end of the range of $k_q(H)$ values obtained in the second experiment.

Comparing the magnitude of the values obtained for the quenching rate constants of the various probes was of interest. For the ethylnaphthalenes, the quenching rate constants recovered were lower than the upper limit for the quenching rate constants for the hydroxyl and carbonyl substituted naphthalenes. Although the upper limit for the $k_q(H)$ values for the carbonyl and hydroxyl substituted Nps were on average an order of magnitude higher than those for the ethyl substituted Nps, they were an order of magnitude lower than the k_q for the probe molecules in water. The exceptions were 2-NpOH and 2-NpO in the presence of 10 mM of NaCh, where the upper limit for the quenching rate constants was of the same order of magnitude as the quenching rate constants in aqueous solutions.

Using the ranges (or value) of $k_q(H)$ determined above, Equation 1.16 was used to determine the values of the dissociation rate constants (k_-) and association rate constants (k_+/N) for all the systems studied. For the probes where only a range of $k_q(H)$ values was determined, a rather complex procedure led to the values quoted in Tables 4.7 and 4.8. For each independent experiment the upper and lower values for k_- (or k_+/N), based on the range of $k_q(H)$, were averaged. These averaged values (with errors) from the two

independent experiments were then used to determine the values outlined in Tables 4.7 and 4.8. For the alkane substituted derivatives, this procedure was not necessary as precise values for $k_q(H)$ were determined from the fit of the data, thus the values for k_- and (k_r/N) were also determined from the fit.

Table 4.7 Dissociation rate constants for the triplet naphthalene derivatives in the presence of 10 mM, 20 mM, and 40 mM of NaCh. The number in parentheses represents the number of independent experiments performed.

Probe	$k_- / 10^6 s^{-1}$		
	10 mM of NaCh	20mM of NaCh	40mM of NaCh
1-EtNp	0.20 ± 0.04 [b] (2)	0.3 ± 0.1 [b] (2)	0.14 ± 0.03 [b] (2)
2-EtNp	0.31 ± 0.06 [b] (2)	0.31 ± 0.08 [b] (3)	0.4 ± 0.2 [b] (2)
1-NpOH	---	9 ± 1 [b] (2)	7 ± 1 [a] (2)
2-NpOH	~40 [c] (2)	5.3± 0.9 [a] (2)	5 ± 2 [a] (2)
1-NpO	4.6 ± 0.8 [a] (2)	3 ± 1 [a] (2)	3 ± 1 [a] (2)
2-NpO	10 ± 8 [a] (2)	5 ± 1 [b] (2)	5 ± 2 [a] (2)

a) The errors correspond to average deviations (when two experiments were performed) and standard deviations (when more than two experiments were performed). b) Errors of individual values from two independent experiments were taken into account. c) The error associated with the value was large, thus only an estimate is presented.

For the acetonaphthones, within the $k_q(H)$ range mentioned in Table 4.6, the %RSD associated with the average dissociation rate constants obtained when using Equation 1.16 was less than 30 %. The exception was 2-NpO in the presence of 10 mM of NaCh where the value recovered for the dissociation rate constant had much larger %RSD associated with it. For 1-NpOH, within the $k_q(H)$ range obtained, the %RSD associated with the average dissociation rate constants was less than 15 %. For 2-NpOH in the presence of 10 mM of NaCh there was a large %RSD of 75 % associated with the dissociation rate constant. Within the $k_q(H)$ range reported for 2-NpOH in 20 mM of NaCh, the %RSD associated with the average dissociation rate constants was less than 15 %.

The k_- values for the alkyl substituted derivatives were at least an order of magnitude lower than those for the other probe molecules. For 1-EtNp and 2-NpEt, no change was noted in the dissociation rate constants as the bile salt concentration was increased. The k_- value decreased for 2-NpOH between NaCh concentrations of 10 mM and 20 mM. In the presence of secondary aggregates ([NaCh] $\geq$ 20 mM), as the NaCh concentration was increased, there was no change in the dissociation rate constant for the naphthylethanols. The most significant contrast in the data, due to the position of the hydroxyl substituent on the naphthalene ring, was noted in the presence of 10 mM of NaCh. The quenching plot for 1-NpOH was linear, while the plot of 2-NpOH displayed signs of interaction with the host system leading to a curved quenching plot (Fig. 4.12). The values in the presence of 20 mM and 40 mM of NaCh were similar for both probes, regardless of the substituent position.

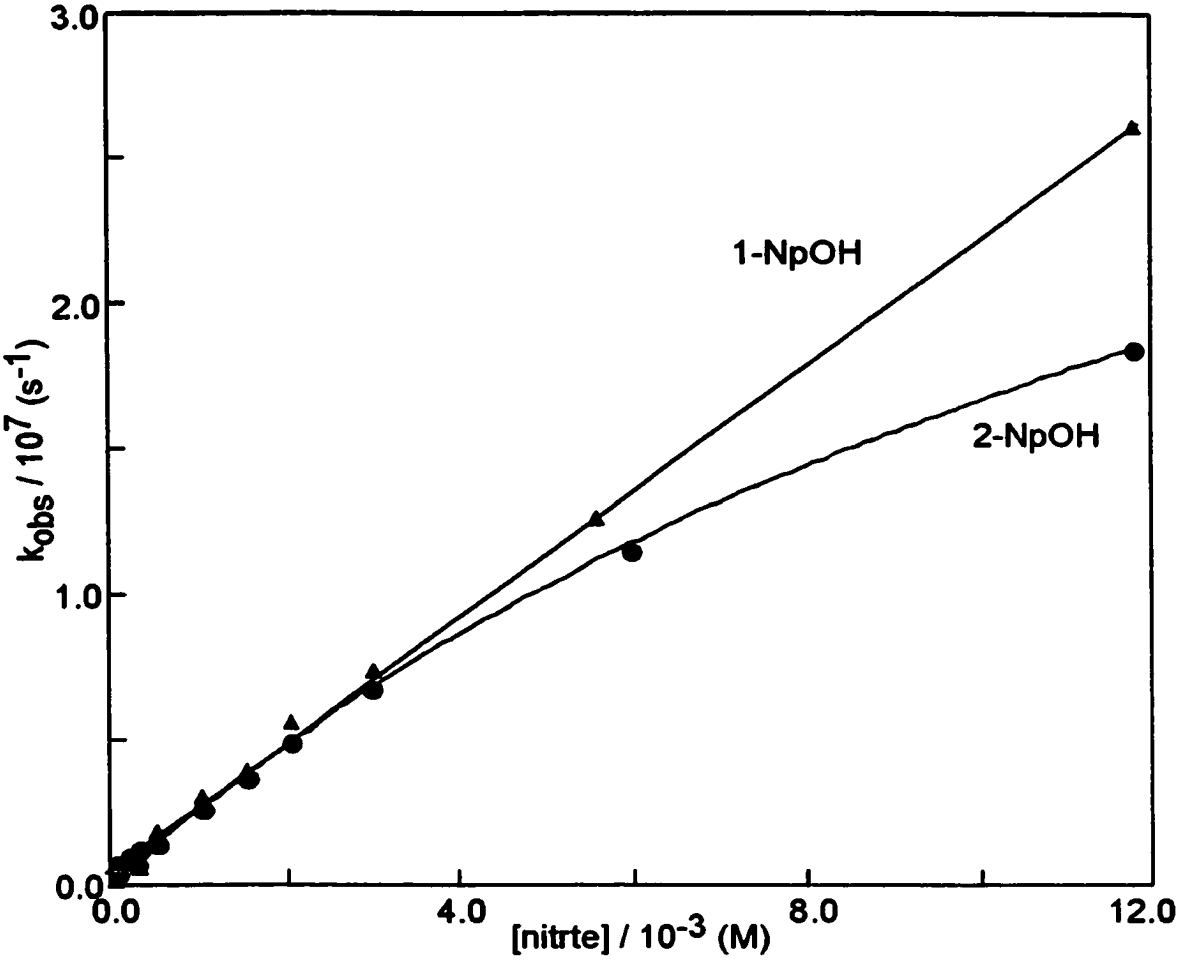

Figure 4.12 Nitrite quenching plot for 1-NpOH and 2-NpOH in the presence of 10 mM of NaCh to show the difference in curvature based on the position of the substituent on the Np ring structure.

The dissociation rate constants for 1-NpO and 2-NpO were similar at all NaCh concentrations. There was no difference observed in the value for the dissociation rate constant based on the position of the carbonyl substituent on the Np ring structure.

In the presence of NaCh, in order to obtain the association rate constant, the value for the aggregation number (N) must be known. As the value for the aggregation number

is still unknown (as mentioned in Chapter 1), the value for the association rate constant was reported as k_+/N (Table 4.8).

For the ethylnaphthalenes in the presence of secondary aggregates, the curvature for the triplet quenching plots was not well defined. As the association rate constant is only contained within the curved portion of the quenching plot, based on Equation 1.16, it was not possible to report reliable values for k_+/N in these cases. The dissociation rate constant (k_-) and quenching rate constant ($k_q(H)$) are contained within the linear portion of the plot, based on Equation 1.16, and were therefore unaffected by the lack of curvature.

Table 4.8 Values for the association rate constants divided by the aggregation number for the naphthalene series of probes, in the presence of 10 mM, 20 mM, and 40 mM of NaCh. The number in parentheses represents the number of independent experiments performed.

Probe	$(k_+/N) / 10^8\ M^{-1}s^{-1}$		
	10 mM NaCh	20 mM NaCh	40 mM NaCh
1-EtNp	0.8 ± 0.5 [a] (2)	N/A [c] (2)	N/A [c] (2)
2-EtNp	2 ± 1 [b] (2)	N/A [c] (3)	N/A [c] (2)
1-NpOH	---	7 ± 2 [a] (2)	4 ± 1 [b] (2)
2-NpOH	50 ± 30 [a] (2)	4 ± 1 [a] (2)	3 ± 1 [a] (2)
1-NpO	3 ± 1 [b] (2)	3 ± 1 [b] (2)	2 ± 1 [a] (2)
2-NpO	11 ± 8 [b] (2)	4 ± 1 [b] (2)	4 ± 1 [a] (2)

a) The errors correspond to average deviations (when two experiments were performed) and standard deviations (when more than two experiments were performed). b) Errors of individual values from two independent experiments were taken into account. c) The curvature in this experiment was insufficient to extract a reliable value for k_+/N.

4.2 Results of experiments done at a constant ionic strength

In this section, the effect of the ionic strength of the solution on the interaction between probe molecules and NaCh aggregates was investigated. It was hypothesized that increasing the ionic strength would assist in the aggregation of the bile salts (see

below). As ionic quenchers were used in these studies, it was important to keep the ionic strength constant throughout the course of an experiment (Section 2.3).

4.2.1 Steady-state fluorescence: Location of probe molecules within NaCh aggregates

The steady-state fluorescence quenching data gave an indication of where the probes were located within the NaCh aggregates. In the varying ionic strength experiments (Section 4.1) it was found that the trend in the Stern-Volmer constants was consistent with the trends in the average quenching rate constants. Consequently, in the constant ionic strength project, it was assumed that the Stern-Volmer constants would give an accurate idea of the trend of the quenching rate constants; therefore, time-resolved fluorescence experiments were not carried out. For the purpose of this study, 1-EtNp and 1-NpOH were selected to give an understanding of the effect of ionic strength on the interactions of the probes with NaCh aggregates.

4.2.1.1 Emission spectra

No shifts or changes in the fluorescence emission spectra were observed when the ionic strength of the solutions was increased. The spectra were measured between 300 nm and 500 nm.

4.2.1.2 Singlet excited state quenching of naphthalene probes by sodium iodide

The fluorescence quenching experiments were performed in the presence of 0 mM, 3 mM, 5 mM, 10 mM, 20 mM, 30 mM, and 40 mM of NaCh. The three ionic

strengths investigated were 0.03 M, 0.2 M, and 0.4 M. Tables 4.9 and 4.10 show the K_{sv} values recovered from Stern-Volmer plots using Equation 1.13.

Table 4.9 Effect of ionic strength on the Stern-Volmer constants for 1-EtNp in the presence and absence of NaCh. The number in parentheses indicates the number of independent experiments performed.

[NaCh] / mM	K_{sv} / 10^1 M^{-1}		
	μ = 0.03 M	μ = 0.2 M	μ = 0.4 M
0	14 ± 2 [b] (3)	14 ± 1 [a] (3)	14 ± 1 [b] (2)
3	13 ± 2 [a] (2)	7.5 ± 0.8 [b] (2)	8 ± 2 [b] (2)
5	6.5 – 16.9 [c] (4)	8.3 – 17.7 [c] (4)	7 ± 1 [b] (2)
10	10 ± 2 [a] (3)	3.1 ± 0.7 [a] (4)	5.4 ± 0.6 [b] (2)
20	1.4 ± 0.3 [b] (2)	1.1 ± 0.2 [b] (4)	0.9 ± 0.3 [a] (2)
30	0.9 ± 0.2 [b] (2)	0.7 ± 0.2 [a] (4)	1.0 ± 0.2 [a] (2)
40	0.6 ± 0.2 [a] (2)	0.6 ± 0.2 [a] (3)	1.1 ± 0.1 [b] (2)

a) The errors correspond to average deviations (when two experiments were performed) and standard deviations (when more than two experiments were performed). b) Errors of individual values from the independent experiments were taken into account. c) Represents a range of values for the data at this NaCh concentration and ionic strength. Data were not reproducible, as was the case for all other concentrations.

Table 4.10 Effect of ionic strength on the Stern-Volmer constants for 1-NpOH in the presence and absence of NaCh. The number in parentheses indicates the number of independent experiments performed.

[NaCh] /mM	K_{SV} /10^1 M^{-1}		
	μ = 0.03 M	μ = 0.2 M	μ = 0.4 M
0	16.3 ± 0.6 [b] (2)	14 ± 1 [a] (3)	15.0 ± 0.9 [a] (2)
3	15.7 ± 0.6 [b] (2)	15.4 ± 0.9 [b] (2)	14.6 ± 0.6 [b] (2)
5	15.7 ± 0.4 [b] (2)	15.0 ± 0.5 [b] (2)	16 ± 1 [b] (2)
10	14.4 ± 0.8 [a] (2)	12.4 ± 0.5 [a] (2)	13 ± 2 [b] (2)
20	10 ± 1 [a] (2)	8 ±1 [a] (2)	8.2 ± 0.7 [b] (2)
30	6.5 ± 0.8 [b] (2)	5.5 ± 0.6 [a] (2)	6.1 ± 0.4 [b] (2)
40	4.6 ± 0.5 [a] (2)	4.7 ± 0.3 [a] (2)	4.7 ± 0.8 [a] (2)

a) The errors correspond to average deviations (when two experiments were performed) and standard deviations (when more than two experiments were performed). b) Errors of individual values from two independent experiments were taken into account.

The majority of the data for the fluorescence quenching experiments suggested the following: for 1-NpOH, in the presence of all concentrations of NaCh, there was no effect of ionic strength on the Stern-Volmer constants. In the presence of 10 mM of NaCh, it appeared that the Stern-Volmer constant was decreasing with increasing ionic

strength. The decrease was small and considered insignificant, based on the fact that some variation in the K_{SV} values was noted even in the absence of NaCh.

For 1-EtNp in the presence of primary aggregates ([NaCh] < 20 mM), with increasing ionic strength, the Stern-Volmer constant was decreased. The exception to this trend was the data collected in the presence of 5 mM of NaCh, where the values at ionic strengths of 0.03 M and 0.2 M were not reproducible. Why the data at an ionic strength of 0.2 M were not similar to that observed in the varying ionic strength experiments is puzzling. It would have been expected that, although the values may have been slightly different due to the different methods of preparing the samples, the value would have been reproducible. In the presence of secondary aggregates of NaCh ([NaCh] $\geq$ 20 mM), the Stern-Volmer constants did not change with increasing ionic strength.

The trends for each probe with changing NaCh concentration were also examined. Similar trends to those observed in the varying ionic strength experiments were noted in most cases, with the exception of the following. In the fluorescence quenching experiments the trend for the K_{sv} between 0 mM and 10 mM of NaCh, for 1-EtNp was affected by the ionic strength. In the varying ionic strength experiments above (Section 4.1), it was noted that the Stern-Volmer constant decreased significantly between NaCh concentrations of 5 mM and 10 mM. A similar trend, with a drop in the K_{SV} between 3 mM and 10 mM, was noted in the constant ionic strength experiments, when the ionic strength was 0.2 M. When the ionic strength was low, at a concentration of 0.03 M, there was little decrease noted between host concentrations of 3 mM and 10 mM. The data at 3 mM was used for this analysis in place of 5 mM because the data in the presence of 5 mM of NaCh were non reproducible. It was further observed that the large drop in the

Stern-Volmer constant at an ionic strength of 0.4 M occurred between 0 mM and 3 mM of NaCh. A second substantial decrease was observed in the presence of 20 mM of NaCh at all ionic strengths.

4.2.2 Laser flash photolysis: investigation of the effect of ionic strength on the complexation dynamics of the triplet excited states of the Np probes with NaCh aggregates

4.2.2.1 Transient spectra and kinetic decays

The characteristics of the transient spectra were not studied in the constant ionic strength experiment. The goal of this work was to understand the binding dynamics of the naphthalene probes to the NaCh aggregates. In the earlier study (Section 4.1.3.1) it was determined that the peak maximum for the excited triplet state of the Np derivatives was centered at 420 nm; thus, the experiments were carried out at this monitoring wavelength. The kinetic traces were monoexponential at all host and quencher concentrations studied, as well as at all ionic strengths.

4.2.2.2 Quenching studies of the excited triplet states of Np with nitrite

The interaction of the triplet excited states of the probe molecules with the NaCh aggregates was examined using quenching studies with nitrite. As previously mentioned, there were two different possibilities for the plots when these experiments were conducted in the presence of NaCh: the quenching plots could be linear or they could be curved. The data in the constant ionic strength project agreed with the previous data at varying ionic strength. All plots in the absence of NaCh and 1-NpOH in the presence of

10 mM of NaCh gave rise to linear quenching plots, while in the presence of 10 mM of NaCh (except 1-NpOH) and at higher NaCh concentrations curved quenching plots were observed. The data obtained from the analysis of the linear quenching plots are presented in Table 4.11 below.

Table 4.11 Quenching rate constants for 1-EtNp in the absence of NaCh, and 1-NpOH in the absence of NaCh and in the presence of 10 of mM of NaCh, at constant ionic strength. Two independent experiments were performed for each probe at each bile salt and NaCl concentration.

Probe	[NaCh] /mM	$k_q / 10^9\ M^{-1}s^{-1}$		
		μ = 0.03 M	μ = 0.2 M	μ = 0.4 M
1-EtNp	0	3.0 ± 0.4 [a]	2.7 ± 0.8 [a]	2.6 ± 0.3 [a]
1-NpOH	0	3.2 ± 0.2 [a]	3.1 ± 0.1 [a]	3.0 ± 0.1 [a]
1-NpOH	10	3.3 ± 0.4 [a]	2.5 ± 0.2 [a]	2.6 ± 0.1 [a]

a) Errors represent the average deviation between two experiments.

The quenching rate constants in water were the same for both probes, with an average quenching rate constant of (3 ± 1) x $10^9\ M^{-1}s^{-1}$. The quenching rate constant for 1-NpOH in the presence of 10 mM of NaCh was similar to this value at all ionic strengths studied.

The data for the curved quenching plots were analyzed in the same manner as was described for the experiments carried out at varying ionic strengths (Section 4.1.1.2). The data for the quenching rate constants in the presence of bile salts (k_q(H), the dissociation rate constant (k_-), and the association rate constant divided by the aggregation number (k_+/N)) are presented in Tables 4.12, 4.13 and 4.14, respectively.

Table 4.12 Quenching rate constants (or ranges) for 1-EtNp in the presence of 10 mM, and 40 mM of NaCh and 1-NpOH in the presence of 40 mM of NaCh at constant ionic strengths. Two independent experiments were performed for each probe at each bile salt and NaCl concentration.

Probe	[NaCh] /mM	$k_q(H)$ / $M^{-1}s^{-1}$		
		μ = 0.03 M	μ = 0.2 M	μ = 0.4 M
1-EtNp	10	$0-2 \times 10^8$ [d]	$(4.0 \pm 0.7) \times 10^7$ [a]	$(2.9 \pm 0.3) \times 10^7$ [b]
1-EtNp	40	$(1.9 \pm 0.3) \times 10^7$ [a]	$(2.6 \pm 0.9) \times 10^7$ [a]	$(2.5 \pm 0.3) \times 10^7$ [b]
1-NpOH	40	$0-1 \times 10^8$ [c]	$0-1 \times 10^8$ [c]	$0-1 \times 10^8$ [c]

a) Errors represent the average deviation between two experiments. b) Errors of individual values from two independent experiments were taken into account. c) Only a range of values could be reported. d) Only one experiment was used.

It was of interest to note that for 1-EtNp in the presence of 10 mM of NaCh, at low ionic strength, a range of values for $k_q(H)$ gave rise to reasonable fits for the data. This is in contrast to all other data for the alkane substituted probe, where precise values for $k_q(H)$ were obtained. In a similar fashion to the experiments carried out at varying ionic strengths, ranges for the $k_q(H)$ values for 1-NpOH in the presence of 40 mM of NaCh are reported.

Table 4.13 Dissociation rate constants for 1-EtNp in the presence of 10 mM, and 40 mM of NaCh and 1-NpOH in the presence of 40 mM of NaCh at constant ionic strengths. Two independent experiments were performed for each probe at each bile salt and NaCl concentration.

Probe	[NaCh] /mM	$k_- / 10^6\ s^{-1}$		
		μ = 0.03 M	μ = 0.2 M	μ = 0.4 M
1-EtNp	**10**	~20 [c]	0.4 ± 0.1 [a]	0.18 ± 0.04 [b]
1-EtNp	40	0.23 ± 0.06 [b]	0.16 ± 0.08 [b]	0.14 ± 0.06 [b]
1-NpOH	40	6 ± 1 [a]	6 ± 1 [a]	4 ± 1 [a]

a) Errors represent the average deviation between the two experiments. b) Errors of individual values from two independent experiments were taken into account. c) Only one experiment was used.

The dissociation rate constants aided in the investigation of the interactions of the naphthalene probes with the NaCh aggregates. The values for the dissociation rate constants of 1-NpOH and 1-EtNp in the presence of 40 mM of NaCh were not affected by varying the ionic strength of the solution. The only data that were affected by an increase in the ionic strength was the data for 1-EtNp in the presence of 10 mM of NaCh. The dissociation rate constant was decreased by more than an order of magnitude when the ionic strength was increased from 0.03 M to 0.2 M. No further substantial decrease was noted when the NaCl concentration was increased to 0.4 M.

The trends due to the hydrophobicity of the probe observed in the varying ionic strength experiments (Section 4.1) were present in the study done at constant ionic strength. The dissociation rate constant for 1-EtNp in the presence of 40 mM of NaCh was an order of magnitude lower than the dissociation rate constant for 1-NpOH at the same host concentration. In the presence of 0.2 M and 0.4 M ionic strength, the

dissociation rate constant for 1-EtNp in the presence of 10 mM of NaCh and 40 mM of NaCh were comparable within the error of the experiments. It was also noted that increasing or decreasing the salt concentration did not affect the quenching efficiency observed for 1-NpOH in the presence of 10 mM of NaCh. This system gave rise to linear quenching plots at all ionic strengths.

Table 4.14 Values for the association rate constants divided by the aggregation number for 1-EtNp in the presence of 10 mM, and 40 mM of NaCh and 1-NpOH in the presence of 40 mM of NaCh at constant ionic strengths. Two independent experiments were performed for each probe at each bile salt and NaCl concentration.

Probe	[NaCh] /mM	$(k_+/N) / 10^8\ M^{-1}s^{-1}$		
		μ = 0.03 M	μ = 0.2 M	μ = 0.4 M
1-EtNp	10	~ 20 [d]	N/A [c]	N/A [c]
1-EtNp	40	2 ± 1 [a]	N/A [c]	N/A [c]
1-NpOH	40	3 ± 1 [b]	3 ± 1 [b]	2.5 ± 0.9 [a]

a) Errors represent the average deviation between the two experiments. b) Errors of individual values from two independent experiments were taken into account. c) The curvature in this experiment was insufficient to extract a reliable value for k_+/N. d) Only one experiment was used.

It is of interest to note that the data at an ionic strength of 0.2 M in the constant ionic strength experiment were in close agreement to the data found in the varying ionic strength experiments. The latter experiments were carried out at an ionic strength varying from 0.2 M to 0.25 M, due to the presence of ionic quenchers. As this concentration

range was small, it was expected that the values from the two different experimental methods would be comparable and this data are presented in Tables 4.15 and 4.16.

Table 4.15 Comparison of the triplet excited state quenching rate constants between the varying ionic strength experiments and the constant ionic strength experiments at $\mu = 0.2$ M.

Probe	[NaCh] (mM)	k_q / 10^9 $M^{-1}s^{-1}$	
		varying ionic strength	constant ionic strength
1-EtNp	0	2.7 ± 0.2	2.7 ± 0.8
1-NpOH	0	3.4 ± 0.2	3.1 ± 0.1
1-NpOH	10	2.4 ± 0.2	2.5 ± 0.2

Table 4.16 Comparison of the dissociation rate constants for the triplet excited states between the varying ionic strength experiments and the constant ionic strength experiments at $\mu = 0.2$ M.

Probe	[NaCh] (mM)	k_- / 10^6 s^{-1}	
		varying ionic strength	constant ionic strength
1-EtNp	10	0.20 ± 0.04	0.4 ± 0.1
1-EtNp	40	0.14 ± 0.03	0.16 ± 0.08
1-NpOH	40	7 ± 1	6 ± 1

All the values agree within experimental error in Table 4.15. In Table 4.16 the values for 1-EtNp in the presence of 10 mM differ slightly, while the values for both probes in the presence of 40 mM of NaCh are the same within error.

4.3 Discussion on the dynamics of probe binding to bile salt aggregates at varying ionic strength

The sharpening in the fluorescence emission spectra of the ethylnaphthalenes upon addition of NaCh was the first indication that an interaction was occurring between the Np probe molecules and the NaCh aggregates. It is possible to see vibrational fine structure in the fluorescence emission spectrum of a molecule if the various vibrational levels of the electronic ground state are distinguishable from one another. Molecule-solvent interactions decrease vibrational fine structure of the emission spectra. When solvated within a protected binding site such as the primary aggregate, the interaction of the probes and solvent is diminished, allowing for fine structure in the emission spectra.

In previous work it has been suggested that two distinct binding sites are present in sodium cholate aggregates.[51-53,94] The series of naphthalene probes was chosen in order to probe both the hydrophilic and hydrophobic binding sites. The hydrophobicity increased upon progressing from carbonyl, to hydroxyl, to alkyl substituents (vide infra). Consequently, the ethyl substituted naphthalenes were chosen, with the hypothesis being that they would bind to the primary site, while the more hydrophilic ketone and alcohol derivatives would bind to the secondary site.

The hydrophobicity scale was based on analyzing substituent polarity[99] and K_s values (values for the incorporation of probe molecules within micelles).[100] It was obvious that the ethylnaphthalenes were the most hydrophobic probe molecules in the study, as the molecule is a pure hydrocarbon not bearing any hydrophilic substituents. The distinction in the hydrophobicity difference for the hydroxyl and carbonyl substituted Nps was not as obvious.

In order to compare the polarity of the hydroxyl substituted Np to the carbonyl substituted Np, representative model compounds were chosen. Acetone and 2-propanol were used to compare the effect of substituents, assuming that the difference observed would be the same when a Np ring was the base for either compound. The dipole moments of the above compounds were compared to measure polarity. The dipole moment of acetone is 2.9 D while that of 2-propanol is 1.7 D.[101] These values are the dipole moments in the gas phase, and though the values will differ slightly in water, it is still expected that acetone's dipole moment will be greater than that of 2-propanol. The higher the dipole moment, the more polar the molecule. Thus, the acetonaphthones (represented by acetone) are more polar than the naphthylethanols (represented by 2-propanol). The solvation of probes will be affected by more than the polarity of the molecule; however, the hypothesis of this work is that the polarity will be an important factor in determining the location of the probe molecules within the aggregate system.

To further validate the fact that this change in polarity can effect the incorporation of probes within a supramolecular binding site, a comparison was made to a study done by Farah and co-workers, in which the partitioning of probe molecules between SDS micelles and water was investigated.[100] In spite of the fact that the current study is interested in the incorporation within NaCh aggregates, the partitioning within micelles was used as a guideline to determine the hydrophobicity scale. Data in this study did not include the carbonyl substituted Nps; thus model compounds were compared. The incorporation of probes within micelles was quoted as a K_S value (incorporation constant for the probe molecule). The larger the value of K_S, the more likely the probe is contained within the binding region of the micelle, and thus the more "hydrophobic" the probe.

Comparing 2-heptanol to 2-heptanone, the K_S value decreased from 100 to 48,[100] suggesting that the ketone derivative was more likely to be located within the aqueous phase than within the binding region of SDS. Thus, based on these observations, it was concluded that the carbonyl was the most hydrophilic of the substituents.

Figure 4.13 shows the evidence for two distinct binding sites. The fact that there was little change in the quenching plot for 1-NpOH when the NaCh concentration was changed from 0 mM to 10 mM suggests that the probe was not included within the primary site. The dramatic change for 1-NpOH in the presence of 40 mM of NaCh shows that at this NaCh concentration the probe was located within a protected binding area, that is, the secondary binding site. A very different trend was observed for 1-EtNp. As can be seen in Figure 4.13, in the presence of 10 mM of NaCh a large decrease in the quenching efficiency was noted, suggesting incorporation of the probe within the primary aggregate. Upon increasing the host concentration to 40 mM, secondary binding sites were introduced and no change in quenching efficiency was noted, suggesting the probe was located mainly within the primary site.

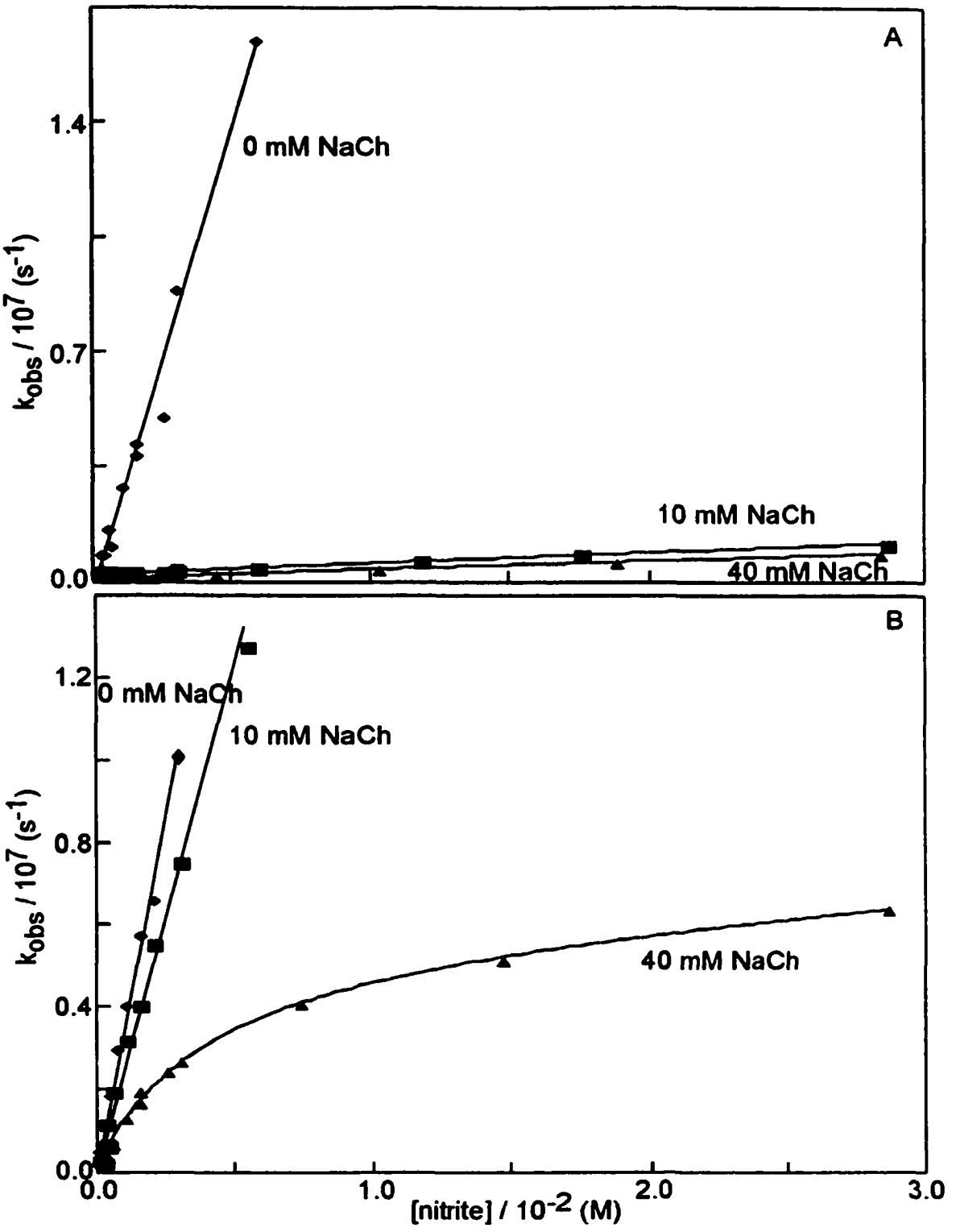

Figure 4.13 Comparison of the triplet excited state quenching plots for (A) 1-EtNp and (B) 1-NpOH by nitrite in the presence of 0 mM, 10 mM and 40 mM of NaCh to highlight the presence of two distinct binding sites.

4.3.1 Mechanism of quenching for singlet excited state Np probe molecules

Elucidating the quenching mechanism for the singlet excited state of the Np probe molecules was achieved by comparing the data obtained from steady-state and time-resolved fluorescence experiments. As the steady-state and time-resolved data gave rise to similar Stern-Volmer constants, the mechanism for quenching in these studies was dynamic quenching (see Section 1.1.3.1). Thus, no static quenching is believed to occur for any of the systems investigated, and the interaction under investigation within the quenching experiments is truly the accessibility of the aqueous quencher to the probe within the supramolecular system (vide infra).

4.3.2 Effect of the probe hydrophobicity on guest binding with NaCh aggregates

When analyzing the results obtained in the fluorescence quenching experiments, general observations were made. The trends in the Stern-Volmer constants were the same as the trends in average quenching rate constants. Consequently, in most cases, only the average quenching rate constants ($<k_q>$) are discussed, and the discussion is the same for the K_{SV} values.

The $<k_q>$ values are the average quenching rate constants arrived at by dividing the K_{SV} value by the average lifetime in the absence of quencher of each probe molecule at each bile salt concentration. This average value takes into account the fraction of probe molecules involved in each of the two separate decays. Thus, it is important to state that the fraction of molecules located within a particular environment in the bile salt aggregates did not change with the addition of quencher. This observation comes from

examining the pre-exponential factors recovered in the SPC experiments. It was found that in most cases the pre-exponential factors remained reasonably constant for a given probe at a constant NaCh concentration, as the quencher concentration was increased. Therefore, the only factor affecting the quenching rate constant was the quenching efficiency. As the average quenching rate constant decrease, it can be stated that the accessibility of the quencher to the probe is decreased. The quencher used in this study is an aqueous quencher that resides mainly within the aqueous phase, thus as the $<k_q>$ values decrease, the probe is most likely located within a more protected environment.

Within the bile salt aggregates the most protected environment is the primary aggregate. Thus, if probe molecules are located within the primary aggregate they will be more protected from the aqueous quencher and this in turn leads to a decrease in the value of $<k_q>$. Probe molecules located within the secondary site are more protected than those located within the aqueous phase. Thus, a decrease in the $<k_q>$ value (compared to the value for the probe in water) will occur for probe molecules located within the secondary site; however, the level of protection of the secondary site is lower than that of the primary site. Thus, the largest decreases in the $<k_q>$ values were observed when the probe molecule was located within the primary aggregate.

4.3.2.1 1-Ethylnaphthalene and 2-ethylnaphthalene as probe molecules in NaCh aggregates

All the data acquired in this study suggests that the ethylnaphthalenes are located within the primary aggregates. It was of interest to note at which concentrations of NaCh the value for the $<k_q>$ in the fluorescence quenching experiments would decrease

significantly. For the ethylnaphthalenes, the largest change in the value of $<k_q>$ occurs at 10 mM of NaCh. It is believed that the onset of primary aggregation occurs at 10 mM of NaCh. Thus, this decrease noted for the ethylnaphthalenes in the presence of 10 mM suggests that upon the formation of primary aggregates, the hydrophobic ethylnaphthalenes are located within a protected binding site. No decrease in the Stern-Volmer constant (from steady-state data) was noted at NaCh concentrations lower than 10 mM, suggesting that aggregates do not form at lower NaCh concentrations.

A second, smaller, decrease in the values of $<k_q>$ was noticed in the presence of 20 mM of NaCh, and was due to the increase in the number of primary aggregates present at this host concentration. At 20 mM of NaCh, more probe molecules were incorporated within the primary aggregates, thus value of $<k_q>$ was decreased. For 2-EtNp, the pre-exponential factors from SPC in the presence of 10 mM of NaCh were 0.46 (for the most accessible species), and 0.54 (for the most protected species). For 1-EtNp the pre-exponential factors in the presence of 10 mM of NaCh were 0.42 (for the most protected species), and 0.58 (for the most accessible species). In the presence of 20 mM of NaCh the pre-exponential factors for both of the ethylnaphthalenes were ca. 0.15 and 0.85 for the least and most protected species, respectively. This SPC data shows a larger fraction of probe molecules were included within a more protected environment, which decreased the accessibility of the quencher to the probe molecules, as the NaCh concentration was increased from 10 mM to 20 mM. Thus, the value for $<k_q>$ was decreased as the NaCh concentration was increased.

The study done by McGown and coworkers,[42] discussed in Chapter one, suggested an increased protection for hydrophobic probes when the bile salt concentration was increased to between 8 mM and 12 mM. This would be consistent with our findings that the onset of primary aggregation occurs around 10 mM.

For 1-EtNp in the presence of 10 mM of NaCh, a downward curvature was noted in the Stern-Volmer quenching plot. This was the only singlet quenching data that did not give rise to a linear plot. In previous work by Webber and co-workers[4] the downward curvature in a singlet quenching plot is explained in terms of a "hindered access" model. This model suggests that two species of excited singlet states exist with similar lifetimes; however, the access to the different species by the quencher is different. If this were the case, it would have been expected that in the lifetime quenching data, a third, long lived, component would be present as the quencher concentration was increased. Unfortunately, the time-resolved experiments were done at lower quencher concentrations and it is therefore possible that the presence two different singlet species was not observed.

Examining the quenching of the two separate excited states with different lifetimes in the time-resolved fluorescence experiments supported the assignments made based on the average quenching rate constants. In most cases, the excited state corresponding to the first component was located in the aqueous phase because the quenching rate constant was of the same order of magnitude as that obtained for the probes in the absence of bile salt. This was the case for 1-EtNp at all bile salt concentrations, and for 2-EtNp in the presence of 10 mM of NaCh.

The value for the k_q of the excited state that corresponds to the first component of 2-EtNp in the presence of 20 mM appears to be an order of magnitude lower than that

observed in water. This value is only an estimate due to a fluctuation in the pre-exponential factor; however, the decrease in the value suggests the excited state corresponding to the first species of 2-EtNp decaying was located within the secondary aggregate, a slightly more protected environment. The second component for both ethylnaphthalenes gave rise to fluorescence quenching rate constants that were two orders of magnitude lower than the values for the k_q in water. Furthermore, the values recovered were all very similar, suggesting that the environment in which the probe molecules were located was the same at all NaCh concentrations. The exited states corresponding to this signal are believed to be located within the primary aggregate. From the SPC data, only two species were detected for 1-EtNp in the presence of 10 mM. One species was located in the primary aggregate and one in the aqueous phase. Thus, if two species existed within the primary aggregate, as was hypothesized from the steady-state results, they must have the same singlet lifetimes.

The two different excited state species for the ethylnaphthalenes in the presence of secondary aggregates appear to be located in different environments when the substituent position is altered. In the case of 1-EtNp the two excited state species were located within the aqueous phase and within the primary aggregate, while for 2-EtNp the two excited state species were located within the secondary and primary aggregates.

A comparison of k_q values for the separate species with different lifetimes can be made to a similar fluorescence study done previously, and using pyrene as a probe molecule within the NaCh system.[52] The previous study for pyrene in the presence of NaCh aggregates found that the fluorescence lifetime decay traces were the sum of two decaying species. The k_q for the first of the two species varied from 0.4 - 1.1 x 10^9 $M^{-1}s^{-1}$,

while the k_q of the second species was much smaller with a value of ca. 3×10^7 $M^{-1}s^{-1}$. The assignments made for these species were that the first species was located within the aqueous bulk, while the second was contained within the hydrophobic binding site of the NaCh aggregates. Thus, the data presented for the ethylnaphthalenes agrees with the earlier findings for pyrene. This is consistent with hydrophobicity affecting the binding of probes within bile salt aggregates, as pyrene is also a hydrophobic probe.

In another study carried out by our research group, Np was analyzed in a similar fashion using SPC.[53] The results found a similar trend in the values for k_q of the first component, with all values being greater than 1×10^9 $M^{-1}s^{-1}$. The values for k_q of the second component were an order of magnitude lower, with values ranging from 1.5×10^8 $M^{-1}s^{-1}$ to 2.07×10^8 $M^{-1}s^{-1}$. All the other research carried out was consistent with a drop of 1.5 to 2 orders of magnitude in the k_q value, when the probe was included within the primary site. Why this was not observed for Np in the previous study is unknown.

The assignments for the location of the ethylnaphthalenes were supported, in most cases, by the trends in dissociation rate constants of the triplet excited states of these probe molecules. The dissociation rate constants obtained for the ethylnaphthalenes were of an order of magnitude lower than those obtained for other probe molecules in this study, suggesting that these probes are located within the most protected binding site, that is, the primary aggregate. The triplet quenching rate constants were also lower than any of the values obtained for the alcohol or ketone derivatives, suggesting that the access to the ethylnaphthalenes by an aqueous quencher was lower than for the acetonaphthones or the naphthylethanols. The triplet quenching studies provide information on the dynamics of the excited state system as well as the access of the aqueous quencher to the probe

molecules. The Np probes, in the excited state, interacted with the host system, and thus the interaction of the quencher with the excited state probe molecules was dependent upon the exit of the probe from the aggregate system. This differs from the fluorescence quenching experiments where the only process investigated was the ability of the quencher to enter the bile salt aggregate and access an excited state probe molecule. Thus, in the triplet studies a lower quenching rate constant suggests the probe molecule was located within a rigid binding site, and therefore the quencher has less access to the excited state probe molecules.

Comparing the dissociation and quenching rate constants for the ethylnaphthalenes to those previously obtained for Np, further supports the assignments made above. In a previous study,[51] the k_- value for Np in the presence of 40 mM of NaCh was found to be $(1.0 \pm 0.4) \times 10^6\ s^{-1}$, while the value of k_q was $(2.2 \pm 0.4) \times 10^7\ M^{-1}s^{-1}$. Np was located within the primary aggregate. The ethylnaphthalenes have the added ethyl groups making the molecules more hydrophobic; thus, it would be expected that the k_- value would be lower. In the current study, the value for the k_- for the ethylnaphthalenes in the presence of 40 mM of NaCh was $(1.4 \pm 0.3) \times 10^5\ s^{-1}$, for 1-EtNp and $(4 \pm 2) \times 10^5\ s^{-1}$, for 2-EtNp. Thus, the dissociation rate constant was at least halved with the addition of the ethyl group, and lend further support to the assignment of these probe molecules as being located within the primary aggregate. No change was noted in the dissociation rate constant as the NaCh concentration was increased from 10 mM to 40 mM; thus it was reasonable to assume that the probe was located within the same environments at all bile salt concentrations.

The triplet data does not support the finding from SPC that 2-EtNp in the presence of 20 mM of NaCh was located within the two binding sites, while 1-EtNp was located within the primary binding site and the aqueous phase. The data recovered for the ethylnaphthalenes in the LFP studies suggested that similar behavior was observed for both probes. Further, no change was observed for the triplet quenching data when the NaCh concentration was increased from 10 mM to 20 mM. Thus, as secondary aggregates were introduced, the interaction of the probe with the host system was not altered. As the finding in the SPC experiment for 2-EtNp was only an estimate and is not confirmed by the LFP data, it is most likely that both ethyl substituted probes are located solely within the primary binding site (and in the aqueous phase).

The behaviour of 1-EtNp in the presence of 10 mM of NaCh is also puzzling. The singlet steady-state data suggested that two species of 1-EtNp were present when the NaCh concentration was 10 mM. Though the singlet lifetimes of the two species were the same, the accessibility of the quencher to the two species was not the same. The quenchers used in both singlet and triplet studies were aqueous, ionic quenchers. This being the case, it was assumed that the accessibility to the probe molecules would be similar when performing singlet and triplet quenching studies. If this were the case, two species should have been observed in the triplet quenching data; however, all the decay traces were mono-exponential and thus, only one species was present within the primary aggregate. A possible explanation for the differences observed may be based on the difference in time scale for the experimental procedures. As mentioned previously, fluorescence measurements occur on much faster time scale than the corresponding triplet measurements. It is possible that the two species were therefore indistinguishable

from one another in the triplet quenching decays, as the deactivation occurs in the hundred of nanoseconds to millisecond time-domain.

4.3.2.2 1-Naphthyl-1-ethanol and 2-naphthyl-1-ethanol as probe molecules in NaCh aggregates

All the data acquired in this study suggests that the naphthylethanols were located within the secondary aggregates. In the fluorescence quenching experiments, it was of interest to note at which concentrations of NaCh the value for the $<k_q>$ (or K_{SV}) would decrease significantly. For the hydroxyl-substituted naphthalenes, only one large drop was noted in this value, between NaCh concentrations of 10 mM and 20 mM. This is the concentration at which secondary aggregates are formed. It is believed that the naphthylethanols were not included within the primary binding site; thus, no decrease was expected in the $<k_q>$ value until secondary aggregates were present. A gradual decrease was observed in the average quenching rate constants as the NaCh concentration was increased from 20 mM to 40 mM.

Analyzing the fluorescence quenching rate constants for the various excited state species from SPC separately lends further support to the naphthylethanols being located solely within the secondary binding site. For both alcohol derivatives in the presence of 20 mM and 40 mM of NaCh the quenching rate constant for the second of the two excited state species observed was an order of magnitude lower than in water, suggesting it was located within the secondary binding site. In the previous section (Section 4.3.2.1) it was noted that the k_q values for the ethylnaphthalenes in the presence of primary aggregates were two orders of magnitude lower than in water. The primary aggregate is a

more protected environment than the secondary aggregate, which leads to lower k_q values. It is therefore reasonable to assign a decrease of one order of magnitude in the k_q value as compared to the aqueous phase to correspond to the quencher accessing a probe molecule located within the secondary aggregate.

In general, no decrease was noted in the average fluorescence quenching rate constant (or K_{SV} value) for 1-NpOH below 20 mM of NaCh. This result suggests that 1-NpOH did not interact with the primary aggregates. This observation was supported by the findings in the triplet excited state data. The quenching plots for the triplet excited state of 1-NpOH in the presence of 10 mM were linear. At 10 mM NaCh, only primary aggregates are present, and a linear quenching plot suggests that the probe molecules were not incorporated within or interacting with the binding site.

For 2-NpOH, a decrease was noted in the K_{SV} value in the presence of 10 mM of NaCh, but not at lower bile salt concentrations. The decrease in the presence of 10 mM of NaCh was small, indeed, much smaller than the decrease observed for the ethyl-substituted derivatives at the same NaCh concentration, suggesting that the interaction of 2-NpOH with the primary site was not the same as that of the ethylnaphthalenes. This observation was supported by the time-resolved fluorescence results, as well as the results in the triplet excited state quenching experiments. In the singlet state time-resolved study, though two components were present, the k_q was of the same order of magnitude as the quenching of the probes in water for both components. For 2-NpOH in the presence of 10 mM of NaCh, a curved quenching plot was obtained for the quenching of the triplet excited state by nitrite. The upper value in the range obtained for the $k_q(H)$ was of the same order of magnitude as the k_q in water, suggesting the probe was not fully

incorporated within a protected site. The dissociation rate constant obtained for 2-NpOH in the presence of 10 mM of NaCh was two orders of magnitude larger than that obtained for the ethylnaphthalenes bound within primary aggregates, and an order of magnitude larger than when 2-NpOH was located within the secondary site.

All these findings suggest that only a weak interaction occurred between 2-NpOH and the primary aggregates. The most likely explanation for the weak interaction observed is that the probe molecule was interacting with the outside of the primary aggregate. A combination of hydrophobic interactions and hydrogen bonding may account for the results that were observed. It is possible that the Np ring structure was located in close proximity to the rings of the NaCh monomer. The bond distance between the hydroxyl groups on the B and C rings within the NaCh monomer is ca. 5.3 Å, while the length of the Np molecule is ca. 5.1 Å. Therefore, it is possible for the probe molecule to be located between the two hydroxyl groups on the B and C rings of the NaCh molecule on the outside of the primary aggregate. Further, it is likely that 2-NpOH formed hydrogen bonding interactions with one of the hydroxyl groups of the NaCh monomer. The hydroxyl groups are separated by 6 Å; thus only one hydroxyl group per monomer would be able to interact with the probe molecule. In the case of 1-NpOH, no interaction was observed. The subtle changes in the structure of the molecule excluded its interaction with the primary aggregate. Thus, no interaction occurred between 1-NpOH and the primary aggregate, while an interaction leading to a weak protection was observed for 2-NpOH.

In the presence of secondary aggregates ([NaCh] $\geq$ 20 mM), 1-NpOH and 2-NpOH behaved similarly. This was expected, as these probe molecules were located

mainly within the secondary aggregate. The pre-exponential factors recovered in the SPC experiments did not change with increasing NaCh concentration above 20 mM, thus it is likely that the partitioning of the probe molecules between the aqueous phase and the secondary aggregate was constant. For the triplet excited state data, the values remained an order of magnitude greater than the dissociation rate constants for the ethylnaphthalenes in the presence of primary aggregates, supporting the fact that the naphthylethanols were located within a less rigid binding site, that is, the secondary aggregate.

4.3.2.3 1-Acetonaphthone and 2-acetonaphthone as probe molecules in NaCh aggregates

To a large extent, analyzing the fluorescence data for 2-NpO was not possible. It appeared that the ketone derivative was not included within the aggregate. No shift in the emission spectra was noted and the Stern-Volmer constants were the same in water and in the presence of 40 mM of NaCh. 1-NpO did not fluoresce.

As a result, the analysis for the most polar of the Np probes is based solely on triplet excited state data. In the presence of 10 mM of NaCh, both ketone derivatives gave rise to curved quenching plots, suggesting that the ketone derivatives did interact with the NaCh primary aggregates. The interaction 2-NpO was similar to that observed for 2-NpOH in the presence of 10 mM of NaCh, and thus it is believed that 2-NpO was also interacting with the outside of the primary aggregate as described previously. This assignment was based on the fact that the dissociation rate constant, as well as the range

of the quenching rate constant for 2-NpO were similar to those observed for 2-NpOH in the presence of 10 mM of NaCh.

The behaviour of 1-NpO in the presence of 10 mM of NaCh was unique. The value for the dissociation rate constant was an order of magnitude lower than those observed for 2-NpO and 2-NpOH in the presence of 10 mM of NaCh. The dissociation rate constant for 1-NpO was an order of magnitude larger than those recovered for the ethylnaphthalenes at the same host concentration. A range of values for the kq(H), similar to the other polar probes, was recovered for 1-NpO; however, the upper limit was 1 $x10^8$ $M^{-1}s^{-1}$, as opposed to the diffusional limit of 1 $x10^9$ $M^{-1}s^{-1}$ obtained for 2-NpO and 2-NpOH. Again, the upper limit for the quenching rate constant for 1-NpO exceeds that observed for the ethylnaphthalenes within primary aggregates. The observations that the dissociation rate constant, as well as the quenching rate constant are larger than those for the ethylnaphthalenes suggests that the probe molecules are not located within the primary binding site. The most likely explanation for these findings is that 1-NpO is perhaps forming slightly stronger interactions with the outside of the primary aggregate, due to the slight structural differences between the probes. As no singlet excited state results were available for this probe molecule, the analysis must be solely based on the triplet quenching data.

The values for the dissociation rate constants of 1-NpO and 2-NpO in the presence of 20 mM and 40 mM of NaCh were similar to the dissociation rate constants for the alcohol derivatives at the same NaCh concentrations. This observation is consistent with the acetonaphthones being located within the secondary site. The

quenching rate constant ranges for the acetonaphthones in the presence of secondary aggregates were also similar to those of the naphthylethanols.

4.3.2.4 Summary of the findings for Np probe complexation in experiments carried out with varying ionic strength

It was interesting to note that the decrease in the $<k_q>$ for the alcohol derivatives between host concentrations of 10 mM and 20 mM was minor compared to the decrease observed for the $<k_q>$ for the ethylnaphthalenes in the presence of 10 mM and 20 mM of NaCh. The fact that the values for the ethylnaphthalenes $<k_q>$ decreased by an order of magnitude, while the naphthylethanols $<k_q>$ values were only halved, suggested that the former were located in a much more protected environment than the latter. Comparing the average quenching rate constants in the presence of 40 mM of NaCh gave further evidence for this interpretation. The values for the $<k_q>$s of 1-EtNp and 2-EtNp were of the order of magnitude of 10^7 $M^{-1}s^{-1}$, while the values for 1-NpOH and 2-NpOH were an order of magnitude larger ($10^8 M^{-1}s^{-1}$).

The most obvious trend noted in the dissociation rate constants was that the values for the alkyl substituted derivatives were of an order of magnitude lower than those for the hydroxyl and carbonyl substituted naphthalenes. Thus, the assignment of the ethylnaphthalenes being contained within the primary aggregate while the naphthylethanols were contained within the secondary site is reasonable.

Previous dynamic data for bile salt aggregates are very limited. Dynamic data for the interaction between pyrene and NaTC was previously reported in the literature.[40] A dissociation rate constant of $(3.8 \pm 0.4) \times 10^6$ s^{-1} was recovered by the researchers. In the

current study, this value falls within the same range as the values recovered for acetonaphthones in the presence of secondary aggregates. It is difficult to relate the previous data to the current study as the earlier work on pyrene was carried out at a NaCl concentration of 1 M. Further, the dissociation rate constant appears to be the average value of experiments carried out in presence of 10 mM, 15 mM, 20 mM, and 25 mM of NaTC.[40] Thus a comparison of the results in this work to the previous study is not possible to a large extent.

In another dynamic study, Thomas and co-workers attempted to estimate the dissociation rate constant of anthracene from NaTC.[54] The authors estimated the lower limit for k_- to be $3 \times 10^4\ s^{-1}$. This estimation was based on measuring the triplet-triplet annihilation rate constant. The researchers assumed that a triplet exiting from the aggregate would encounter a second triplet in the aqueous phase, and triplet-triplet annihilation would occur. Based on previous research in our group, using SDS micelles, this model is incorrect because the triplets would most likely interact with one another within the aggregates (or micelles), and not within the aqueous phase.[102] The assumption made within the SDS micelle model is that the association rate constant is close to the diffusion controlled limit. As a similar assumption may be made for the NaTC aggregates, it is reasonable that triplet-triplet annihilation would more likely occur within the NaTC aggregate than within the aqueous phase. Though this study does not directly relate to the research in this thesis, the work is mentioned to point out the very narrow scope of previous dynamic work carried out for bile salt aggregates.

In a study by Seret and co-workers, the lower limit for the exit rate constant of a common synthetic dye, rose bengal, from NaTC was examined.[103] The researchers found

Table 4.17 Association rate constants for the triplet excited state of the probe molecules located within the primary aggregate of NaCh calculated based on an aggregation number of 4.

Probe	$k_+ / 10^9$ ($M^{-1}s^{-1}$)		
	10 mM of NaCh	20 mM of NaCh	40 mM of NaCh
1-EtNp	0.3 ± 0.2 [a]	N/A [c]	N/A [c]
2-EtNp	0.8 ± 0.4 [b]	N/A [c]	N/A [c]

a)Errors represent the average deviation between the two experiments. b) Errors of individual values from two independent experiments were taken into account. c) The curvature in this experiment was insufficient to extract a reliable value for k_+.

Table 4.18 Association rate constants for the triplet excited state of the probe molecules located within the secondary aggregate of NaCh calculated, based on an aggregation number of 10.

Probe	$k_+ / 10^9$ ($M^{-1}s^{-1}$)		
	10 mM of NaCh	20 mM of NaCh	40 mM of NaCh
1-NpOH	---	7 ± 2 [a]	4 ± 1 [b]
2-NpOH	50 ± 30 [a]	4 ± 1 [a]	3 ± 1 [a]
1-NpO	3 ± 1 [b]	3 ± 1 [b]	2 ± 1 [a]
2-NpO	11 ± 8 [b]	4 ± 1 [b]	4 ± 1 [a]

a) Errors represent the average deviation between the two experiments. b) Errors of individual values from two independent experiments were taken into account.

The association rate constants were arrived at by assuming that the ethylnaphthalenes were located within the primary aggregate while the naphthylethanols and acetonaphthones were located within the secondary aggregate. The association rate

constants in the presence of 20 mM and 40 mM of NaCh for the naphthylethanols and acetonaphthones were all very similar. Considering these numbers were based on an average N value, it was difficult to draw conclusions from the values recovered.

4.4 Discussion on the dynamics of probe binding to bile salt aggregates at constant ionic strength

The data collected at constant ionic strengths gave insight into the role of ionic strength on aggregation behavior of bile salts. Work has been done previously by other groups on the effect of ionic strength on aggregation of bile salts (Chapter 1).[27,40,43,48] Most researchers working on the effect of ionic strength with relation to bile salts were not looking specifically at the effect of increased ionic strength on the structure of primary or secondary aggregates, but their data can be used to support the findings of the research in this thesis. Based on the past work carried out by the above researchers, it was hypothesized that the increase in ionic strength of the solution causes aggregation to occur at lower bile salt concentrations. Each cholate monomer, when dissolved in aqueous medium, has a negative charge associated with it due to the presence of the carboxylate group. Thus, it was hypothesized that increasing the ionic strength would affect aggregation of NaCh considering the added counter ions would shield the negatively charged carboxylate groups. This would allow the monomers to approach one another in order to form primary aggregates as well as the primary aggregates to approach in order to form secondary aggregates. The hydrophobic driving force for the monomers in solution is the key supramolecular force involved in the formation of primary aggregates. For the formation of secondary aggregates, it is believed that the

main driving force is the hydrogen bonding interactions of the primary aggregates to form secondary aggregates. The electrostatic repulsion of the carboxylate group would counter both of the above interactions making it more difficult for the aggregates to form. Thus, by shielding the negative charge, the favorable interactions would be enhanced.

4.4.1 Effect of ionic strength on primary aggregate formation

1-EtNp is located within the primary binding site, as discussed above (Section 3.3). The K_{sv} values for 1-EtNp in the absence of NaCh were, as expected, unaffected by the increase in the ionic strength of the solutions. In the presence of 3 mM and 10 mM of NaCh, as the ionic strength was increased, there was a decrease in the Stern-Volmer constant. Why the effect was not noted at 5 mM is a puzzle. Though the experiments at 5 mM were repeated under the same conditions multiple times, only a range of values was obtained. This observation aside, it would appear that a change in the ionic strength did affect the aggregation of the primary aggregates to a large extent, cutting the value for the K_{sv} in half with an increase in ionic strength of 0.37 M.

The one trend in the K_{SV} values that differed from the experiments carried out at varying ionic strengths was the onset of primary aggregation. In the varying ionic strength experiments, and at a $\mu = 0.2$ M in the constant ionic strength experiments, the onset of primary aggregates was noted at a host concentrations of 10 mM of NaCh. At an ionic strength of 0.03 M, aggregate formation was only noted at a NaCh concentration of 20 mM. This suggests that at low ionic strength primary aggregates did not form at 10 mM of NaCh as previously observed. At an ionic strength of 0.4 M, primary aggregate formation was noted at a host concentration of 3 mM of NaCh. This suggested that an

increase in the ionic strength of the solution allowed primary aggregates to be formed at lower host concentrations. This is reasonable as the formation of primary aggregates is a matter of balancing the hydrophobic driving force for aggregation with the electrostatic repulsion of the negative charge on the carboxylate groups. At high ionic strength the repulsion of the hydroxyl groups would be decreased and primary aggregation would occur at lower bile salt concentrations.

Work done previously supports the finding that at very low ionic strength aggregation is inhibited. Kratohvil and co-workers observed that, in the absence of NaCl, aggregates of NaTC would not form.[28] This study was done at very low bile salt concentrations, but the findings support the observation that formation of primary aggregates is decreased at low ionic strength. Work done by Mazer and co-workers looked at bile salt aggregation at host concentrations lower than 11 mM,[48] so the researchers were observing the effect of ionic strength on primary aggregates. Here, the researchers' findings suggest that at a high ionic strength, aggregates were formed at lower concentration of bile salt. This observation is consistent with the current study observation that primary aggregation occurs at lower bile salt concentration as the ionic strength is increased.

Using the triplet excited state quenching results, the fluorescence findings for 1-EtNp in the presence of primary aggregates were confirmed. A decrease in the dissociation rate constant, for 1-EtNp in the presence of 10 mM of NaCh, of more than one order of magnitude was noted when the ionic strength was increased from 0.03 M to 0.4 M. This observation lends support to the conclusion that ionic strength was important for the formation of primary aggregates of sodium cholate. No other significant changes

in the dissociation rate constants were noted due to a change in ionic strength as the NaCh concentration was increased to 40 mM.

The observation that no ionic strength dependence was noted on 1-EtNp in the presence of 40 mM of NaCh was difficult to understand. Regardless of the host concentration, 1-EtNp was located within the primary binding site of the NaCh aggregates. The most likely explanation for the loss of ionic strength dependence as the bile salt concentration was increased comes from considering the intermolecular forces involved. Despite the fact that secondary binding sites are present, it is the primary aggregation pattern that was of interest. As was previously mentioned, primary aggregation is a balance between hydrophobic interactions and electrostatic repulsions. As the monomer concentration was increased, so was the density of negative charge in the solution. By nature, the negative charges would still repel one another, but the total distance possible between charges would be decreased. Thus, as the negative charges could not repel one another as easily as at lower bile salt concentration, it is possible that the hydrophobic driving force for primary aggregation dominated, and aggregates formed even at low ionic strength. This effect would not occur at low bile salt concentrations, as the density of negative charges is lower, thus the electrostatic repulsion would have a much larger effect on the system.

The comparison between data carried out at μ = 0.2 M in the constant ionic strength experiments with data at varying ionic strengths revealed that only the data for 1-EtNp in the presence of primary aggregates were effected by the different sample preparation methodology. The difference in the k_- value of two preparation methods was small, which was reasonable because the change in ionic strength was small. The study

at constant ionic strength showed that the data for 1-EtNp in the presence of primary aggregates was the only data that were affected by changes in ionic strength. This being the case, the only data that should have been affected by the change in the sample preparation method was the data for 1-EtNp in the presence of 10 mM of NaCh. The varying ionic strength experiments led to a higher ionic strength (0.25 M) and it has been seen that this leads to a smaller dissociation rate constant. Thus, the findings when comparing the differing sample preparation methods are consistent with those observed in the constant ionic strength experiments.

4.4.2 Effect of ionic strength on secondary aggregate formation

No effect of ionic strength was observed for any of the singlet or triplet excited state data recorded for 1-NpOH. The naphthylethanols reside solely in the secondary aggregate. Therefore, the preliminary work carried out by this study found no effect of ionic strength when using NaCl, on secondary aggregate formation of NaCh.

It may be hypothesized that ionic strength does not affect the structure of secondary aggregates because electrostatic repulsions are minimal within the secondary binding sites. Secondary aggregation is postulated to occur due to hydrogen bonding, ion-diple and ion-ion interactions. The size of the cavity for the secondary aggregates is not known, and as such it is possible that the negative charges of the carboxylate groups are kept far enough apart from each other even as the secondary aggregates are formed. If this were the case, electrostatic repulsions would be minimized as would be the need for increased ionic strength, as added counterions would not be necessary for secondary aggregate formation.

The work done by McGown and co-workers has presented the most information on the effect of counter ions on the aggregation of bile salts to date.[43,45,49,76] All the work done by these researchers is consistent with ionic strength having an effect on bile salt aggregation in the presence of primary aggregates. The most relevant study showed that by using sodium as the counter ion, an effect was noted at NaCh concentrations below 10 mM, whereas no effect was noted on the aggregation of secondary sites.[43] For sodium as the counterion, this is consistent with our findings that only 1-EtNp in the presence of primary aggregates was affected by an increase in the ionic strength. In the presence of larger counter ions (Al and Tb) an effect of ionic strength was noted on secondary aggregation[43]; therefore, it is likely that the effect of ionic strength on aggregation of bile salts is also dependent upon the size and valency of the counter ion introduced.

5 Conclusions

The main objective of this work was to understand the complexation of probe molecules within the two distinct binding sites present in NaCh aggregates. The findings within this study aid in the growing support for the primary and secondary aggregation model of bile salts in solution.

5.1 Benzophenone complexation

Benzophenone and 4,4'-dimethylbenzophenone were used to study the interaction of probes within NaCh aggregates, as well as to gain an understanding of how photochemical reactivity is altered for probe molecules, based on their location within the two different binding sites. It was found that, for both ketones, the reactivity in the presence of primary aggregates was different than in the presence of secondary aggregates. It was also found that in the case of DMBp, the added hydrophobic moieties affected reactivity.

In the presence of only primary aggregates, both ketones reacted similarly. Three different populations of triplet excited states, with different reactivities, were identified. The first of these triplet excited states was located within the aqueous phase. The other two populations of triplet excited states were located in the primary aggregate. Most of the triplets in the primary aggregate reacted within the laser pulse (<10 ns) to form ketyl radicals, while some longer-lived triplets were unreactive within the laser pulse. The long-lived triplet excited states in the primary aggregate were observed to form ketyl radicals over 10 to 20 μs. The ketyl radicals exited the primary aggregate, and were

observed to react in a diffusion-controlled process that occurred within the aqueous phase.

The presence of secondary sites added complexity to the system. All the processes occurring in the presence of primary aggregates were still present, but with the interaction of primary aggregates to form secondary binding sites, additional reactions occurred. The processes unique to the secondary site were observed to occur on a much faster time scale than those occurring solely in the presence of primary aggregates. It was found that most of the ketyl radicals were formed by the reaction of triplet excited states within the primary aggregates. The decay of the ketyl radicals was slowed in the presence of secondary aggregates, suggesting that the radical-radical reactions were taking place within the secondary binding site, which is a more protective environment than the aqueous phase. In the secondary sites, it was found that the hydrogen abstraction reaction did not compete with self-quenching and exit of the excited state probe to the aqueous phase. Bp was found to have a shorter residence time within the secondary site than DMBp, leading to the conclusion that hydrophobicity changes, even small ones, lead to changes in the complexation dynamics for probe molecules with NaCh aggregates.

Analyzing the self-quenching data for Bp suggested that a small number of NaCh monomers are necessary in order to define both the primary and the secondary sites. It was found that the product of N_1 (number of monomers in the primary aggregate) and N_2 (number of primary aggregates that form the secondary site) lies between 6 and 13.

5.2 Naphthalene complexation

The hydrophobicity of the probe molecules was found to affect probe incorporation within the two different binding sites of NaCh aggregates. The ethyl-substituted Nps were located within the primary binding site, while the naphthylethanols and acetonaphthones were found to be located within the secondary aggregates. In the absence of secondary aggregates, all of the probes, with the exception of 1-NpOH, interacted with the primary aggregate. It is believed that the ethylnaphthalenes were completely incorporated within the binding site, the other probes interacted with the outside of the aggregates.

Conclusive evidence for the location of two distinct binding sites was also presented in the comparison of both the quenching rate constants (of the singlet as well as the triplet excited state) and the dissociation rate constants. The values for the hydrophobic probes were found to be, on average, an order of magnitude lower than the more hydrophilic probes. As both k_- and k_q values decrease with an increase in the level of protection, the difference of an order of magnitude suggests the probes are located in different environments.

The position of the substituent on the Np ring was also found to have a limited effect on the binding dynamics within the aggregate system. In general, it was found that the dynamics when the probe was bound to either the primary site or the secondary site were not affected by the position of the substituent. For the naphthylethanols the most striking differences were noted in the presence of 10 mM of NaCh because 2-NpOH appeared to interact with the outside of the aggregate, while 1-NpOH appeared to be unaffected by the presence of NaCh. For the acetonaphthones in the presence of 10 mM

of NaCh, 1-NpO appeared to form a stronger interaction with the outside of the aggregate than 2-NpO. Therefore, it would appear that the position of the substituent affects its interaction with the outside of the aggregate but not its incorporation within one of the binding sites.

Studying the effect of ionic strength on aggregation also provided insight into the role of ionic strength on bile salt aggregate formation. It was found that changing the ionic strength of the solution had an effect on the primary aggregation of NaCh, but not on the secondary aggregate formation. At low ionic strength, primary aggregates did not form, whereas, as the ionic strength was increased, primary aggregates formed at lower concentrations of NaCh.

6 References

(1) Klessinger, M.; Michl, J. *Excited States and Photochemistry of Organic Molecules*; VCH Publishers Inc.: New York, **1995**.

(2) Gilbert, A.; Baggott, J. *Essentials of Molecular Photochemistry*; CRC Press: London, **1991**.

(3) Turro, N. J. *Modern Molecular Photochemistry*; The Benjamin/Cummings Publishing Company, Inc.: Menlo Park, **1978**.

(4) Webber, S. E. *Photochem. Photobiol.* **1997**, *65*, 33.

(5) Sillen, A.; Engelborghs, Y. *Photochem. Photobiol.* **1998**, *67*, 475.

(6) Clements, J. H.; Webber, S. E. *J. Phys. Chem. A.* **1999**, *103*, 2513.

(7) Almgren, M.; Grieser, F.; Thomas, J. K. *J. Am. Chem. Soc.* **1979**, *101*, 279.

(8) Kleinman, M. H.; Bohne, C., Use of Photophysical Probes to Study Dynamic Processes in Supramolecular Structures in *Molecular and Supramolecular Photochemistry*; Ramamurthy, V., Schanze, K. S., Eds.; Marcel Dekker, Inc: New York, **1997**; *1*, 391.

(9) Bolt, J. D.; Turro, N. J. *J. Phys. Chem.* **1981**, *85*, 4029.

(10) Norrish, R. G. W.; Porter, G. *Nature* **1949**, *164*, 658.

(11) Liao, Y.; Bohne, C. *J. Phys. Chem.* **1996**, *100*, 734.

(12) Atkins, P. W. *Physical Chemistry*; Fourth ed.; Oxford University Press: New York, **1990**.

(13) Birch, D. J. S.; Imhof, R. E., Time-Domain Fluorescence Spectroscopy Using Time-Correlated Single-Photon Counting in *Topics in Fluorescence Spectroscopy*; Larkowicz, J. R., Ed.; Plenum Press: New York, **1991**; *1*, 1.

(14) Hofmann, A. F.; Mysels, K. J. *Coll. Surf.* **1988**, *30*, 145.

(15) Stedronsky, E. R. *Biochim. Biophys. Acta.* **1994**,1012, 255.

(16) Carey, M. C.; Small, D. M. *J. Colloid Interface Sci.* **1969**, *31*, 382.

(17) Hofmann, A. F.; Small, D. M. *Ann. Rev. Med.* **1967**, *18*, 333.

(18) Small, D. M., The Physical Chemistry of Choloanic Acids in *The Bile Acids*; Nair, P., Kritchevsky, D., Eds.; Plenum Press: New York, **1971**; *1: Chemistry*, 249.

(19) Small, D. M.; Penkett, S. A.; Chapman, D. *Biochim. Biophys. Acta.* **1969**, *176*, 178.

(20) Hjelm, R. P. J.; Thiyagarajan, P.; Alkan-Onyuksel, H. *J. Phys. Chem.* **1992**, *96*, 8653.

(21) Spink, C. H.; Lieto, V.; Mereand, E.; Pruden, C. *Biochemistry* **1991**, *30*, 5104.

(22) Cohen, D. E.; Thurston, G. M.; Chamberlin, R. A.; Benedek, G. B.; Carey, M. C. *Biochemistry* **1998**, *37*, 14798.

(23) Bandyopadhyay, A.; Moulik, S. P. *J. Phys. Chem.* **1991**, *95*, 4529.

(24) Carey, M. C.; Small, D. M. *Amer. J. Med.* **1970**, *49*, 590.

(25) Freeman, K. S.; Beck Tan, N. C.; Trevino, S. F.; Kline, S.; McGown, L. B.; Keserow, D. J. *Langmuir* **2001**, *17*, 3912.

(26) Janich, M.; Lange, J.; Graener, H.; Neubert, R. *J. Phys. Chem. B.* **1998**, *102*, 5957.

(27) Kratohvil, J. P.; Hus, W. P.; Jacobs, M. A.; Aminabhavi, T. M.; Mukunoki, Y. *Colloid Polym. Sci.* **1983**, *261*, 781.

(28) Kratohvil, J. P.; Hsu, W. P.; Kwok, D. I. *Langmuir* **1986**, *2*, 256.

(29) Kratohvil, J. P. *Adv. Colloid Interface Sci.* **1986**, *26*.

(30) O'Connor, C. J.; Wallace, R. G. *Adv. Colloid Interface Sci.* **1985**, *22*, 1.

(31) Mukerjee, P.; Cardinal, J. R. *J. Pharm. Sci.* **1976**, *65*, 882.

(32) Jover, A.; Meijide, F.; Rodriguez, N.; Tato, J. V. *Langmuir* **1997**, *73*, 101.

(33) Li, G.; McGown, L. B. *J. Phys. Chem.* **1994**, *98*, 13711.

(34) Oakenfull, D. G.; Fisher, L. R. *J. Phys. Chem.* **1977**, *81*, 1838.

(35) Oakenfull, D. G.; Fisher, L. R. *J. Phys. Chem.* **1978**, *82*, 2443.

(36) Zakrzewska, J.; Markovic, V.; Vucelic, D.; Feigin, L.; Dembo, A.; Mogilevsky, L. *J. Phys. Chem.* **1990**, *94*, 5078.

(37) Zana, R. *J. Phys. Chem.* **1978**, *82*, 2440.

(38) Zana, R.; Guveli, D. *J. Phys. Chem.* **1985**, *89*, 1687.

(39) O'Connor, C. J.; Ch'ng, B. T.; Wallace, R. G. *J. Colloid Interface Sci.* **1983**, *95*, 410.

(40) Hashimoto, S.; Thomas, J. K. *J. Colloid Interface Sci.* **1984**, *102*, 152.

(41) Schurtenberger, P.; Mazer, N. A.; Känzlg, W. *J. Phys. Chem.* **1983**, *87*, 308.

(42) Meyerhoffer, S. M.; McGown, L. B. *Langmuir* **1990**, *6*, 187.

(43) Meyerhoffer, S. M.; McGown, L. B. *J. Am. Chem. Soc.* **1991**, *113*, 2146.

(44) Meyerhoffer, S. M.; McGown, L. B. *Anal. Chem.* **1991**, *63*, 2082.

(45) Nithipatikom, K.; McGown, L. B. *Anal. Chem.* **1988**, *60*, 1043.

(46) Nithipatikom, K.; McGown, L. B. *Photochem. Photobiol.* **1988**, *47*, 797.

(47) Nithipatikom, K.; McGown, L. B. *Anal. Chem.* **1989**, *61*, 1405.

(48) Mazer, N. A.; Carey, M. C.; Kwasnick, R. F.; Benedek, G. B. *Biochemistry* **1979**, *18*, 3064.

(49) Li, G.; McGown, L. B. *J. Phys. Chem.* **1993**, *97*, 6745.

(50) Kawamura, H.; Murata, U.; Yamaguchi, T.; Igimi, H.; Tanaka, M.; Sugihara, G.; Kratohvil, J. P. *J. Phys. Chem.* **1989**, *93*, 3321.

(51) Ju, C.; Bohne, C. *J. Phys. Chem.* **1996**, *100*, 3847.

(52) Ju, C.; Bohne, C. *Photochem. Photobiol.* **1996**, *63*, 60.

(53) Ju, C.: Characterization of Bile Salt Aggregates Using Singlet and Triplet Excited Probe Molecules. Masters Thesis, University of Victoria (Victoria) 1996.

(54) Chen, M.; Grätzel, M.; Thomas, J. K. *J. Am. Chem. Soc.* **1975**, *90*, 2052.

(55) D'Alangni, M.; Forcellese, M. L.; Giglio, E. *Colloid Polym. Sci.* **1985**, *263*, 160.

(56) D'Alangni, M.; Giglio, E.; Petriconi, S. *Colloid Polym. Sci.* **1987**, *265*, 517.

(57) D'Archivio, A. A.; Galantini, L.; Gavuzzo, E.; Giglio, E.; Scaramuzza, L. *Langmuir* **1996**, *12*, 4660.

(58) Conte, G.; Blasi, R. D.; Giglio, E.; Parretta, A.; Pavel, N. V. *J. Phys. Chem.* **1984**, *88*, 5720.

(59) Campanelli, A. R.; De Sanctis, S. C.; Giglio, E.; Pavel, N. V.; Quagliata, C. *Incl. Phenom.* **1989**, *7*, 391.

(60) Esposito, G.; Giglio, E.; Pavel, N. V.; Zanobi, A. *J. Phys. Chem.* **1987**, *91*, 356.

(61) Almgren, M.; Grieser, F.; Thomas, J. K. *J. Chem. Soc., Faraday Trans. I.* **1979**, *75*, 1674.

(62) Meirovitch, E. *J. Phys. Chem.* **1982**, *86*, 5237.

(63) Meirovitch, E. *J. Phys. Chem.* **1985**, *89*, 2385.

(64) Djavanbakht, A.; Kale, K. M.; Zana, R. *J. Colloid Interface Sci.* **1977**, *59*, 139.

(65) Giglio, E.; Loreti, S.; Pavel, N. V. *J. Phys. Chem.* **1988**, *92*, 2858.

(66) Coello, A.; Meijide, F.; Rodriguez Nunez, E.; Tato, J. V. *J. Phys. Chem.* **1993**, *97*, 10186.

(67) Coello, A.; Meijide, F.; Rodriguez Nunez, E.; Tato, J. V. *J. Pharm. Sci.* **1996**, *85*, 9.

(68) Kalyanasundaram, K.; Thomas, J. K. *J. Am. Chem. Soc.* **1977**, *99*, 2039.

(69) Murov, S. L.; Carmichael, I.; Hug, G. L. *Handbook of Photochemistry*; 2nd, revised and expanded ed.; Marcel Dekker, Inc.: New York, **1993**.

(70) McGarry, P. F.; Doubleday, C. D.; Wu, C.-H.; Staab, H. A.; Turro, N. J. *J. Photochem. Photobiol. A: Chem* **1994**, *77*, 109.

(71) Webster, D.; Baugher, J. F.; Lim, B. T.; Lim, E. C. *Chem. Phys. Lett.* **1981**, *77*, 294.

(72) Selinger, B. K. *Aust. J. Chem.* **1966**, *19*, 825.

(73) Treinin, A.; Hayon, E. *J. Am. Chem. Soc.* **1976**, *18*, 3884.

(74) Barros, T. C.; Stefaniak, K.; Holzwarth, J. F.; Bohne, C. *J. Phys. Chem. A.* **1998**, *102*, 5639.

(75) Takenura, T.; Hara, K.; Baba, H. *Bull. Chem. Soc. Jpn.* **1971**, *44*, 997.

(76) Li, Y.; Holzwarth, J. F.; Bohne, C. *Langmuir* **2000**, *16*, 2038.

(77) Okano, L. T.; Barros, T. C.; Chou, D. T. H.; Bennet, A. J.; Bohne, C. *J. Phys. Chem. B.* **2001**, *105*, 2122.

(78) Elisei, F.; Favaro, G.; Görner, H. *J. Photochem. Photobiol. A: Chem* **1991**, *59*, 243.

(79) Boch, R.; Whittlesey, M. K.; Scaiano, J. C. *J. Phys. Chem.* **1994**, *98*, 7854.

(80) Okano, L. T.; Ovans, R.; Zunic, V.; Moorthy, J. N.; Bohne, C. *Can. J. Chem.* **1999**, *77*, 1356.

(81) Baral-Tosh, S.; Chattopadhyay, S. K.; Das, P. K. *J. Phys. Chem.* **1984**, *88*, 1404.

(82) Boyle, J. W.; Ghormely, J. A.; Hochanadel, C. J.; Riley, J. F. *J. Phys. Chem.* **1969**, *73*, 2886.

(83) Janata, E.; Schuler, R. H. *J. Phys. Chem.* **1982**, *86*, 2078.

(84) Topp, M. R. *Chem. Phys. Lett.* **1975**, *32*, 144.

(85) Bensasson, R. V.; Gramain, J.-C. *J.C.S. Faraday I.* **1980**, *76*, 1801.

(86) Lougnot, D. J.; Jaques, P.; Fouassier, J. P.; Casal, H. L.; Kim-Thuan, N.; Scaiano, J. C. *Can. J. Chem.* **1985**, *63*, 3001.

(87) Favaro, G.; Bufalini, G. *J. Phys. Chem.* **1976**, *80*, 800.

(88) Lutz, H.; Duval, M.-C.; Bréhéret, E.; Lindqvist, L. *J. Phys. Chem.* **1972**, *76*, 821.

(89) Turro, N. J.; Okubo, T.; Chung, C.-J. *J. Am. Chem. Soc.* **1982**, *104*, 1789.

(90) Turro, N. J.; Bolt, J. D.; Kuroda, Y.; Tabushi, I. *Photochem. Photobiol.* **1982**, *35*, 69.

(91) Lowry, T. H.; Richardson, K. S. *Mechanism and Theory in Organic Chemistry*; 3rd ed.; Harper and Row: New York, **1987**.

(92) Griller, D.; Kanabus-Kaminska, J. M.; MacColl, A. *J. Molec. Struct.* **1988**, *163*, 125.

(93) Kanabus-Kaminska, J. M.; Gilbert, B. C.; Griller, D. *J. Am. Chem. Soc.* **1989**, *111*, 3311.

(94) Infelta, P. P.; Grätzel, M.; Thomas, J. K. *J. Phys. Chem.* **1974**, *78*, 190.

(95) Wolf, M. W.; Brown, R. E.; Singer, L. A. *J Am. Chem. Soc* **1977**, *99*, 526.

(96) Tedesco, A. C.; Nogueira, L. C.; Carreiro, J. C.; Batista da Costa, A.; Boniha, J. B. S.; Moreira, P. F.; Alonso, E. O.; Quina, F. H. *Langmuir* **2000**, *16*, 134.

(97) Kalanasundaram, K. *Photochemistry in Microheterogeneous Systems*; Academic Press. Inc.: New York, **1987**.

(98) Scaiano, J. C.; Selwyn, J. C. *Can. J. Chem.* **1981**, *59*, 2368.

(99) Solomons, T. W. G. *Organic Chemistry*; 5th ed.; John Wiley & Sons, Inc.: Toronto, **1992**.

(100) Quina, F. H.; Alonso, E. O.; Farah, J. P. S. *J. Phys. Chem.* **1995**, *99*, 11708.

(101) *CRC Handbook of Chemistry and Physics*; 49th ed.; The Chemical Rubber Co.: Cleveland, **1969**, Vol.49.

(102) Kleinman, M. H.; Shevchenko, T.; Bohne, C. *Photochem. Photobiol.* **1998**, *68*, 710.

(103) Seret, A.; Van de Vorst, A. *J. Photochem. Photobiol. B: Biol.* **1993**, *17*, 47.